INFORMATION TO USERS

This manuscript has been reproduced from the microfilm master. UMI films the text directly from the original or copy submitted. Thus, some thesis and dissertation copies are in typewriter face, while others may be from any type of computer printer.

The quality of this reproduction is dependent upon the quality of the copy submitted. Broken or indistinct print, colored or poor quality illustrations and photographs, print bleedthrough, substandard margins, and improper alignment can adversely affect reproduction.

In the unlikely event that the author did not send UMI a complete manuscript and there are missing pages, these will be noted. Also, if unauthorized copyright material had to be removed, a note will indicate the deletion.

Oversize materials (e.g., maps, drawings, charts) are reproduced by sectioning the original, beginning at the upper left-hand corner and continuing from left to right in equal sections with small overlaps.

Photographs included in the original manuscript have been reproduced xerographically in this copy. Higher quality 6" x 9" black and white photographic prints are available for any photographs or illustrations appearing in this copy for an additional charge. Contact UMI directly to order.

ProQuest Information and Learning
300 North Zeeb Road, Ann Arbor, MI 48106-1346 USA
800-521-0600

Molecular Modeling of the Bacterial Chemotaxis Receptors Tar and Trg

Megan L. Peach

A dissertation submitted in partial fulfillment
of the requirements for the degree of

Doctor of Philosophy

University of Washington

2001

Program Authorized to Offer Degree: Department of Bioengineering

In presenting this dissertation in partial fulfillment of the requirements for the Doctoral degree at the University of Washington, I agree that the Library shall make its copies freely available for inspection. I further agree that extensive copying of this dissertation is allowable only for scholarly purposes, consistent with "fair use" as prescribed in the U.S. Copyright Law. Requests for copying or reproduction of this dissertation may be referred to Bell and Howell Information and Learning, 300 North Zeeb Road, Ann Arbor, MI 48106-1346, to whom the author has granted "the right to reproduce and sell (a) copies of the manuscript in microform and/or (b) printed copies of the manuscript made from microform."

Signature 

Date December 17, 2001

University of Washington

Graduate School

This is to certify that I have examined this copy of a doctoral dissertation by

Megan L. Peach

and have found that it is complete and satisfactory in all respects,
and that any and all revisions required by the final
examining committee have been made.

Chair of Supervisory Committee:

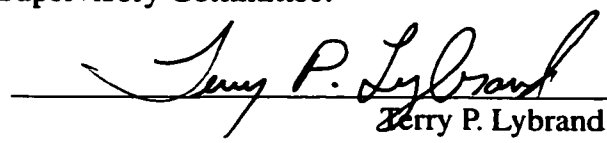

Terry P. Lybrand

Reading Committee:

Terry P. Lybrand

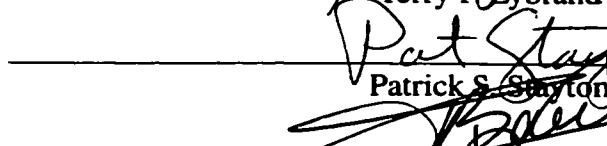

Patrick S. Stayton

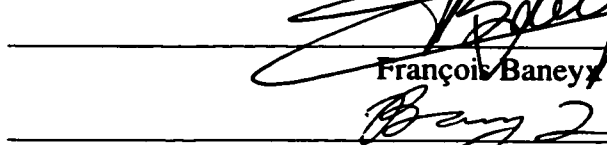

François Baneyx

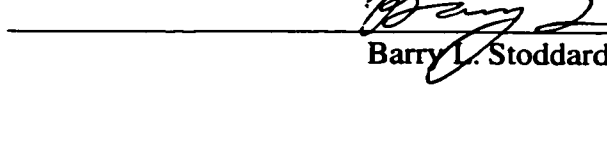

Barry L. Stoddard

Date: December 12, 2001

University of Washington

Abstract

Molecular Modeling of the Bacterial Chemotaxis Receptors Tar and Trg

by Megan L. Peach

Chair of Supervisory Committee:

Professor Terry P. Lybrand
Department of Bioengineering

Bacterial chemotaxis receptors signal across the membrane by a conformational change that traverses their periplasmic, transmembrane, and cytoplasmic domains. The mechanism of this conformational change is controversial and is not completely understood. Molecular models of the periplasmic and transmembrane domains of the homodimeric chemotaxis receptors Trg and Tar were constructed, using the coordinates of an unrelated four-helix coiled coil as a template and the X-ray structure of the periplasmic domain of Tar to establish register and positioning. The models were tested and refined using the extensive experimental data for cross-linking propensities between cysteines introduced into adjacent transmembrane helices.

These refined models were used to assess the effects of inter-helical disulfides, using a measure of disulfide potential energy, on two previously proposed mechanisms for ligand-induced conformational changes in the receptor structure: an axial sliding motion of one helix in a subunit, and a rotational motion between the two subunits in the dimer. These proposed mechanisms were tested further, along with the theory that receptor signaling might involve a change in dynamics, using molecular dynamics simulations of the fully

solvated periplasmic and transmembrane domains.

Testing of disulfide effects on receptor motion showed that a sliding motion of transmembrane helix 2 is consistant with experimental data on receptor signaling. However, inter-helical disulfides would not significantly constrain an inter-subunit rotational motion. The molecular dynamics simulations showed that the transmembrane domain has a high degree of dynamic flexibility, and that in the isolated periplasmic domain ligand binding induces an inter-subunit rotation that is of much greater magnitude than was previously concluded from analysis of the periplasmic domain crystal structures.

These results suggest a new model for transmembrane signaling in which an inter-subunit rotational motion is converted into a helical sliding motion via a flexible transmembrane domain and linker region. Thus, both proposed mechanisms occur and have functional roles.

TABLE OF CONTENTS

LIST OF FIGURES

ACKNOWLEDGMENTS

This work would not have been possible without the collaboration of Gerald Hazelbauer and his lab group, especially Bryan Beel and Wing-Cheung Lai. I am grateful to them for sharing their data and for many helpful discussions.

I would also like to thank my advisor, Terry Lybrand, my supervisory committee: Barry Stoddard, Pat Stayton, François Baneyx, and my graduate faculty representative, Arthur Nowell.

Two former members of the Lybrand lab, Randy Henne and André Krammer, did the pioneering studies on molecular dynamics simulations of lipid bilayers; my own work stands on their shoulders.

I am indebted to Viola Vogel for giving me space in her lab during the last 18 months of my work. I am also thankful for the friendship of my office mates: Lynn Amon, David Craig, John Saeger, and Wendy Thomas.

Last but not least, I would like to thank my parents, David and Janet Peach, my brother, Michael Peach, and my friends, especially Kiril Korsunsky, for their unconditional support and encouragement.

Chapter 1

INTRODUCTION

Most bacteria have the ability to swim toward nutrients and away from repellents in their environment. This behavior, called chemotaxis, is mediated by a simple two-component signaling pathway. The best studied chemotaxis system is that of *Escherichia coli*, *Salmonella typhimurium*, and other closely related enteric bacteria [57]. The functions of all the proteins in this system are known, and almost all of them have been studied on a structural level [53]. For this reason, the bacterial chemotaxis system is seen as a paradigm for other two-component histidine kinase/response regulator signaling pathways, which are ubiquitous in bacteria. The bacterial chemotaxis system also has structural and functional similarities to eukaryotic tyrosine kinase signaling systems [138]. Thus, a complete understanding of signaling in the bacterial chemotaxis system is an important step toward understanding the mechanisms of cell signaling in general.

1.1 The mechanism of chemotaxis

A schematic of the chemotaxis pathway and its components is shown in Figure 1.1. Chemical attractants that can be sensed by *E. coli* and *Salmonella* include the amino acids aspartate, glutamate, serine, alanine, and glycine; dipeptides; the sugars maltose, glucose, galactose, and ribose; and the carboxylic acids malate and citrate. Repellents include small aliphatic alcohols and phenol; the hydrophobic amino acids leucine, isoleucine, valine and tryptophan; and the inorganic ions Co(II) and Ni(II) [103]. These ligands interact with the transmembrane receptors either directly (as in the case of aspartate), or indirectly through

periplasmic binding proteins (such as ribose binding protein).

The dimeric transmembrane receptors are non-covalently and stably associated with a coupling protein, CheW, and the dimeric histidine kinase CheA. In the absence of ligand, CheA is autophosphorylated. The aspartate kinase CheY binds temporarily to phosphorylated CheA until it receives the phosphoryl group, then it dissociates and diffuses through the cytoplasm. Ultimately, phosphorylated CheY interacts with a switch (FliM) at the base of the flagellar motor which affects bacterial swimming. CheY is dephosphorylated by the phosphatase CheZ. When ligand binds to the periplasmic domain of a receptor, a conformational change is sent through the receptor to its cytoplasmic domain, which reduces the autophosphorylation of CheA, hence the concentration of phosphorylated CheY [57].

A second branch of the chemotaxis pathway is involved in adapting receptor signaling to the current level of ligand. The methyltransferase CheR binds to the C-terminal end of some of the transmembrane receptors. From this position, it also interacts with neighboring receptors that do not have a binding site. CheR adds methyl groups to a series of glutamate residues in the cytoplasmic domain of the receptor, which modifies its signaling, increases the kinase activity of CheA, and restores the amount of phosphorylated CheY to the basal level. The methyl groups are removed by the methylesterase CheB. CheB is structurally homologous to CheY, and is also phosphorylated by CheA, but unlike CheY it is not dephosphorylated by CheZ and instead undergoes fairly rapid auto-dephosphorylation [57].

The methylation level of the receptor acts as a memory for the bacterium, and allows the bacteria to follow a spatial gradient of attractant. The cell can compare the current level of ligand, as measured by receptor occupancy, to the past level of ligand, as measured by the amount of receptor methylation. If the level of ligand has increased, CheA is inhibited, leading to a decrease in phosphorylated CheY concentration. If the level of ligand has decreased, CheA is stimulated, leading to an increase in phosphorylated CheY [57].

The sum of the signals from all the chemotaxis receptors in the cell ultimately determines the total cellular concentration of phosphorylated CheY, which directs the direction of rotation of the bacterial flagella. The default rotational direction of the flagella is

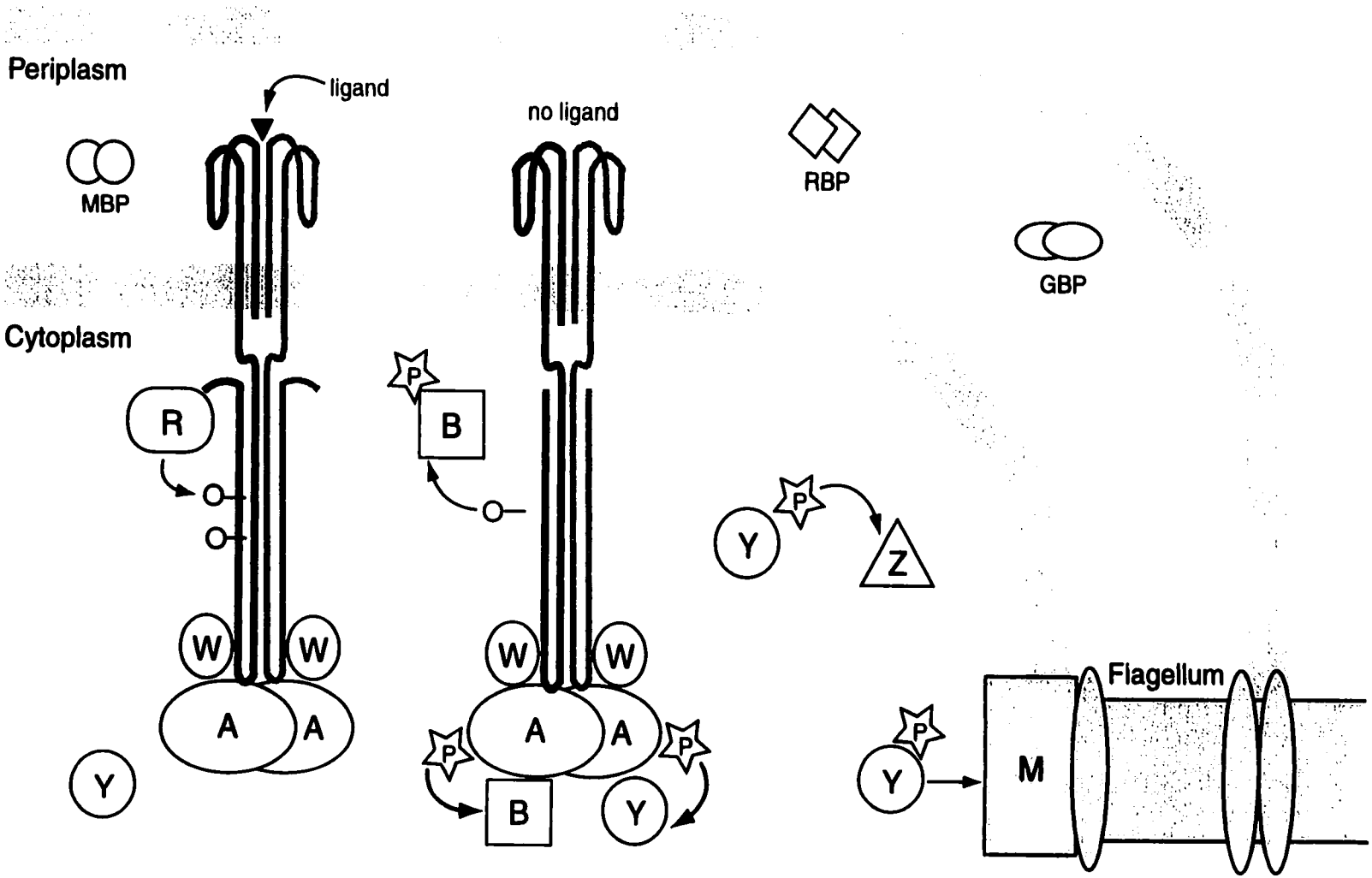

Figure 1.1: Schematic drawing of the bacterial chemotaxis pathway, showing the dimeric chemotaxis receptors as thick black and gray lines. Other chemotaxis proteins are indicated with abbreviations: A, B, R, W, Y, Z = CheA, CheB, CheR, CheW, CheY, and CheZ; P = phosphoryl group; small open circle = methyl group; M = FliM; MBP = maltose binding protein; GBP = glucose/galactose binding protein; RBP = ribose binding protein; small filled triangle = aspartate.

counter-clockwise, so that the left-handed helical filaments exert a pushing force on the cell, causing all the filaments around the bacterium to come together in a single bundle and produce a directed swimming motion, at an approximate speed of 25 mm/second. When phosphorylated CheY interacts with the flagellar motor it changes the direction of rotation to clockwise, so that the filaments are dispersed and the bacterium moves in a chaotic tumbling motion (Figure 1.2A and B). Under conditions where no stimuli are present in the environment, the basal level of phosphorylated CheY in the cell allows the bacterium to move in a random walk, with alternating swimming and tumbling. When a gradient of attractant is present, however, the amount of phosphorylated CheY is decreased and the pattern of swimming and tumbling is biased toward longer swimming intervals to allow an overall movement toward the source of the attractant (Figure 1.2C and D) [103].

The chemotaxis receptors are found *in vivo* in large clusters, perhaps so that ligand binding to one receptor can send a signal through the whole cluster to dramatically increase the cellular response to low concentrations of chemicals [32]. The exact stoichiometry between receptors, CheA, and CheW is not known. It was traditionally thought to be 2:2:2, as shown in Figure 1.1, but new evidence suggests that there may be as many as 14 receptors per CheA dimer [99, 130].

1.2 Other bacterial two-component pathways

Similar signaling pathways control many other functions in bacteria. It has been estimated that 50 or more of these two-component pathways operate simultaneously [2], controlling functions as diverse as sporulation, nitrogen fixation, osmolarity and temperature sensing, antibiotic resistance, cell division, and virulence [57]. Since two-component systems are not found in mammals, since they are essential for the survival of nearly every species of bacteria, and since they are responsible for the expression of virulence factors in pathogenic bacteria, they are good targets for new antibiotic compounds [15, 136].

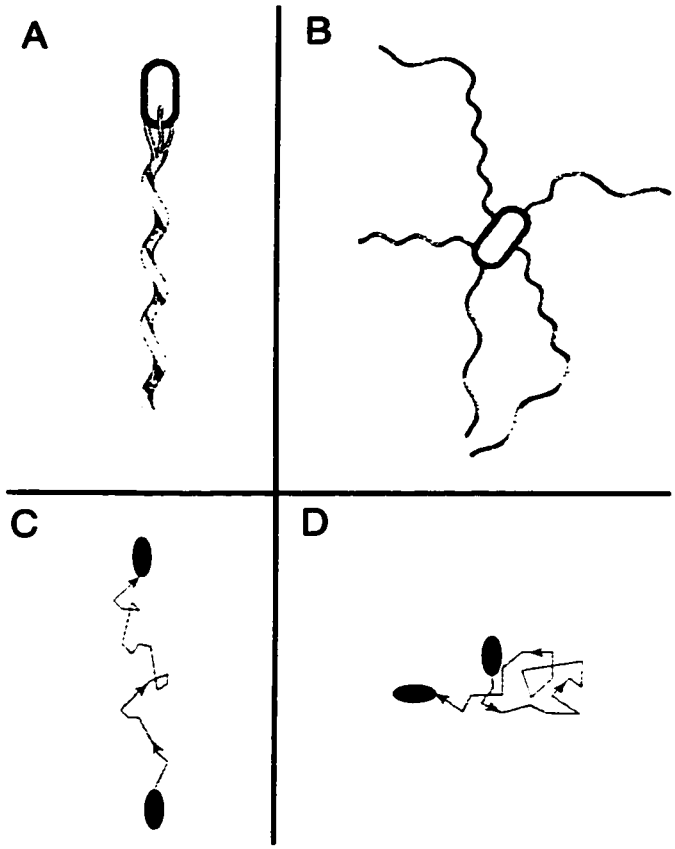

Figure 1.2: Positioning of the bacterial flagella when swimming (A) or tumbling (B). Swimming allows the bacterium to move toward an attractant source (C), whereas during tumbling the bacterium moves in a random walk (D). Modified from [103].

1.3 Similarities to eukaryotic receptors

The membrane receptors in bacterial two-component pathways are structurally similar to the eukaryotic tyrosine kinase receptors, such as the insulin receptor and growth factor receptors. They have a similar overall topology, consisting of an extracellular or periplasmic ligand binding domain, a transmembrane domain with one or two helices, and a cytoplasmic signaling domain [138].

The first step in both sensory pathways is ligand binding to the periplasmic domain of a receptor, followed by a structural change in the receptor that changes the activity of a kinase. The periplasmic domains of these receptors are not structurally homologous, since they sense a wide variety of chemical and environmental stimuli. However, their signaling mechanism seems to be quite similar. Although the eukaryotic tyrosine kinase receptors are known to signal through dimerization, whereas the chemotaxis receptors are always found in dimeric form, there is a common organization of two transmembrane helices per signaling unit. The common mechanisms for signaling may involve reorientation of the transmembrane helices following ligand binding [107]. This reorientation may facilitate (or be facilitated by) dimerization in the growth factor receptors [139].

The idea of a common signaling mechanism for this entire superfamily of membrane receptors is supported by experiments constructing functional chimeric proteins: between chemotaxis receptors in the same family [140, 154], between a chemotaxis receptor and an osmolarity sensing receptor [20], and between a chemotaxis receptor and the insulin receptor [24]. Other evidence for a common signaling mechanism includes sequence analysis studies, which have identified a section of conserved sequence located directly downstream of the membrane spanning helices in the chemotaxis receptors, in the linker region which links the transmembrane domain to the cytoplasmic domain. This 50-residue long sequence is termed the HAMP domain, since it is conserved across Histidine kinases, Adenylyl cyclases, Methyl-accepting proteins (i.e. the chemotaxis receptors) and Phosphatases. These HAMP domains were also found along with other signaling domains in an even wider

variety of proteins, in prokaryotes and eukaryotes alike, and were most often found immediately adjacent to a membrane-spanning region. Thus, these domains may be a conserved structural element that senses a conformational change transmitted across the membrane by membrane-spanning helices, and acts to control the signaling of a kinase [8].

In humans, tyrosine kinase receptor mutations are implicated in a variety of diseases including cancer susceptibility, dwarfism, and some forms of diabetes. Some of these mutations affect protein folding or ligand binding but others seem to cause abnormal receptor dimerization and signaling [123]. Studies are underway to develop drugs that inhibit signaling in the hepatocyte growth factor receptor, which is encoded by a protooncogene, and which is overexpressed in many types of cancer [101].

Thus, a complete understanding of the mechanism of transmembrane signaling by the chemotaxis receptors will, due to their similarities with a wide variety of other receptors, be useful for the development not only of new antibiotics but also of potential treatments for a wide variety of inherited diseases.

1.4 Chemotaxis receptor structure

This work focuses on a family of chemotaxis receptors involved in sugar and amino acid sensing, and on the conformational change that occurs in these receptors upon ligand binding. These homodimeric transmembrane receptors have three domains: a periplasmic domain that binds ligand, a cytoplasmic domain that binds and regulates the associated kinase CheA, and a transmembrane domain that couples the other two domains structurally and functionally. The cytoplasmic domains are all highly homologous, since they share the same CheA and CheW interactions and regulation. The periplasmic domains are more varied in sequence, according to the ligand that is sensed by the receptor. They are homologous enough, however, that they are thought to have the same tertiary structure.

The two chemotaxis receptors that have been studied the most thoroughly are the aspartate receptor of *Salmonella*, Tar_S, and the ribose and galactose receptor of *E. coli*, Trg.

X-ray crystal structures have been determined for the periplasmic domain of Tar_S [106, 162] along with that of the the *E. coli* aspartate receptor Tar_E [31]. The structure of most of the cytoplasmic domain of the *E. coli* serine receptor, Tsr, has also been determined [85].

In addition to these crystal structures, the transmembrane domains of Tar (both Tar_S and Tar_E) and Trg, as well as the cytoplasmic domain of Tar_S, have been extensively analyzed using disulfide cross-linking. In these studies, site-directed mutagenesis is used to introduce two cysteine residues at different positions in the protein, then the ability of the cysteines to form a disulfide bond in the presence of an oxidizing agent is assessed. These disulfide scanning studies have allowed the secondary and tertiary structure of the transmembrane domain to be characterized at a medium resolution [116, 93, 80].

The combination of the crystal structures and the disulfide scanning studies gives a comprehensive picture of the overall receptor structure as an extended helical bundle [85] (Figure 1.3). The periplasmic domain contains two four-helix bundles, one from each subunit. The two central helices from each bundle, $\alpha 1$ and $\alpha 4$, extend through the membrane where they become TM1 and TM2, respectively. The transmembrane domain consists of four transmembrane helices: TM1 and TM2 from one monomer and TM1′ and TM2′ from the other. TM2 and TM2′ continue into the cytoplasmic domain through the linker region and become CD1 and CD1′. The cytoplasmic domain is a long helical coiled-coil of two helical hairpins, one from each subunit.

Engineered disulfides have also been used to gather information about the conformational change that occurs during receptor signaling [128, 96, 43, 41, 79]. However, the results of these studies are somewhat different from the conformational change seen in the crystal structures of the ligand-bound (holo) vs. the ligand-free (apo) periplasmic domains [106, 162, 44]. Thus, there is still some controversy over the exact nature of this conformational change, and two different mechanisms have been proposed: a rotation between the two subunits in the dimer [87], or a translation of the $\alpha 4$/TM2 helix relative to the other helices within a subunit [42, 58]. A third possibility is that ligand binding might affect the dynamics of the receptor rather than inducing an overall change in conformation [86].

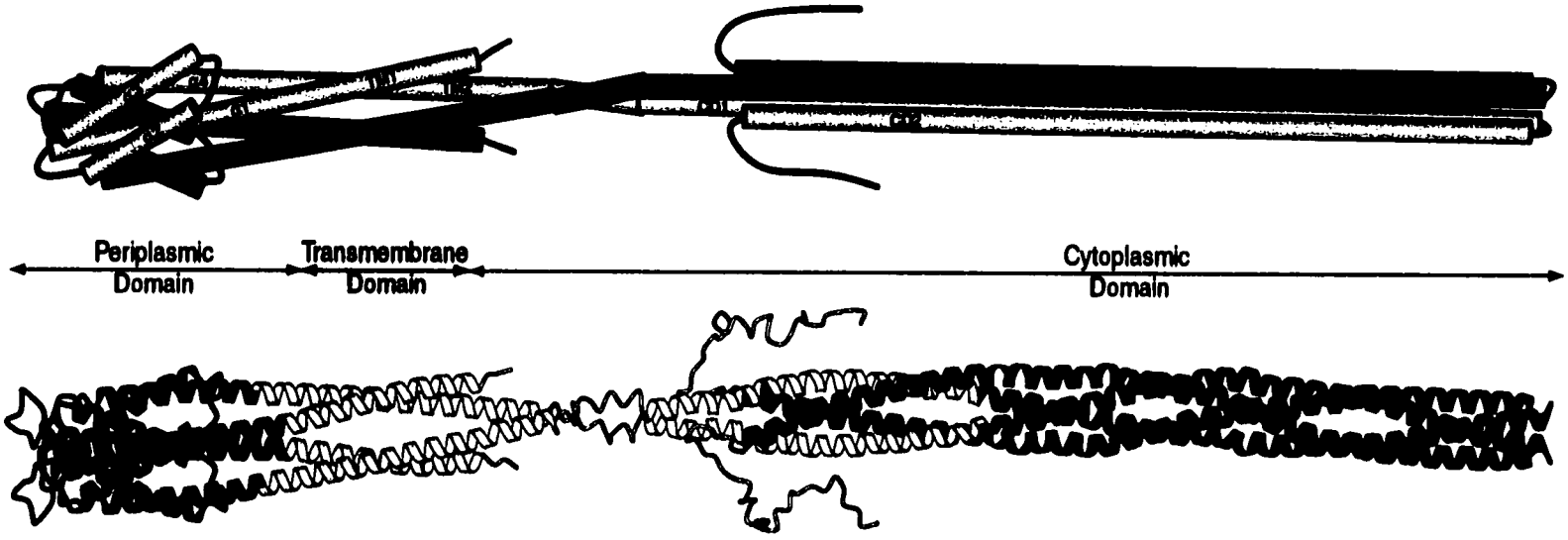

Figure 1.3: Model of chemotaxis receptor structure. A ribbon diagram (left) and a schematic (right) of a composite model of a homodimeric bacterial chemotaxis receptor. In the ribbon diagram, the portions of the model based on X-ray crystallography of receptor fragments are colored red. Regions of the receptor which are known to be helical are drawn as a ribbon, and non-helical regions are shown as coil. In the schematic diagram, the helices are labeled, the two subunits are shown in yellow and blue, and helix super-coiling is omitted for clarity. Each ~60 kDa subunit begins on the cytoplasmic side of the membrane, crosses the membrane as transmembrane helix 1 (TM1), becomes helix α1 of the periplasmic domain, turns to make a four-helix bundle, extends to the membrane as helix α4, crosses the membrane as TM2, extends into the cytoplasm, and makes a membrane-distal turn to create the extended helical hairpin of cytoplasmic helices 1 and 2 (CD1 and CD2). The ligand-binding site is at the top end of the periplasmic domain and the kinase-interaction site is at the bottom end of the cytoplasmic domain. This figure was made using Molscript [89].

1.5 Modeling the chemotaxis receptors

The structure and signaling of the chemotaxis receptors are highly relevant to membrane proteins and transmembrane signaling in general, yet neither is completely understood due to the technical difficulties in obtaining structural information on membrane proteins. In the absence of an atomic-resolution structure for the intact receptor, a molecular model is an attractive alternative. In spite of the large amount of experimental data available on the structure of the chemotaxis receptors, to date no large-scale molecular modeling or simulation studies have been performed on them. In this work, we constructed detailed molecular models of the periplasmic and transmembrane domains of Tar_S (hereinafter referred to simply as Tar) and Trg (Chapter 2). These models provide a platform for the integration of all the available experimental data, and allowed us to examine the different proposed signaling mechanisms in terms of their effects on the receptor structure (Chapter 3). We have also performed molecular dynamics simulations of the periplasmic domain of Tar (Chapter 4) as well as the transmembrane domain of Trg (Chapter 5), which allowed us to examine their dynamic behavior in a fully solvated environment.

Chapter 2

MOLECULAR MODEL BUILDING

2.1 Homology modeling

The first step in our model building was to construct a homology model for the periplasmic domain of Trg, whose structure is unknown, using the available crystal structures of the periplasmic domain of Tar. Homology modeling is based on the general principle that two evolutionarily related proteins with similar sequences will also have similar three-dimensional structures. Thus, a model for a protein of unknown structure can be constructed using the backbone of a homologous protein whose structure is known as a template [13].

2.1.1 Sequence alignment

The first and most crucial step in building a homology model is to align the sequence of the target protein with the sequence of the template protein, because if the sequence alignment is wrong, the model will definitely be wrong as well [108]. If the target protein is not very homologous to the template, i.e. less than about 40-50% sequence identity, computer-generated sequence alignments can often contain errors. Tar and Trg are closely related in sequence in their cytoplasmic domains, but exhibit few residue matches in the periplasmic and transmembrane domains. To optimize the alignment of minimally related sequences such as these, it is useful to include the sequences of related proteins from the same family in the alignment, which helps to characterize patterns of conserved and variable residues across the family [67].

The periplasmic domain of Trg does not have very high sequence homology to any of

the other chemotaxis receptors, leading early researchers to hypothesize that it might have arisen via gene-splicing of an unrelated ribose/galactose transport protein to the cytoplasmic signaling domain common to all the receptors [29]. Nevertheless, in a PSI-BLAST search [7] with the periplasmic and transmembrane domains of Trg (residues 14-229), using the non-redundant database at NCBI and the BLOSUM-62 matrix with the default gap penalty of 11 [75], other chemotaxis receptors are detected. The first PSI-BLAST iteration finds only Trg sequences with strict significance ($e<0.001$), but the *Salmonella* aspartate receptor (Tar_S) is found with an e-value of 0.002, along with the *Salmonella* citrate receptor (Tcp) with an e-value of 0.074. These are the two highest-scoring matches, other than Trg itself. Including these three sequences in the next PSI-BLAST iteration produces additional significant alignments: the aspartate and serine receptors from *E. coli* (Tar_E and Tsr) and *Enterobacter aerogenes* (Tas and Tse). Including all of these sequences in a third iteration finds the *E. coli* dipeptide receptor (Tap). After this, the search converges and no new sequences are added in subsequent iterations. This suggests that the periplasmic and transmembrane domains of these eight receptors are indeed homologous with similar structures.

Another way to improve the accuracy of an alignment between sequences with low homology is to include structural information along with the sequences to be aligned [67]. Since the structures of the periplasmic domains of Tar_S and Tar_E are known, these two sequences were aligned first, using the program AMPS (Alignment of Multiple Protein Sequences) [18]. AMPS first performs a pairwise alignment of each sequence with every other sequence, using the Needleman and Wunsch algorithm [110], and the PAM-250 matrix with the default gap penalty of 8. Then the sequences are shuffled and re-compared 100 times to give a significance score to the alignment, as well as a percentage identity for each sequence with every other sequence. The alignment between Tar_S and Tar_E is simple, since these sequences are very similar and can be aligned without any gaps. The output file of this alignment was edited to indicate the locations of the loops in the periplasmic domain. The remaining six sequences (Trg, Tcp, Tsr, Tas, Tse, and Tap) were then aligned to this

first alignment, increasing the gap penalty 100-fold in the helical regions of the periplasmic and transmembrane domains. This had the effect of confining all the gaps in the alignment to loop regions, where they are evolutionarily more likely to occur [17].

This computer-generated alignment was examined closely by hand, and the sequence of Trg was adjusted slightly to improve the alignment near the end of loop 1 and the beginning of helix α2. The final version of the alignment is shown in Figure 2.1. Helical periodicity can be observed in the positions of conserved residues in the periplasmic domain. The alignment is also consistent with additional structural features. In the transmembrane helices there is alignment of the hydrophobic cores, charged residues at the membrane boundaries, and a band of aromatic residues at the periplasmic end. In the periplasmic domain, residues identified as important for interaction with ligands [160, 65] are at identical or adjacent positions.

2.1.2 Backbone and sidechain construction

The next step in the modeling process was to decide which crystal structure of Tar_S provided the best template for the periplasmic domain of the receptor. The two sets of high-resolution structures in the Protein Data Bank (PDB) are 1LIH/2LIG, the apo and holo forms of a mutant receptor with a cysteine at residue 36 that forms a disulfide bond across the subunit interface of the dimer, and 1VLS/1VLT, the wild-type apo and holo structures.

The main difference between the two apo structures 1VLS and 1LIH is a 12.6° rotation of the subunits relative to one another [161]. This rotation affects the inter-subunit interface, so that in the wild-type structure the membrane-proximal ends of the helices α1 and α1′ diverge, with residues 36 and 36′ facing away from one another, at a Cα–Cα distance of 20.6 Å. It is unclear whether this is due to differences in crystal packing, or because of the absence of the transmembrane domains. However, studies have shown that a cross-link between 36-36′ does not affect ligand binding or receptor signaling [59, 128, 43], which implies that these residues should be close to one another in the intact receptor. For this reason, we chose the cross-linked crystal structure 1LIH as a template for the periplasmic

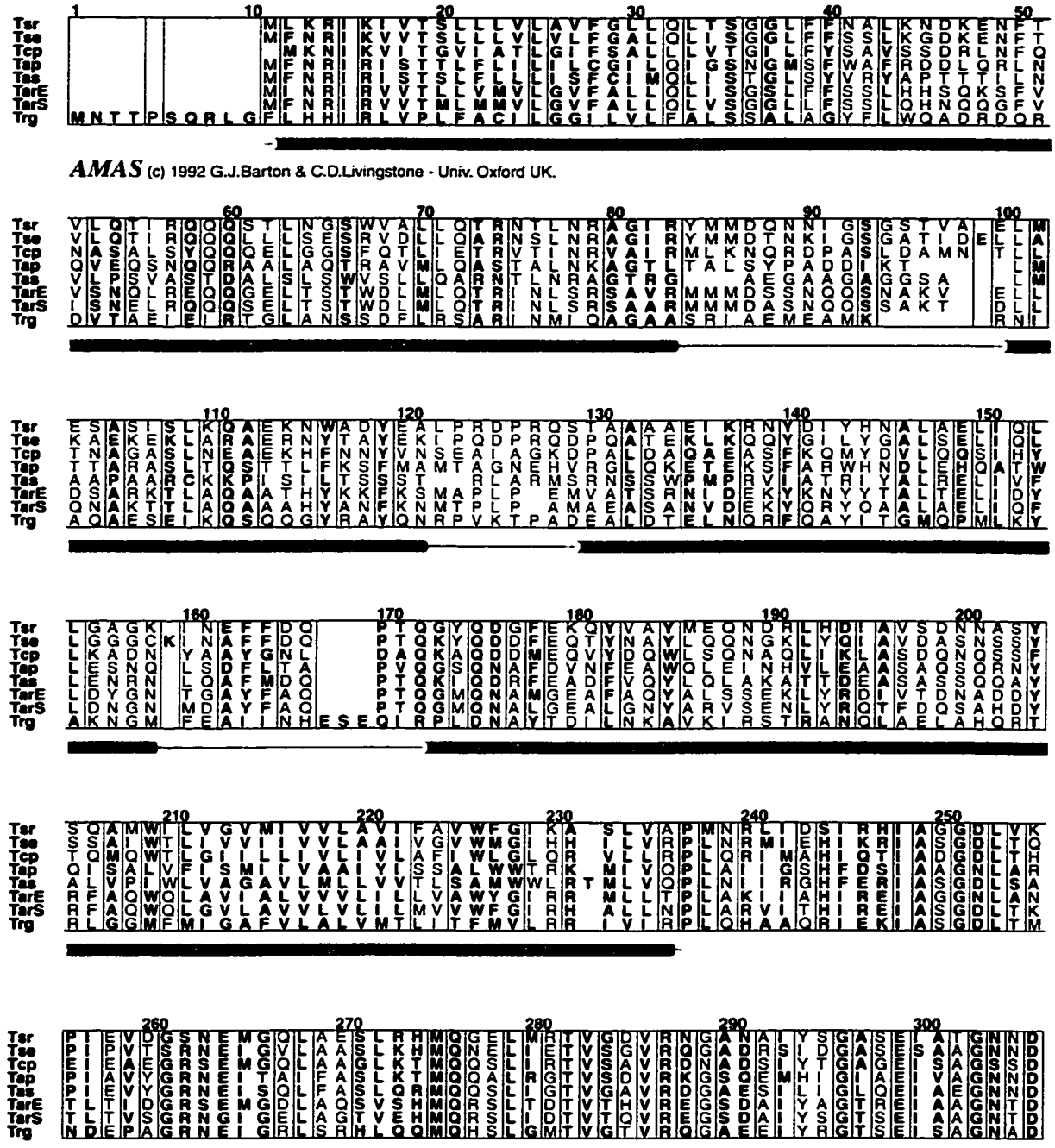

Figure 2.1: Multiple sequence alignment of eight homologous chemotaxis receptors. The positions of conserved residues were calculated using AMAS (Analysis of Multiply Aligned Sequences) [100], and are shown in bold type. The positions of secondary structural elements in the periplasmic and transmembrane domains are indicated by the cartoon helices below the sequences. The alignment was formatted using Alscript [16].

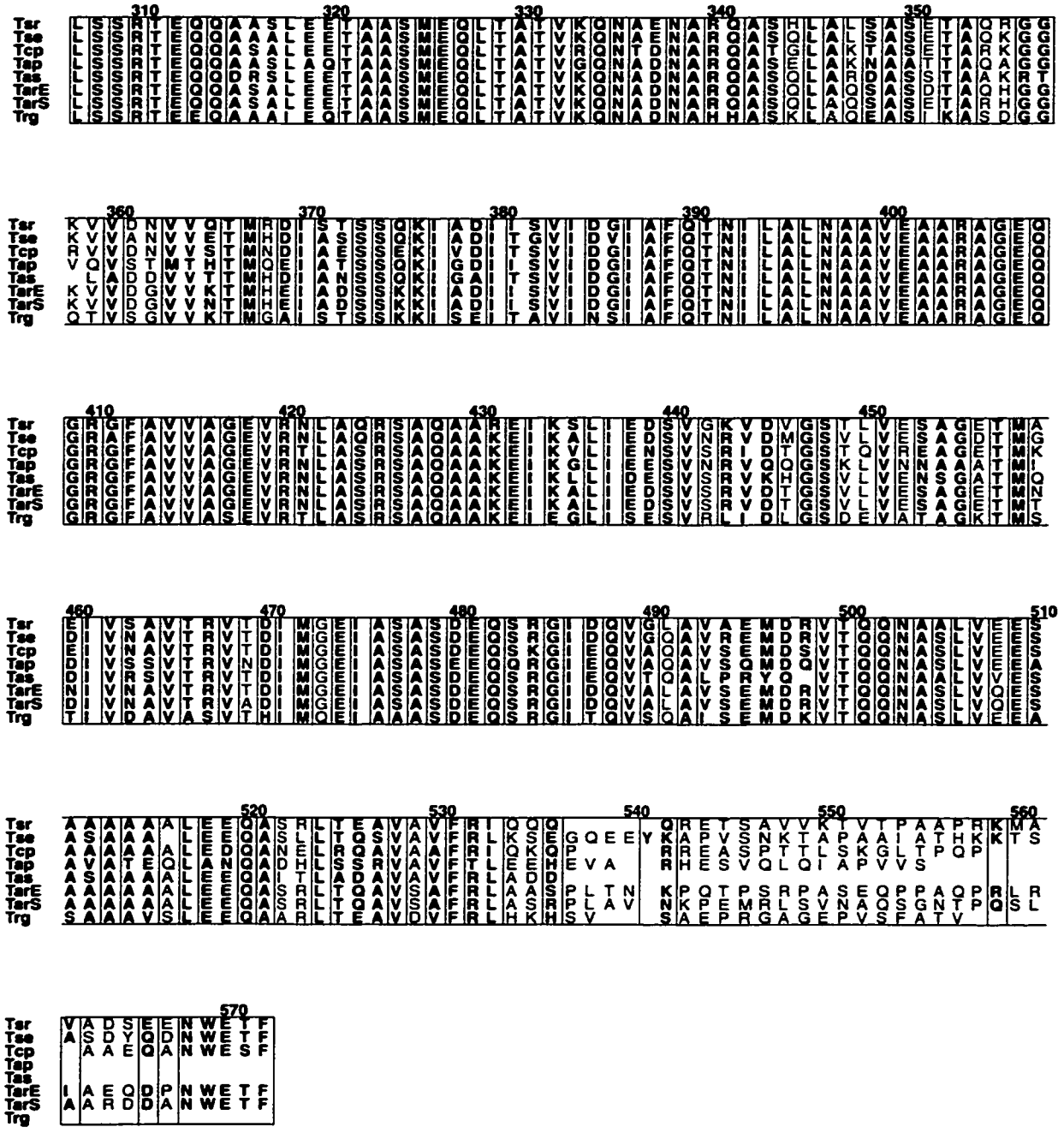

Figure 2.1: *(continued).* Multiple sequence alignment of eight homologous chemotaxis receptors.

domain.

We used a four-helix coiled-coil structure of a mutant leucine zipper (1GCL in the PDB) [72] to extend helices $\alpha 1$, $\alpha 4$, $\alpha 1'$, and $\alpha 4'$ of the cross-linked crystal structure 1LIH, creating a backbone structure for the periplasmic plus transmembrane domain of the receptor. This strategy for modeling the transmembrane domain was based on the approach of Scott and Stoddard [128], who used the coordinates of a natural two-helix leucine zipper as the template for a model of TM1 and TM1′.

The helices in the mutant leucine zipper structure were only 30 residues long, and so they were extended by stacking the helices along their axes, preserving the pattern of hydrophobic residues and thus the coiling structure. We aligned each extended helical backbone individually to the top of a corresponding helix in the periplasmic domain. Since the ends of these helices are somewhat disordered in the crystal structure, we merged the leucine zipper helices with the periplasmic helices approximately midway along their length, at residues 51 and 171.

Both receptors have a small N-terminal cytoplasmic tail (residues 1-4 in Tar and 1-14 in Trg) that is not necessary for transmembrane signaling or chemotaxis [39], so the TM1 helices were terminated in the model at residue 4 for Tar and residue 14 for Trg. To neutralize the charged ends of the receptor backbone, we capped the helix ends with acetyl (Ace) and methyl amide (Nme) terminal residues.

We placed the sidechains for the correct sequence of both Tar and Trg onto separate backbone templates using the program SCWRL (Side-Chains With a Rotamer Library), which uses a backbone-dependent rotamer library [54] to position sidechains in the most likely rotamer based on the conformation of the backbone at that residue, followed by a combinatorial search to remove steric conflicts [30]. For the Tar structure we retained the crystal structure placement of residues 51 through 171. Since all the gaps in the sequence alignment of Trg and Tar_S occur in the loops, the sequences for both proteins can be fit on the same helical backbone structure. For the Trg structure we deleted the periplasmic loops and replaced all the helical residues. None of the three loops have the same number of

residues in Trg and Tar, and are probably quite different in conformation, so we generated plausible structures for their structure in Trg by adding the loop residues to the ends of the helices in an extended all-trans configuration, with half of the loop on each helix. We then ran limited molecular dynamics at low temperature using AMBER [38] with only the residues in the loops free to move, and with a distance restraint between the two loop ends which was gradually reduced to pull the loop closed. This was followed by a limited minimization of the loop structures and another limited molecular dynamics run with only the loop residues free to move, in order to relax all the bond lengths in the loops and arrive at a final structure.

2.1.3 Model refinement

We corrected large steric clashes and any asymmetry between corresponding sidechains in the two subunits by manually rotating sidechain dihedral angles. Next, we performed a limited amount of energy minimization (200 steps) *in vacuo* using AMBER [38] to relax the structures slightly and remove any small remaining steric overlaps.

The overall quality of the structures was assessed using the programs QPack [68], which evaluates the sidechain packing density and residue-residue contacts, and WhatIf [152], which checks for buried unsatisfied hydrogen bond donors and acceptors, and reasonable sidechain and backbone torsion angles.

2.2 Comparison with experimental data

In these initial versions of our models of Trg and Tar, the position, orientation and register of the transmembrane helices were determined by the X-ray structures of the Tar_S periplasmic domain and the coiled coil template. To refine and validate these models, it was important to determine the degree to which they were consistent with experimental characterization of the transmembrane domains of the two receptors. It was also important to test our homology model for the periplasmic domain of Trg.

2.2.1 Periplasmic domain of Trg

To verify that our homology model of the periplasmic domain of Trg was reasonably accurate, we suggested a series of residues that could be tested for their cross-linking ability when mutated to cysteine. These cross-linking tests were performed by Wing-Cheung Lai, in the research group of Dr. G. L. Hazelbauer at the University of Missouri–Columbia.

We had assumed that the choice of Tar_S as a template for the backbone of the periplasmic domain of Trg was reasonable, since the outcome of the PSI-BLAST search suggested that in spite of their marginal sequence identity the periplasmic and transmembrane domains of Trg and Tar_S are structurally similar. The question which we wanted the cross-linking experiments to answer is whether the sequence of Trg is correctly "threaded" onto this backbone structure.

The periplasmic domain mutants we used for the cross-linking tests were:

S66C and G109C S66C and Q108C	linking helix α1 and helix α2
I96C and K149C I96C and N150C	linking helix α2 and helix α3
M77C and L145C M77C and K146C	linking helix α1 and helix α3
L130C and A178C N131C and A178C	linking helix α3 and helix α4

As illustrated in Figure 2.2, each pair tests the relative rotational positioning of two helices. We predicted that the first pair in each set should cross-link, since those residues face each other across the helical interface. In the second pair in each set, one of the residues is facing away from the interface, so little or no cross-linking should occur.

Three of these pairs, 66-109, 77-145, and 96-149, show extensive, spontaneous disulfide cross-linking even without the addition of oxidizing agents. For the corresponding 66-108, 96-150, and 77-146 pairs, some inter-chain cross-linking is observed experimentally, but little to no intra-chain cross-linking. These constructs are all very sensitive to proteolysis,

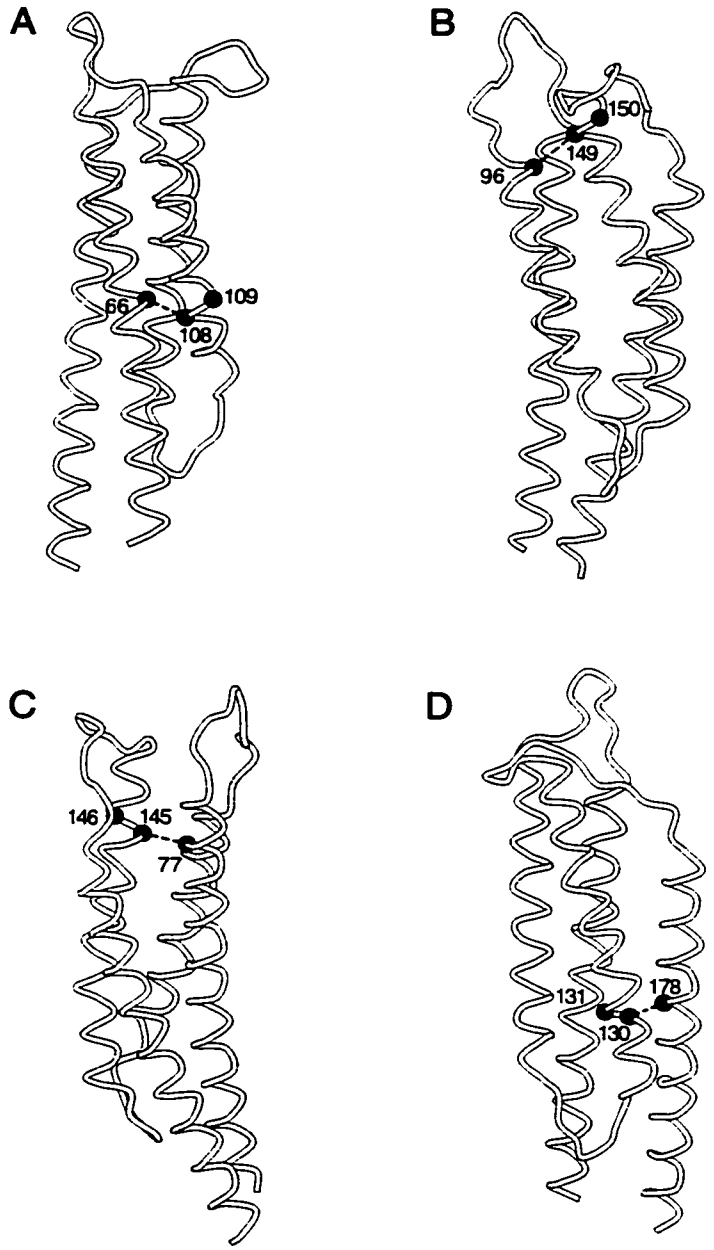

Figure 2.2: Positions of experimental cross-links constructed to test the homology model of the periplasmic domain of Trg. The α-carbon atoms in the mutated residues are shown as dark gray spheres. (A) Cross-links between α1 and α2; (B) Cross-links between α2 and α3; (C) Cross-links between α1 and α3; (D) Cross-links between α3 and α4. Residue pairs which are close to one another in the model and predicted to cross-link are shown connected with dashed lines.

indicating that they may not be stably folded. This suggests that the pairs which we had predicted should be close to one another are indeed in an orientation in the folded protein that is close enough that oxidation by ambient oxygen can occur. Similarly, the pairs that we predicted to be distant from one another are far enough apart in the folded structure that they do not cross-link readily, and any cross-linking that does occur traps the protein in an unstable conformation.

Both pairs linking helix α3 with α4 (130-178 and 131-178) do cross-link partially with ambient oxygen. However, after an oxidizing agent is added, the 130-178 pair cross-links completely, whereas the 131-178 pair does not. In both constructs, significant inter-chain cross-linking is also observed. This may be a indication of flexibility or mobility in the α4/TM2 helix, an idea which is supported by a variety of other data.

Further tests to examine the signaling and chemotaxis abilities of all the mutants are underway [90], but these preliminary results suggest that our model structure for the periplasmic domain of Trg is reasonable.

2.2.2 *Subunit interface in the transmembrane domain*

The most extensive experimental probing of transmembrane structure in the chemotaxis receptors has been done by determining the propensity for oxidative cross-linking between cysteine pairs in homologous positions in the receptor. (Cysteines introduced at a single position in the receptor sequence are present at two homologously placed positions in the two subunits of the receptor homodimer.) These determinations of cross-linking propensity have been made quantitatively for every position in the two transmembrane segments of Trg [93] and qualitatively for almost every position in Tar_E [116], which has 70% residue identity to Tar_S in the periplasmic and transmembrane domains.

Since cross-linking propensity is a function of the distance between reactive sulfhydryls [37], we compared inter-residue Cα–Cα distances in our models to the experimentally determined cross-linking propensities of introduced cysteines at each position along TM1 and TM2. Figure 2.3 shows both the modeled distance between the α-carbons of homologously

placed residues and the experimentally determined cross-linking propensity as a function of position along the TM1 and TM2 sequences. To relate the patterns to the organization of the transmembrane domain, in each graph the sequences are displayed with the periplasmic end on the left, which results in the TM1 sequence reading from higher to lower residue number. The distance between α-carbons is plotted on an inverted scale so that upward peaks correspond to shorter distances and thus greater probabilities of cross-linking.

Our models correspond to experimental data in terms of both general patterns and specific features. Experimentally, there was more extensive cross-linking across the TM1–TM1′ interface than across the TM2–TM2′ interface for both Trg and Tar. In the models of both Trg and Tar, the TM1–TM1′ pair were significantly closer than the TM2–TM2′ pair. Experimentally, local maxima of cross-linking identified the rotational orientation of each helix relative to its homologous partner in the other subunit [95]. This was the same orientation identified by residue pairs separated by the shortest distances in the models for both chemoreceptors. For Trg, in which cross-linking propensities were quantified [93], the distinct local maxima corresponded well to positions that in the model were in closest proximity across the subunit interface. Not all positions in the modeled interface exhibited extensive cross-linking, probably because the chemical oxidation is influenced by other factors in addition to the distance between the reacting residues. The cysteine residues must be accessible to oxidizing agents, the bond between the sidechain atoms must be able to rotate into a favorable conformation, and the redox and electrostatic potentials of the local environment must be within certain limits [48].

Since the four helices of the transmembrane domain were aligned individually with helices α1, α4, α1′, and α4′, and the periplasmic domain does not have a perfect coiled-coil structure [127], the resulting model did not maintain its coiled-coil organization over the entire length of the transmembrane domain. TM1 and TM2 remained in proximity within a subunit, but the distances separating TM1 and TM1′ or TM2 and TM2′ increased from the periplasmic side to the cytoplasmic side of the domain. In essence, the coiled-coil became partially unwound. This modeled unwinding agrees with the experimental data on intact

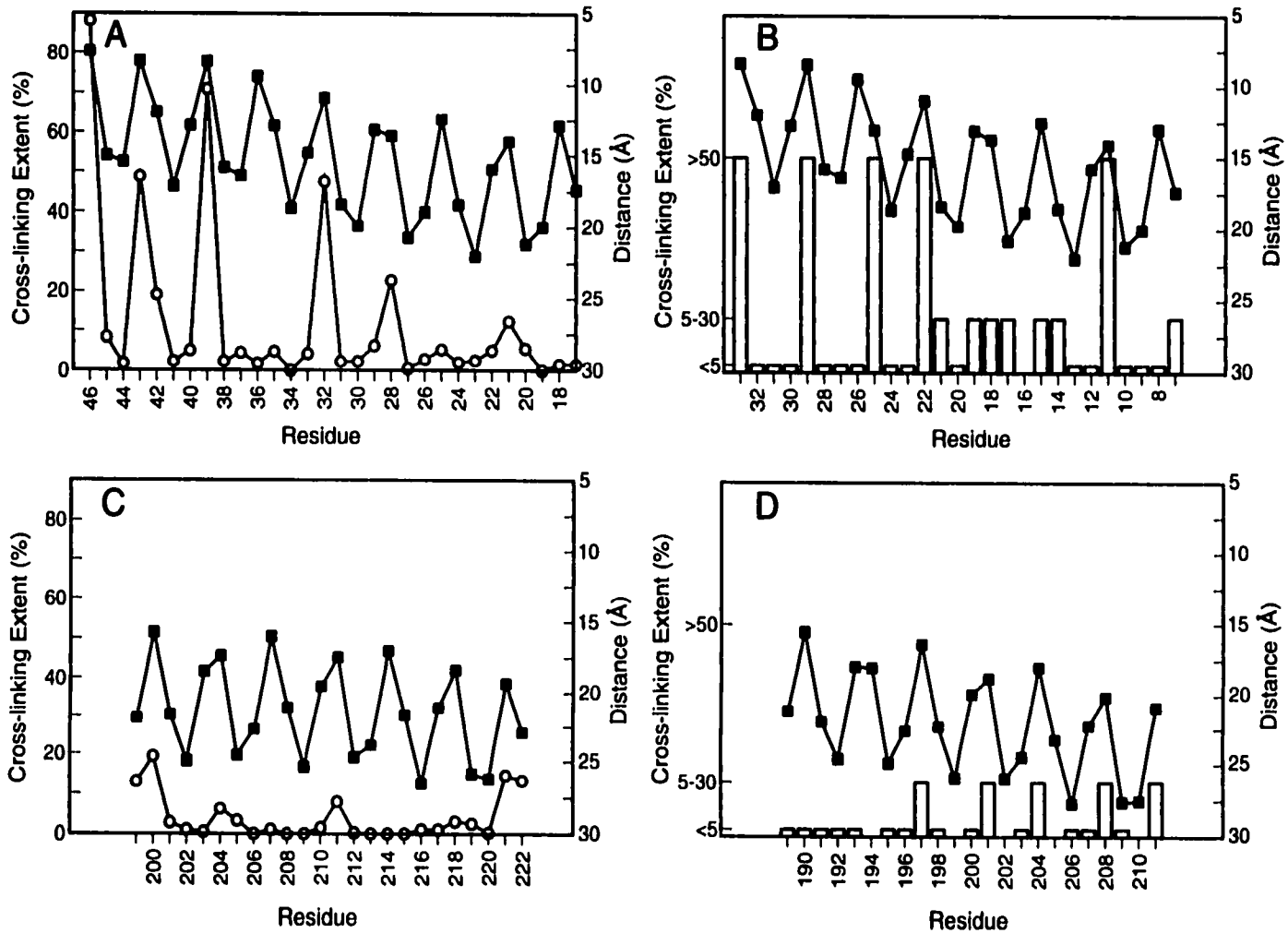

Figure 2.3: Patterns of cross-linking extent and α-carbon distance for homologous cysteines introduced into TM1 of Trg (A) and Tar_E (B), and into TM2 of Trg (C) and Tar_E (D). Cα–Cα′ distances in Å (black squares) are plotted with an inverted scale on the right-hand axes. Values for the extent of oxidative cross-linking (left-hand axes) for Trg (gray circles) are averages of *in vivo* and *in vitro* data with two different oxidizing reagents [80]. Qualitative extents of cross-linking in Tar (gray bars) are from [116].

receptors, which also indicates that the two subunits splay apart as they near the cytoplasm. In the quantitative determinations of cross-linking propensities along the TM1 and TM1′ interface of intact Trg, the maxima in the periodic relationship between cross-linking and residue position decrease from periplasm to cytoplasm (Figure 2.3A), suggesting a gradual separation of the two subunits across the width of the membrane. For cross-linking across the TM1–TM1′ interface of Tar, which was assessed only qualitatively (Figure 2.3B), there is also a general pattern of decreased propensity from periplasm to cytoplasm, suggesting that subunit splaying also occurs in this receptor. Specific evidence for such splaying in Tar is provided by the pattern of effects of TM1–TM1′ cross-links on receptor function, in which cross-links near the periplasm/membrane boundary allow function but those near the membrane/cytoplasm boundary do not [43].

2.2.3 Helix positioning within a subunit

In contrast to the good agreement between our models and experimental data for the TM1–TM1′ and TM2–TM2′ interfaces, there was a disparity for the TM1–TM2 interface between the modeled positions of key residues and the proximities suggested by cross-linking data. Screening of random and engineered combinations of TM1 and TM2 cysteines in both Trg and Tar has identified certain pairs that cross-link readily [116, 93, 21]. These cysteines are thus likely to be among the most closely positioned across the TM1–TM2 interface. The left-hand portions of Figures 2.4 and 2.5 show the positions of these TM1–TM2 cysteine pairs in the initial models of Trg and Tar, respectively. In contrast to the TM1–TM1′ cysteine pairs, none of the extensively cross-linked TM1–TM2 pairs in Trg and only two of six such pairs in Tar were directly opposite each other across the helical interface. All the rest were significantly displaced in the same direction and to roughly the same extent. For each displaced pair the TM2 residue was shifted toward the cytoplasm relative to its optimal position opposite the corresponding TM1 residue.

These displacements were not unique to models based on the 1LIH coordinates, which are for the periplasmic domain fragment of Tar_S containing the disulfide cross-link between

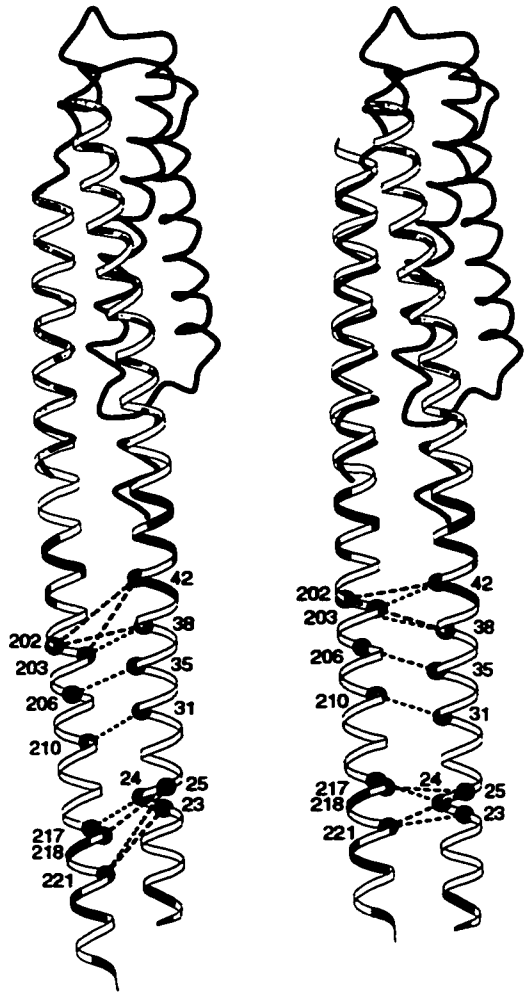

Figure 2.4: Positions of cysteine pairs with high cross-linking propensity between TM1 and TM2 of Trg. Initial (left) and revised (right) positions of TM2 relative to TM1 are diagrammed with cysteine pairs exhibiting high cross-linking propensities [93, 21] marked with red spheres and joined by dashed lines. The shaded coil shows the crystal structure backbone of one monomer of the periplasmic domain (1LIH; [106]) that was used to align the helices of the extended coiled-coil template (ribbon). In the right-hand diagram, the sliding of α4/TM2 toward the periplasm is emphasized by shifting only the long helix, not the template representing the original position of helix α4. The hydrophobic core of the transmembrane domain is shown in yellow, aromatic and amidated residues at the edges of the hydrophobic core are colored green, and charged residues (including histidines) are colored blue. This figure was made using MolScript [89].

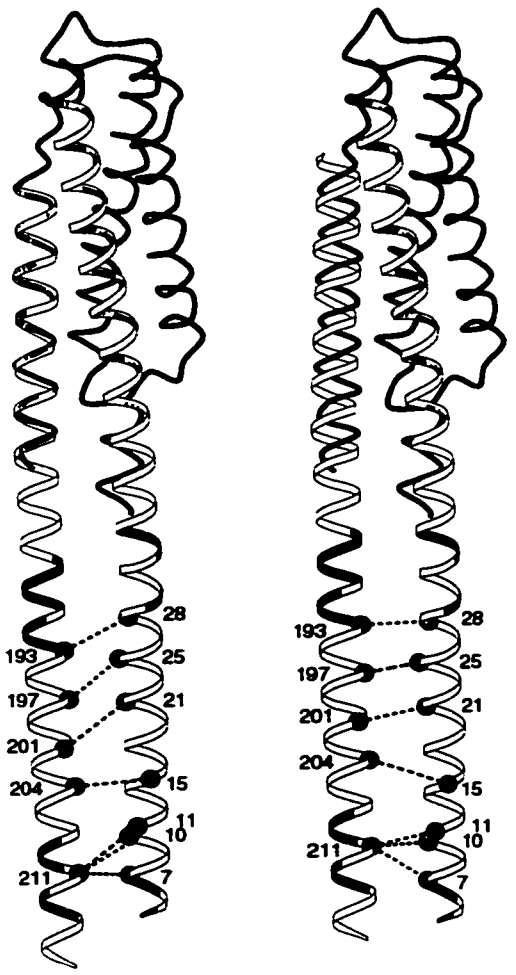

Figure 2.5: Positions of cysteine pairs with high propensity for cross-linking between TM1 and TM2 of Tar. Initial (left) and revised (right) positions of TM2 relative to TM1 are diagrammed with cysteine pairs exhibiting high cross-linking propensities [116] marked with red spheres and joined by dashed lines. Details and symbols are as in Figure 2.4. This figure was made using MolScript [89].

α1 and α1′. Very similar displacements were observed for models based on the coordinates of the Tar_S periplasmic domain lacking the engineering disulfide (1VLS) or on the Tar_E periplasmic domain (2ASR), which is also devoid of cross-links. The systematic nature of this disparity argued that the two models should be adjusted by sliding α4/TM2 along its long axis toward the periplasm. The shift that provided the best positioning of the cysteine pairs with high cross-linking propensities was 3.5 Å for Tar and 6.4 Å for Trg. These refined models are diagrammed in the right-hand parts of Figures 2.4 and 2.5.

As a check on whether this rather large displacement of α4/TM2 was likely to severely perturb the interactions of the transmembrane domain with the membrane, and to determine why the shift for Trg was larger than that for Tar, we examined the sequence/structure relationships in the transmembrane domains of our models. Transmembrane helices have been shown to have a general structure which consists of a central core of hydrophobic residues, flanked on either side by an "aromatic belt" of Phe, Trp, and Tyr along with the amidated residues Asn and Gln, and then a region of charged residues which interact with the charged membrane headgroups [121, 153]. In Figures 2.4 and 2.5, the transmembrane domain structure for the original models with α4/TM2 aligned to the crystal structure backbone can be compared to our refined models of Tar and Trg with α4/TM2 shifted toward the periplasm. The hydrophobic core of the transmembrane domain, aromatic and amidated residues at the edges of the hydrophobic core, and charged residues are shown in different colors along the helical ribbon. In Tar, shifting α4/TM2 up gives a better alignment of the charged and aromatic residues on the periplasmic side of the membrane. In Trg, moving α4/TM2 up even farther than in Tar gives a better alignment on both sides of the membrane, because Trg has an extra arginine residue on the cytoplasmic side of TM2, and because TM1 in Trg is (at least based on the sequence) about 3 residues or one helix turn longer than in Tar. However, the un-shifted position of α4/TM2 still gives a fairly reasonable alignment for the two transmembrane segments. This suggests that the sliding of α4/TM2 does not significantly disrupt its interactions with the membrane, and so would not have a large energy barrier. Thus, differences in the relative positioning of the transmembrane helices between Trg and

Tar are reflected in sequence differences. The improved alignment of features independent of cross-linking data lends substantial support to the validity of the direction and magnitude of the shifts we made in the position of α4/TM2.

2.3 Conclusions

In testing our two first-stage models of Trg and Tar with data on propensities for cross-linking between cysteines introduced into transmembrane segments, we found that many aspects of the models corresponded with experimental observations. There was one striking disparity, the register of TM2 relative to its partner TM1. This disparity could be corrected, however, by a simple change in the first-stage models, a sliding of TM2 toward the periplasm several Ångströms along its long axis.

The implication of this correction is that the position of α4/TM2 captured in the crystal structures of the periplasmic domain is shifted toward the cytoplasm relative to the average conformation of intact, membrane-embedded receptor, the state probed in cross-linking studies. This is plausible because a large body of experimental data (discussed in Chapter 3) indicates that axial sliding of a mobile α4/TM2 relative to a static α1/TM1 occurs during ligand-induced signaling in the chemotaxis receptors [58]. This sliding must have a low energy barrier since it can be induced by single residue substitutions near the ligand-binding site [21], and since the distance between charged residues bracketing the transmembrane domain allows a range of TM1–TM2 registers (Figures 2.4 and 2.5). With a low barrier to α4/TM2 sliding, the helical register could be altered as a consequence of truncating the receptor to create the periplasmic domain or by crystal packing forces or other conditions of crystallization.

Chapter 3

THE CONFORMATIONAL CHANGE OF RECEPTOR SIGNALING

One of the remaining questions about chemotaxis receptor structure and function is the nature of the conformational change that sends a signal from ligand binding in the periplasmic domain of the receptor to its cytoplasmic domain.

3.1 Experimental evidence

Ligand binding does not alter the dimeric state of a chemoreceptor [107] and receptors can signal even if subunit dissociation is prohibited by a covalent cross-link across the dimer interface [59, 128, 43, 96]. This suggests that transmembrane signaling involves a conformational change within the dimeric structure. Many lines of evidence indicate that this conformational change is subtle (reviewed in [58]) and thus high-resolution structural studies by X-ray crystallography are appropriate approaches for identifying its essential nature. However, such studies have been possible only with a receptor fragment, the isolated periplasmic domain of Tar_S [106, 162]. Comparisons of aspartate-bound and aspartate-free structures by the model-independent approach of distance-difference analysis identify two different conformational shifts, depending upon the presence of an engineered, inter-subunit disulfide [42, 162, 28]. When the truncated ends of helices $\alpha 1$ and $\alpha 1'$ are held in their natural proximity by an engineered cross-link, the largest motion seen upon ligand binding is a movement of $\alpha 4$ relative to the rest of the receptor. In the absence of that cross-link, ligand binding causes several changes, the largest of which is a rotation of one subunit relative to the other. The full significance of these different ligand-induced conformational

changes observed in crystals of different forms of the periplasmic fragment is yet to be understood. Thus, there has been a long debate over whether the signaling motion involves a movement between the two subunits of the dimer or within an individual subunit.

3.1.1 Evidence for intra-subunit movement

Aside from the crystal structures, the evidence for an intra-subunit movement includes an experiment in which mutant Tar receptors were constructed, lacking either one cytoplasmic domain or both a cytoplasmic and a transmembrane domain. These truncated receptors were tested for their ability to signal, as measured by the extent of aspartate-induced methylation *in vitro*. Methylation of the receptor lacking one cytoplasmic domain was similar to that of wild-type receptor, but the methylation of the receptor lacking both a cytoplasmic and a transmembrane domain was about 1/5 of wildtype. This suggests that each subunit of the dimer can signal independently, but interactions between the transmembrane domains of the monomers are necessary for full receptor functioning [107].

Other data come from the characterization of inter- and intra-subunit cysteine disulfides in Tar_S and Trg. In Tar_S, α1/TM1–α4/TM2 disulfides that lock the receptor in a state where its associated histidine kinase is either constitutively activated or inhibited have been identified [41], and in Trg, ligand occupancy has been shown to affect rates of cross-linking between TM1–TM2 cysteine pairs [79, 21]. In contrast, cross-links between TM1 and TM1′ do not affect receptor function or chemotactic response [43, 96], and the rate of cross-linking between homologous pairs does not change in the presence of ligand [79]. The conclusion from these experiments was that cross-links should restrain any conformational changes in a helical interface, so that changes in the relative positioning of TM1 and TM2 must occur during signaling, whereas changes in the positioning of TM1 and TM1′ must not.

3.1.2 Evidence for inter-subunit movement

Experimental evidence for an inter-subunit movement includes the fact that, in Tar, aspartate binds across the subunit interface [162] with negative cooperativity, meaning that although the two binding sites in the dimer are structurally equivalent, aspartate is only bound in one site at a time. This indicates that ligand binding at one site must somehow cause an inter-subunit change in binding site conformation or dynamics [25]. Also, several constitutively signaling mutants of Trg [160] have been isolated. These mutations are nearly all located at the interface of TM1 and TM1′ in the periplasmic domain.

In the cytoplasmic domain, changes at the interface between the two subunits seem to be important for signaling, since mutations located between the methylation helices CD1 and CD1′ can cause either activation or inactivation of the kinase CheA regardless of the presence of ligand [50, 144]. Mutants of the isolated cytoplasmic domain of Tar in which the linker region directly below the membrane was replaced with a leucine zipper peptide showed that signaling in the cytoplasmic domain was affected by the register of the coiled coil in the leucine zipper, implying that signaling involves the rotation of the two monomers relative to one another [46].

3.1.3 Evidence for both types of movement

One experiment that showed both inter- and intra-subunit conformational changes upon ligand binding used EPR spectroscopy with nitroxide spin labels in Tar to look for changes in the spectra in the presence and absence of aspartate [115]. Four sets of labeled receptors were constructed, labeled at positions 50-172, 39-176, 39-179, and 31-186. Spin-spin interactions were observed through line broadening in all the doubly labeled receptors, but none of the spectra changed upon ligand binding except that of 39-179. From analysis of singly and doubly labeled receptors, these researchers concluded that aspartate binding causes a motion of residues 39 and 39′ closer to one another, and a motion of residues 39 and 179 further apart. The distances moved are smaller than the uncertainty in the measurement,

but the results are reproducible [115].

3.2 Modeling conformational changes

As outlined above, there is a large amount of experimental data available on the structure of the chemotaxis receptors, yet much of it seems contradictory, and the question of the nature of the conformational change upon ligand binding has not been resolved. Our detailed models for the periplasmic and transmembrane domains of Tar and Trg allow us to examine the precise structural relationships among the four membrane-spanning helices, and observe how these relationships are altered by the proposed conformational changes.

3.2.1 Methods

Many of the studies on ligand-induced conformational changes in the chemotaxis receptors have used cross-links between cysteines introduced into adjacent helical segments, which were thought to constrain receptor motion [128, 43, 41, 96]. We were interested in comparing the degree to which such inter-helical disulfides actually affect the two different ligand-induced conformational changes that have been proposed as the receptor signaling mechanism: sliding of α4/TM2 along its long axis relative to α1/TM1, and rotation of one subunit relative to the other.

We constructed models of cross-linked receptors from our refined models of Trg and Tar by fixing the positions of the backbone atoms, substituting cysteine sidechains at the two designated positions, rotating the cysteine sidechains into the most favorable conformer, and linking the sulfur atoms with a new bond.

We modeled the sliding displacement of TM2 by varying its long-axis position in a series of tiny incremental steps. At each step, TM2 was displaced geometrically by 0.125 Å along its axis, to a final displacement of 10 Å in each direction. Modeling the inter-subunit rotation was less straightforward since there are two pairs of apo/holo crystal structures of the Tar_S periplasmic domain, along with an apo structure for the periplasmic domain

of Tar_E. Furthermore, the three apo structures differ from one another by an inter-subunit rotation that is substantially greater than the differences between either apo/holo pair. We therefore simulated the rotation of the structure between all the available forms, using a method related to targeted energy minimization [56], in which the distance between the starting structure and the target structure is reduced in a series of small steps. Each atom is translated in the direction of the target by a fraction of the total distance at each step. Models for the target structures were built using the method outlined in Chapter 2, with the cross-linked holo Tar_S crystal structure (2LIG), the wild-type apo Tar_S crystal structure (1VLS), the wild-type holo Tar_S crystal structure (1VLT), and the apo Tar_E crystal structure (2ASR) as templates. We quantified the rotational differences between the five structures by aligning the target structures to the starting (1LIH) structure through the backbone atoms of the central helical residues in one subunit (47-70, 90-107, 120-139, and 155-172). We then calculated the root mean square (RMS) displacement of the non-aligned subunit relative to its position in the starting structure. The moving subunit was rotated between the five structures in order of increasing RMS distance from the starting structure. Rotational transitions between apo and holo structures were in approximately the same direction and magnitude for both pairs, whereas rotational transitions between the three different kinds of periplasmic domains (cross-linked Tar_S, Tar_E, and wild-type Tar_S) were not in a single direction.

For both conformational changes, after each step the backbone atoms of the helix were fixed in place and the disulfide linkage was energy minimized to remove any unnecessary conformational strain. For comparing the energy of the structure at different points along a trajectory, it is important that the structures be at the same degree of refinement [147]. It is not feasible to minimize each point along the trajectory to an absolute energy minimum, but each minimization was run until the RMS value of the derivatives reached a convergence of 0.1 kcal/mol·Å.

To assess the amount of strain each introduced disulfide would impose on the receptor structure over the course of a conformational change, we calculated a value for the potential

energy of the introduced disulfide at each step, using the Discover module of the program Insight II from Biosym/MSI [27] and a simplified version of the all-atom AMBER forcefield [155, 156]. This forcefield describes the potential energy of a protein as the sum of quadratic terms for bond length and bond angle deviations from ideality, a trigonometric term for dihedral angle rotation, and a Lennard-Jones potential for van der Waals interactions. The minimizations were run *in vacuo*, so to remove any solvent-based effects we did not include non-bonded terms for hydrogen bonding or for electrostatic interactions. We were interested only in the effects of the conformational change on the geometry of the disulfide residue, so the potential energy of the disulfide was calculated at each step as the sum of the bond, angle, and dihedral terms.

Since the backbone atoms were fixed during the minimization, the final potential energies at each step are somewhat higher than they would be if we allowed small distortions of the helix to accommodate the disulfide. However, this method allows the accurate comparison of energies between different disulfide pairs across different receptors. Since it uses only energy minimization, this method gives a qualitative profile for the energy barriers involved in a conformational change. The energies calculated are not quantitatively accurate, because the process does not account for dynamic fluctuations or the internal mobility of the protein, and therefore the energy calculation does not include the entropy of the system.

3.2.2 Axial sliding of helix α4/TM2

A significant body of experimental data implicates the axial sliding of helix α4/TM2 in conformational signaling [58]. In experiments with disulfide cross-links introduced between TM1 and TM2, Chervitz and Falke found four disulfides that "locked" the signaling state of the receptor: 25-197, 39-183 ("off"—decreased ligand affinity, kinase activation with and without ligand); and 39-179, 43-176 ("on"—enhanced ligand affinity, kinase inhibition with and without ligand); and one disulfide, 36-183, that retained partial signaling [41]. After extending the helices of the periplasmic domain crystal structure to examine the structural consequences of these "lock-on" and "lock-off" disulfide bonds, they concluded that

the lock-on disulfides would seem to trap a sliding movement of TM2 downward (toward the cytoplasm) and that conversely the lock-off disulfides would seem to trap an upward piston-like movement of TM2. Both motions would have a magnitude of about 1 Å [42].

Hughson and Hazelbauer used *in vivo* cross-linking in intact cells to measure the rate of formation of disulfide cross-links between pairs of cysteine residues linking TM1–TM1′ and TM1–TM2. They found no (or very little) change in rates of cross-linking between the TM1–TM1′ pairs 39-39′, 43-43′ and 46-46′, but they found that the rate of cross-linking between the TM1–TM2 pair 42-203 decreases by 30%, and the rate between 42-202 decreases by 20% in the presence of ribose, and that the rate of cross-linking between 38-202 increases 200% in the presence of ribose [79]. A similar increase was found for the rate of cross-linking between 38-203 [21]. They concluded that the motion of TM2 vs. TM1 that best explained their data was an axial sliding movement of the helix down toward the cytoplasm upon ligand binding, which would move residues 202 and 203 on TM2 closer to residue 38 and farther away from residue 42 on TM1 [79]. This motion is the same as that predicted for Tar.

The potential energies of these relevant cysteine pairs in Trg and Tar as a function of the sliding of helix α4/TM2 along its axis are plotted in Figure 3.1A and C. The null position represents the placement of α4/TM2 in the refined models. Sliding toward the cytoplasm or toward the periplasm is represented by positive and negative values, respectively. Kinks in the curves reflect a switch in disulfide dihedral angle from one conformation to another. We expect that oxidative cross-links across the α1/TM1–α4/TM2 interface would tend to stabilize the receptor in the position where the potential energy of the disulfide is at a minimum. In Trg (Figure 3.1A), this energy minimum occurs at a displacement of −0.375 Å and −1.125 Å for the 42-202 and 42-203 pairs respectively, and rises sharply as α4/TM2 is displaced toward the cytoplasm. For the 42-202 disulfide there is a similar rise for displacement toward the periplasm, whereas the potential energy of the 42-203 disulfide remains close to the minimum for displacements toward the periplasm of ≤ 3 Å. Thus formation of either signal-blocking disulfide would cause a minimal shift in the helical register, but

would constrain sliding of α4/TM2 toward the cytoplasm. This implies that these disulfides block signaling by providing a barrier to axial sliding of α4/TM2 toward the cytoplasm, not by causing it to slide. For the 38-202 and 38-203 pairs, however, the disulfide energy minima occur at +5.000 Å and +3.500 Å respectively, suggesting that a displacement of α4/TM2 toward the cytoplasm occurs upon disulfide cross-linking of these pairs. The relatively high potential energy of the 38-202 and 42-202 disulfides reflects the separation of the cysteines and the need for helical rotation to bring the residues within the normal length of a disulfide bond. However, the 42-202 cross-link forms very readily, implying that such rotation is frequent and not an unusual distortion. Similar large twisting motions have been observed in studies of α4–α4′ cross-linking in Tar [41].

Similarly in Tar (Figure 3.1C), the "lock-on" cross-links 25-197 and 39-183 are at minimum-energy positions with α4/TM2 very close to the null position, at −0.125 Å and −0.500 Å respectively, whereas the minimum-energy positions for the "lock-off" disulfides 39-179 and 43-176 occur when α4/TM2 is shifted toward the cytoplasm by +6.125 Å and +3.875 Å, respectively. Figure 3.1C also shows a plot for the 36-183 cross-link, which retains partial functioning of the receptor, allowing ~50% of normal kinase activation and 30% of ligand-induced reduction of that activation [41].

3.2.3 Inter-subunit rotation

Lee et al. examined effects on Trg signaling of disulfide cross-links formed *in vivo* in intact, chemotactically functional cells. The cross-links that could be formed eliminated tactic response when placed between TM1 and TM2 but had no discernible effect on response when placed between α1/TM1 and α1′/TM1′, at positions 32-32′, 39-39′, 46-46′, and 82-82′ [96]. Similarly, Hughson and Hazelbauer used *in vivo* cross-linking in intact cells to measure the rate of formation of cross-links between pairs of cysteine residues in TM1–TM1′. They found no (or very little) change in rates of cross-linking between the TM1–TM1′ pairs 39-39′, 43-43′ and 46-46′ [79].

Figure 3.1B shows plots of the potential energy, using the same energy scale as in Figure

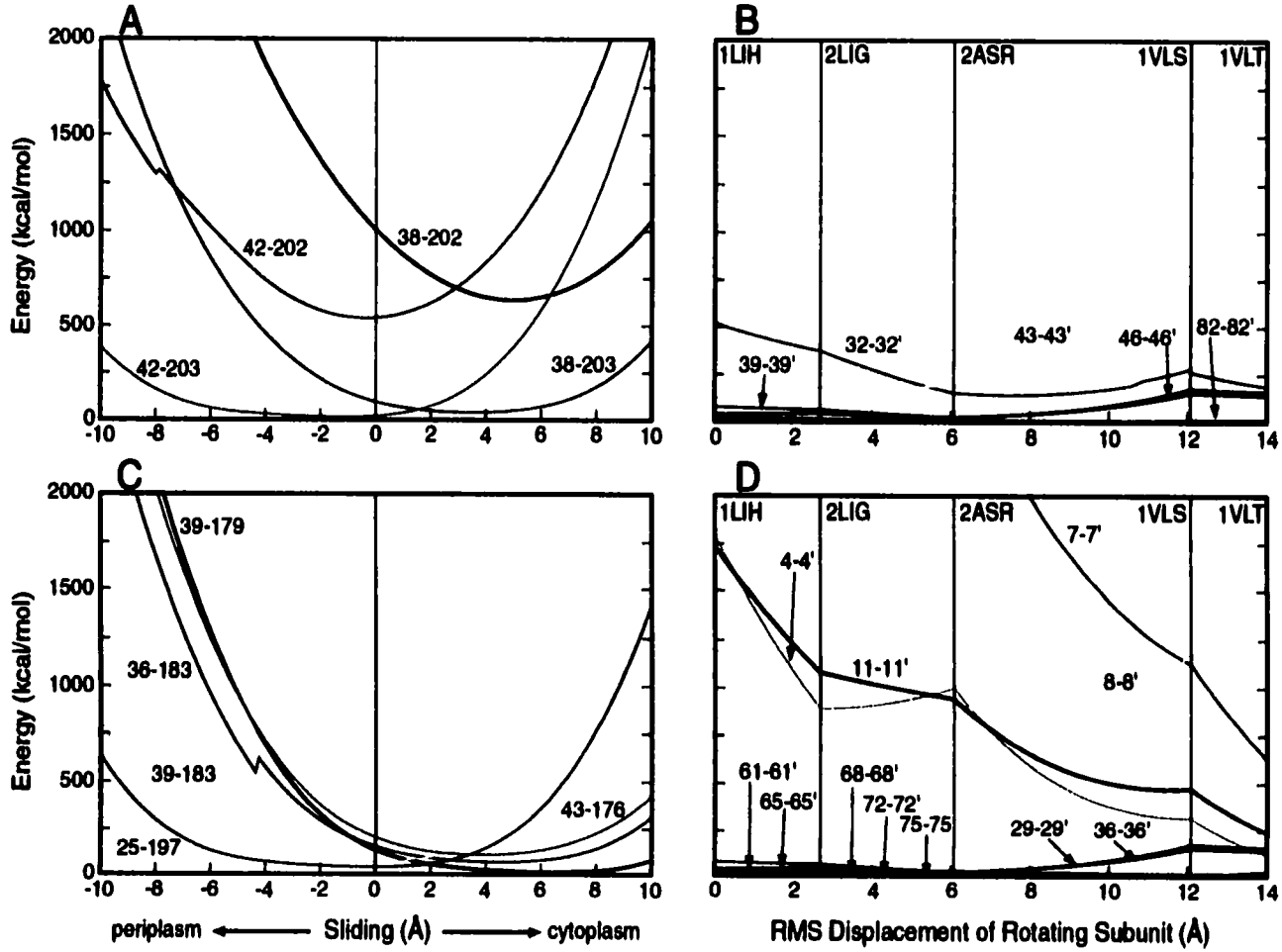

Figure 3.1: Values for the potential energy of inter-helical disulfide bonds, calculated at incremental steps during two receptor motions. Energies of TM1–TM2 disulfides between the indicated positions in Trg (A) and Tar (C) over the course of a sliding motion of helix α4/TM2 along its long axis toward the periplasm (negative) or toward the cytoplasm (positive). Energies of TM1–TM1′ disulfides in Trg (B) and Tar (D) over the course of the rotation of one subunit through the various orientations found in crystal structures of the periplasmic domain. The x-axis shows the total RMS distance traveled by the moving subunit. Positions of the crystal structures are indicated along the top.

3.1A, of these α1/TM1–α1′/TM1′ cross-links in Trg as a function of subunit rotation. The rotation is modeled as a movement of one subunit from its starting position in the crystal structure of the apo cross-linked Tar_S periplasmic domain (1LIH) to its positions in the structures of the holo cross-linked Tar_S domain (2LIG), the Tar_E apo domain (2ASR), the apo wild-type Tar_S domain (1VLS), and the holo wild-type Tar_S domain (1VLT). This path follows the relative ordering of the inter-subunit angles from the smallest to the largest RMS difference from the starting structure. While the ligand-induced rotations between 1VLS–1VLT and 1LIG–2LIG are of similar direction and magnitude, the direction of rotation is not the same between the different apo structures. The x-axis shows the total RMS distance traveled per residue in the moving subunit. It is striking that this inter-subunit movement has little effect on the potential energy of the inter-subunit disulfides, especially within the apo and holo forms of a given structure, indicating that these cross-links would not provide significant constraint on rotation between apo and holo conformations. The 43-43′ and 32-32′ cross-links are somewhat higher in energy than the others. While these cross-links form readily [93, 80], the corresponding cross-link in Tar, 33-33′ and 22-22′, disrupt some aspects of normal receptor signaling [43], indicating that they may perturb the receptor structure.

In an *in vitro* study of Tar, among the eleven cysteine substitutions in α1/TM1 that preserved the ability of the receptor to activate kinase, cross-links across the subunit interface at seven positions allowed signaling [43]. The potential energies of these eleven disulfides as a function of subunit rotation are plotted in Figure 3.1D. For the seven α1/TM1–α1′/TM1′ disulfides that allowed signaling (75, 72, 68, 65, 61, 36 and 29), the potential energy is quite low, reflecting the close apposition of the two helices. As in Trg, there is little change in energy upon subunit rotation from an apo to a holo state. Thus these cross-links would not constrain subunit rotation over the range investigated. Disulfides across the subunit interface at positions 11, 8, 7, and 4 drastically reduced the signaling ability of the receptor [43]. The potential energies of these disulfides are quite high, reflecting distortions that disrupted receptor function. This is consistent with the greater distances between TM1 and

TM1′ near the cytoplasm, the splaying discussed in Chapter 2.

3.3 Receptor flexibility

Measurements of disulfide energy for other TM1–TM2 pairs in Trg and Tar that exhibit a high propensity for cross-linking, but that destroy receptor signaling, are shown in Figure 3.2A (Trg) and 3.2B (Tar). These pairs show a wide variety in the positions of α4/TM2 at which they are in a minimum-energy conformation, ranging from a displacement in the periplasmic direction of −4.875 Å to a cytoplasmic displacement of +4.250 Å.

The potential energy plots of these transmembrane domain residues illustrate that while the receptor has an average conformation as modeled, the α4/TM2 helix may undergo an axial sliding motion in both the periplasmic and cytoplasmic directions even in the absence of ligand. The large displacements of α4/TM2 that are captured by these disulfides with high cross-linking propensities implies that the structure of the receptor is very dynamic.

This idea is supported by a variety of experimental evidence which also suggests that these receptors are quite flexible. For example, cross-links can form between widely different parts of the structure [59] and also can capture large twisting motions of α4/TM2 [41]. In Trg, experiments with nitroxide spin labels have given values for oxygen accessibility that are much larger than for other more closely packed membrane proteins [14]. The relative insensitivity of the transmembrane domain to mutation also suggests a loosely-packed structure [94, 19, 81].

3.4 Conclusions

Our models showed the same pattern of disulfide conformational energies for cross-linked pairs in both Trg and Tar. In each case, disulfides that lock the receptor in an apo-like, kinase-activating state (25-197 and 39-183 in Tar), or whose rate of cross-linking decreases with ligand binding (42-202 and 42-203 in Trg) stabilize the null or starting conformation of the receptor. Disulfides that have the effect of locking the receptor in a holo-like,

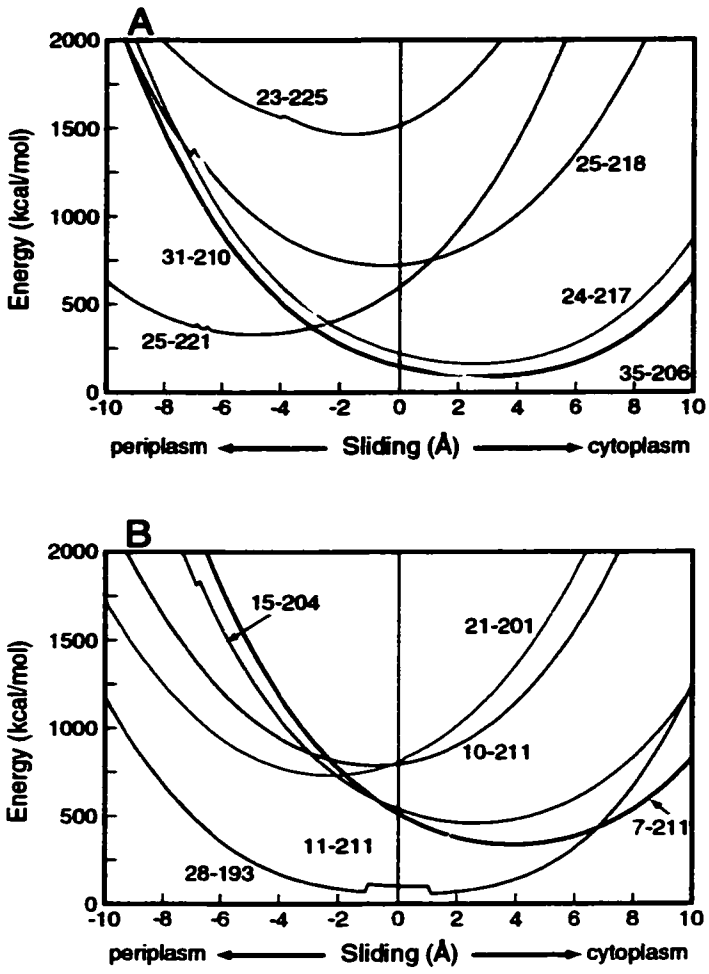

Figure 3.2: The potential energies of the inter-helical disulfide linkages between TM1–TM2 residue pairs in Trg (A) and Tar (B) which have a high propensity for cross-linking [93, 21, 116] over the course of a sliding movement of helix α4/TM2 along its long axis toward the periplasm (negative) or toward the cytoplasm (positive).

kinase-inhibiting state (39-179 and 43-176 in Tar) or whose rate of cross-linking increases upon ligand binding (38-202 and 38-203 in Trg) stabilize a conformation in which TM2 is displaced toward the cytoplasm. These results support the helical sliding mechanism of chemoreceptor signaling, and suggest that the conformational change upon ligand binding is indeed a piston-like sliding of α4/TM2 toward the cytoplasm. A puzzling observation in one of the original studies [41] was that a cross-link between cysteines at positions 36 and 183 created a receptor that exhibited 30% of normal ligand-induced kinase inhibition whereas all other α1/TM1–α4/TM2 cross-links essentially eliminated this signaling. Our modeling does not provide any new insights, since the conformational energy profile for this disulfide is indistinguishable from those of the two lock-off cross-links.

The initial versions of our models were based on the positioning of helices in crystals of the periplasmic domain of Tar_S. As we suggested in Chapter 2, crystallization of the periplasmic domains of Tar_S and Tar_E may have captured receptor fragments in which α4/TM2 was shifted down toward the cytoplasm, i.e shifted toward the signaling conformation. This implies there is a greater difference between the position of α4/TM2 in the ligand-free and ligand-bound conformations than is revealed by comparison of the X-ray structures of the periplasmic domain, and suggests that the $\sim$1 Å shift in the position of α4 that is seen in the crystal structures [42] may underestimate the magnitude of the helical sliding of α4/TM2 upon ligand binding. The potential energy profiles of disulfides that prohibit receptor signaling or whose rate of cross-linking decreases after ligand binding indicate that those cross-links would cause little restraint on axial sliding of α4/TM2 for as much as 2 Å toward the cytoplasm, but would provide increasing restraint for larger movements. This implies that the natural ligand-induced shift should be greater than 2 Å, and in contrast to other measurements of the conformational change [115, 109], the sliding motion of α4/TM2 may be as large as 5 or 6 Å. Since the receptor appears to undergo large fluctuations, ligand binding may affect the frequency of its sliding in the cytoplasmic direction and thus the time-averaged conformation of the receptor. The $\sim$1 Å that is measured in nitroxide spin-labeling [115] and NMR experiments [109] may be a function of the change

in the average positioning of the receptor.

The difference in the subunit interaction angle is much greater between the three available apo structures of the Tar periplasmic domain than between either of the apo/holo pairs of structures. This suggests that the angle of subunit packing is influenced by the crystal environment, and that large fluctuations of the inter-subunit angle may occur spontaneously in the truncated periplasmic domain. Our results indicate that even a large rotation could be accomodated by a disulfide bond at some positions across the subunit interface. However, for both apo/holo structure pairs the direction and magnitude of the small change in inter-subunit rotation angle upon ligand binding is similar, consistent with this rotation being part of receptor function.

Chapter 4

MOLECULAR DYNAMICS OF THE TAR PERIPLASMIC DOMAIN

It has been suggested that ligand binding to the chemotaxis receptors may cause a change in their dynamic properties rather than a discrete change in conformation. Some evidence for this theory comes from the crystal structures of Tar. For example, the mechanism by which aspartate binding at one site prevents binding at the second site is not obvious from the crystal structures: it could be small conformational changes in the positions of sidechains, or it could be that the presence of aspartate simply rotates the receptor into a slightly more closed position, which "closes the entrance" to the second site [162]. Theoretically, a bound molecule of repellent might move the receptor into a more open configuration [86].

Alternatively, the "open" and "closed" rotational conformations of Tar seen in the crystal structures might just be two conformations that are always available to the receptor, that happened to be stabilized by crystal packing forces. In some proteins, open and closed states are only slightly different in energy, and the two states exist in dynamic equilibrium at room temperature. Crystal packing forces have been shown to stabilize closed forms in some proteins (such as lactoferrin) in the absence of ligand [66].

The binding site for aspartate has a very high positive electrostatic potential, caused by three arginine sidechains (R64, R69, and R73), and this potential is partially neutralized by the negatively charged carboxyl groups of aspartate, and the presence of water molecules in the binding site [162]. Thus, in the absence of aspartate these positive charges might act to destabilize the dimer structure, and when aspartate is bound, it might "freeze" the

receptor into a more static conformation, because of the many hydrogen bonds to aspartate from both monomers [86].

Another piece of evidence for a dynamically functioning receptor comes from cross-linking studies. In a study of disulfide cross-links across the interface between TM1 and TM2 in Tar, Chervitz and Falke found that many of these TM1–TM2 cross-linked mutants had *enhanced* aspartate binding ability. Some of the mutants with the lowest K_D for aspartate were "twist-trappers" or structures which were cross-linked between TM1 and the opposite side of TM2 (39-178, 39-180, 39-181, and 39-182). These disulfide bonds all formed rapidly and easily, even though they severely perturbed transmembrane signaling. The authors suggested that the binding energy of aspartate is used by the receptor for moving helix α4/TM2 to signal, so that mutations or perturbations in the receptor that uncouple α4TM2 from the binding site would increase the overall ΔG of aspartate binding, and thus the affinity [41]. There is a conserved proline residue at the top of α4 (P153 in Tar), that may act as a flexible hinge for this decoupling.

Similar cross-links are also seen in Trg, where as we discussed in Chapter 3, cross-links between residues 42-202 and 42-203 form at approximately the same rate even though residue 203 is located in the helical interface and residue 202 is located on nearly the opposite side of the helix, 100 degrees away. Early cross-linking experiments, which were done before the structure of the periplasmic domain was known, showed that cross-links can be observed to form between residues 106-106′ and 128-128′. Both of these pairs are more than 30 Å apart in the folded structure. These results suggest that the periplasmic domain, particularly the α4/TM2 helix, has a large amount of themal mobility, and that large twisting motions of this helix seem to occur naturally in the folded and functioning receptor.

It is possible to determine whether or not a bound aspartate alters the dynamics of the receptor using molecular dynamics simulations. Such simulations have been performed on the *trp* repressor, which binds tryptophan in a manner that is very similar to the binding of aspartate by Tar. The *trp* repressor of *E. coli* is a transcription factor that regulates

tryptophan synthesis. When tryptophan ligand is bound to the repressor, it binds to the *trpR*, *aroH*, and *trpEDCBA* operators and prevents transcription of genes necessary for the synthesis of tryptophan, other aromatic amino acids, and the *trp* aporepressor itself [76]. In a comparison of molecular dynamics simulations of the *trp* repressor and the *trp* aporepressor, Howard and Kollman found that the presence of the tryptophan ligand affected the distance between the DNA-binding helices and their flexibility, as well as the overall mobility of the ligand-binding helices [76]. Both the *trp* repressor and Tar bind their amino acid ligands through an arginine residue which interacts with the α-carboxylate group, and a series of backbone carbonyl oxygen atoms which interact with the α-amino group [102]. The *trp* repressor, like Tar, is also a dimeric, primarily helical protein, with the binding site at the subunit interface between two anti-parallel helices. Although this is probably a result of convergent evolution rather than a conservation of structure and function, it is possible that the conformational and dynamic changes in the protein structure upon ligand binding are similar for the two proteins [102].

In order to test the theory that a bound molecule of ligand might affect the dynamics of the chemotaxis receptors, rather than causing a static conformational change, we performed molecular dynamics simulations of the periplasmic domain of Tar with and without bound aspartate.

4.1 Methods

We began with the four available crystal structures of the periplasmic domain of Tar_S: 1LIH, which is the apo form, cross-linked across the subunit interface at residue 36-36′; 2LIG, the holo cross-linked form [106]; 1VLS, the apo wild-type (not cross-linked) form; and 1VLT, the holo wild-type form [162]. These structures do not all have the same number of residues, so we added or deleted residues as necessary so that each system consisted of residues 35-180. Hydrogens were added to the heavy atoms of the X-ray structures, and the helix ends were capped with neutral acetyl (Ace) and methyl amide (Nme) terminal

residues. Parameters for the zwitterionic aspartate ligand were generated by merging partial charges from the standard N-terminal and C-terminal charged aspartate residues in the AMBER [47] residue library.

The finished structures were briefly minimized for 50 steps *in vacuo* to relax any close atomic contacts due to the modeled hydrogens. We added sodium counter-ions to neutralize the total charge in each system, and each structure was solvated in a periodic box of TIP3P water. All minimization and molecular dynamics was run using AMBER 5.0 [38] and the standard all-atom potential functions [47]. The four systems were first minimized for 100 steps with only water molecules and ions allowed to move, then for 200 steps with all atoms moving. Since the water boxes were constructed by abutting several small equilibrated boxes of water, any periodic structure remaining in the water was removed by running 5000 steps of molecular dynamics at constant volume, allowing only water molecules and ions to move. This eliminates the possibility of spurious forces acting on the protein structure during subsequent dynamics runs [9, 70].

The systems were brought to thermal equilibrium by running constant volume molecular dynamics in 10 runs of 200 steps each, reassigning the atomic velocites to a different Maxwell-Boltzmann distribution at 300 K after each run. We then switched to constant pressure molecular dynamics (NPT ensemble) with periodic boundary conditions for the remainer of the simulation time. A residue-based cutoff of 10 Å for the non-bonded interactions was employed. Long-range electrostatic interactions were modeled by the particle-mesh Ewald summation technique [51]. The integration time step was set to 1 fs, and a dielectric constant of 1 was used. All hydrogen bond lengths were restrained to their equilibrium values using SHAKE [125]. The system temperature of 300 K was maintained using the Berendsen algorithm [22] with time constants for heat bath coupling of 0.5 ps for the solvent and 1.0 ps for the solute. The system pressure was coupled anisotropically to a Berendsen pressure piston [22] at 1 atm with a relaxation time of 1.0 ps. The coordinates of the system were written to disk every 200 steps, or 0.2 ps.

4.2 Equilibration

We monitored the progression of the simulations toward equilibrium by examining the deviation of the backbone structures from their starting coordinates. Any global translation or rotation due to diffusion of the protein was first removed by superimposing the backbone atoms in each frame onto the starting conformation of the protein, using a mass-weighted root-mean-square fitting algorithm. The values of the RMS difference of each frame from the starting structure were calculated using the program PTraj, which is part of AMBER [38]. The time evolution of this RMS deviation from the starting structure for the four systems is shown in Figure 4.1.

For all the systems, the RMSD gradually reaches a stable value of about 1.5–2.0 Å. This is within the atomic resolution of the crystal structures [106, 162], suggesting that the system does not undergo any significant conformational changes. In both the cross-linked and wild-type structures, the apo runs take longer to stabilize, reaching a plateau value after about 400 ps, as compared to 200 ps for the holo runs. The average RMS difference between the starting structure and the simulation structure is also larger for the apo runs. Both the apo and holo forms of the cross-linked structure stay closer to their starting conformations than the wild-type structures.

We also monitored the values of the total system energy (the sum of the kinetic and potential energies) and the density in the periodic box over the course of the simulations (Figure 4.2). All four systems rapidly reach equilibrium values for total energy and density, within about 100 ps. Slight differences in the values for the energy between systems occur because each system has a different total number of atoms. Differences in the density are due to differences in the number of water molecules per system.

These measurements suggest that the system is stable on the time scale of the molecular dynamics simulations. The last 500 ps of each trajectory was used for all subsequent analyses.

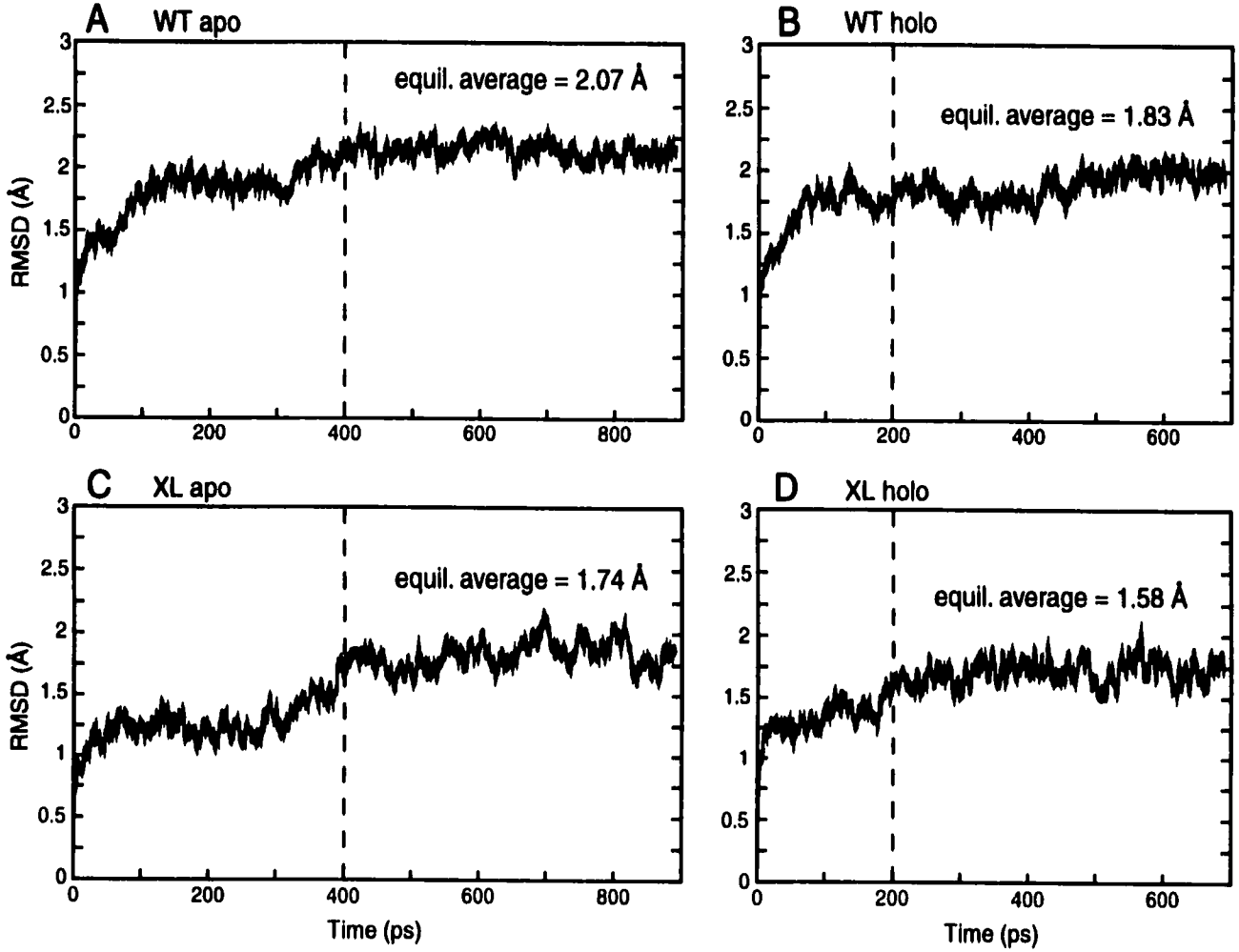

Figure 4.1: Root mean square deviations of the four simulation structures of the Tar periplasmic domain from their starting coordinates, monitored as a function of time. The time at which equilibrium is reached is marked by a dashed line, and the equilibrium RMSD value for each system is indicated. Abbreviations: WT = wild-type structure; XL = cross-linked structure.

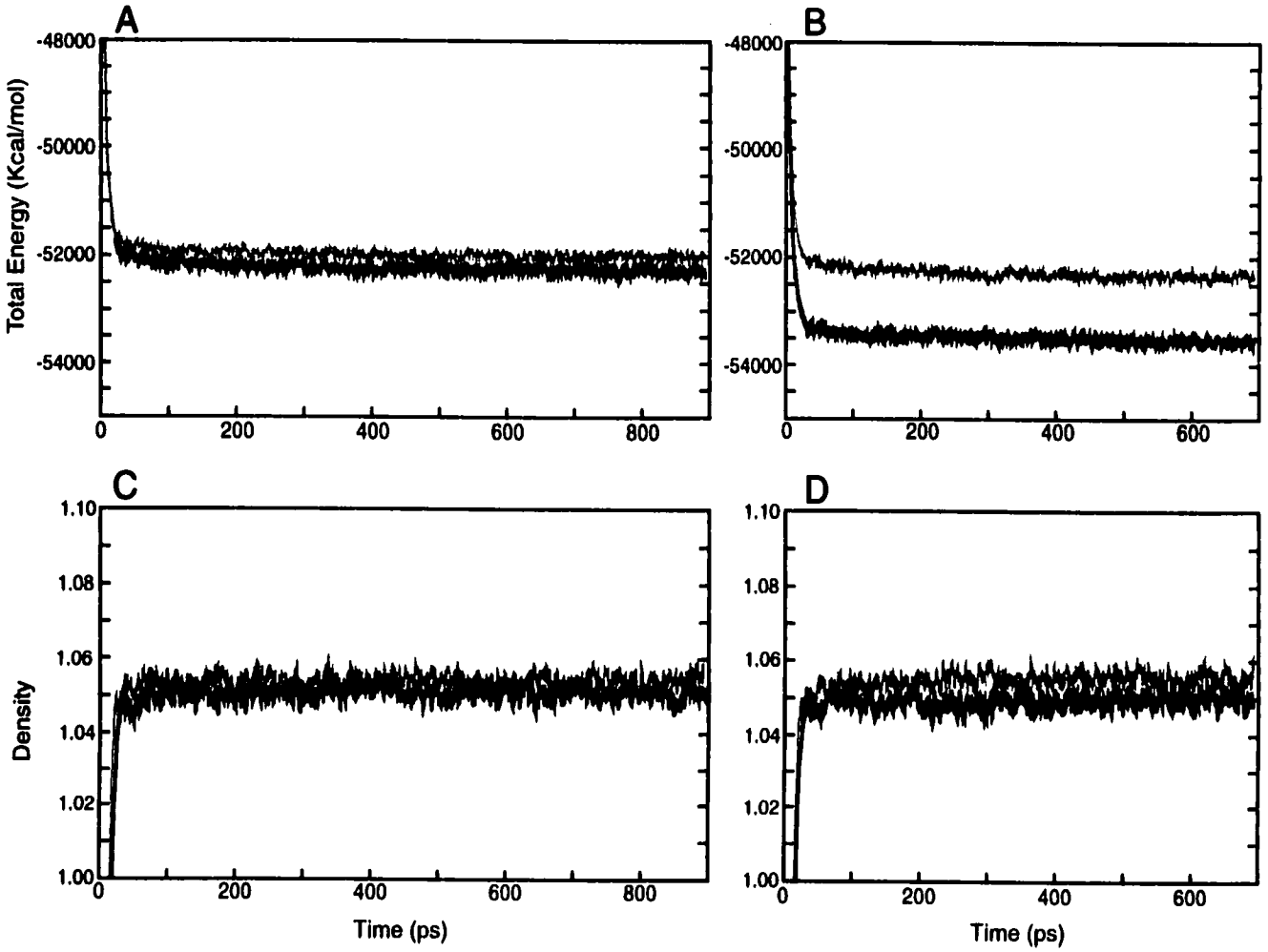

Figure 4.2: Values for total system energy in the apo (A) and holo (B) systems, and values for the density of the periodic box in the apo (C) and holo (D) systems. Values for the wild-type systems are shown as black lines, and the cross-linked systems are indicated with grey lines. Slight differences in values between the four systems are due to differences in the number of atoms and water molecules.

4.3 Dynamic behavior

4.3.1 RMS fluctuations of overall structure

A comparison of the root-mean-square (RMS) fluctuations of the backbone atoms in the two pairs of apo and holo periplasmic domain structures allows an estimate to be made of their relative flexibilities and the relative size of their dynamic fluctuations. If the presence of aspartate does affect the dynamics of the receptor, then there should be a difference in the magnitude of the RMS fluctuations between the apo and the holo structures. Comparing the RMS fluctuations of the backbone atoms over the course of the molecular dynamics simulation with their temperature factors in the crystal structures also provides another indication of the accuracy of the simulation.

The temperature factor, or B-factor, is an indication of the extent of the disorder each atom has in the crystal. The position of the atom becomes less localized as its temperature factor increases. If we assume that the crystal lattice is perfect, then this disorder is due entirely to harmonic thermal vibrations of the atom, and so the temperature factor is related to the RMS fluctuations by the equation

$$\Delta R_j = \frac{3B}{8\pi^2} \tag{4.1}$$

where B is the temperature factor or B-factor and ΔR_j is the magnitude of the RMS atomic fluctuations. In reality, of course, the crystal lattice is not perfect and the temperature factor is also influenced by experimental uncertainty and lattice disorder within and between the unit cells in the crystal [119, 49].

To calculate the RMS fluctuation values from the MD simulations, we first removed any global translation or rotation in the motion of the protein by superimposing the backbone atoms in each frame in the equilibrated portion of the trajectory (2500 frames for each simulation) onto the starting conformation of the protein, using a mass-weighted root-mean-square fitting algorithm. The RMSF values were calculated using the program PTraj [38]. The B-factor values from the crystal structures were averaged for the backbone atoms

(N, Cα, C) in each residue and converted to RMSF values using the equation above. These RMSF values are shown in Figure 4.3. Values for the apo structures are averages of the two subunits.

The agreement between the molecular dynamics simulations and the crystal structures is good. There is a general correspondence between the magnitude of the fluctuations and the secondary structure: residues in helices show less overall motion than residues in loop regions. The first loop, which connects helices α1 and α2, is the most flexible region of the protein. The second loop, between helices α2 and α3, is somewhat less flexible, probably because of its shorter length. The third loop, connecting helices α3 and α4, is much more rigid than the other two. The N-terminal and C-terminal ends of the helices are also flexible, although in the cross-linked structures the N-terminal end of α1 has a reduced mobility relative to the wild-type structures, as would be expected due to the constraining cross-link.

Neither the molecular dynamics runs nor the crystal structures show any significant differences in RMS fluctuation magnitude between the apo and holo systems in the helical regions of the receptor. The cross-linked crystal structure shows slightly less motion in helices α1, α2 and α3 in both monomers of the holo form. The wild-type crystal structure has a somewhat different pattern of fluctuations, with slightly more motion in one region of the apo α4 helix compared to the holo structures, but the other helices have similar fluctuations.

These results suggest that the apo and holo forms of the truncated periplasmic domain do not have any overall difference in their dynamic properties, at least on the time scales surveyed by these molecular dynamics simulations. We looked more closely at the residues that make up the binding site, to see if aspartate binding had a localized effect on receptor dynamics in this region.

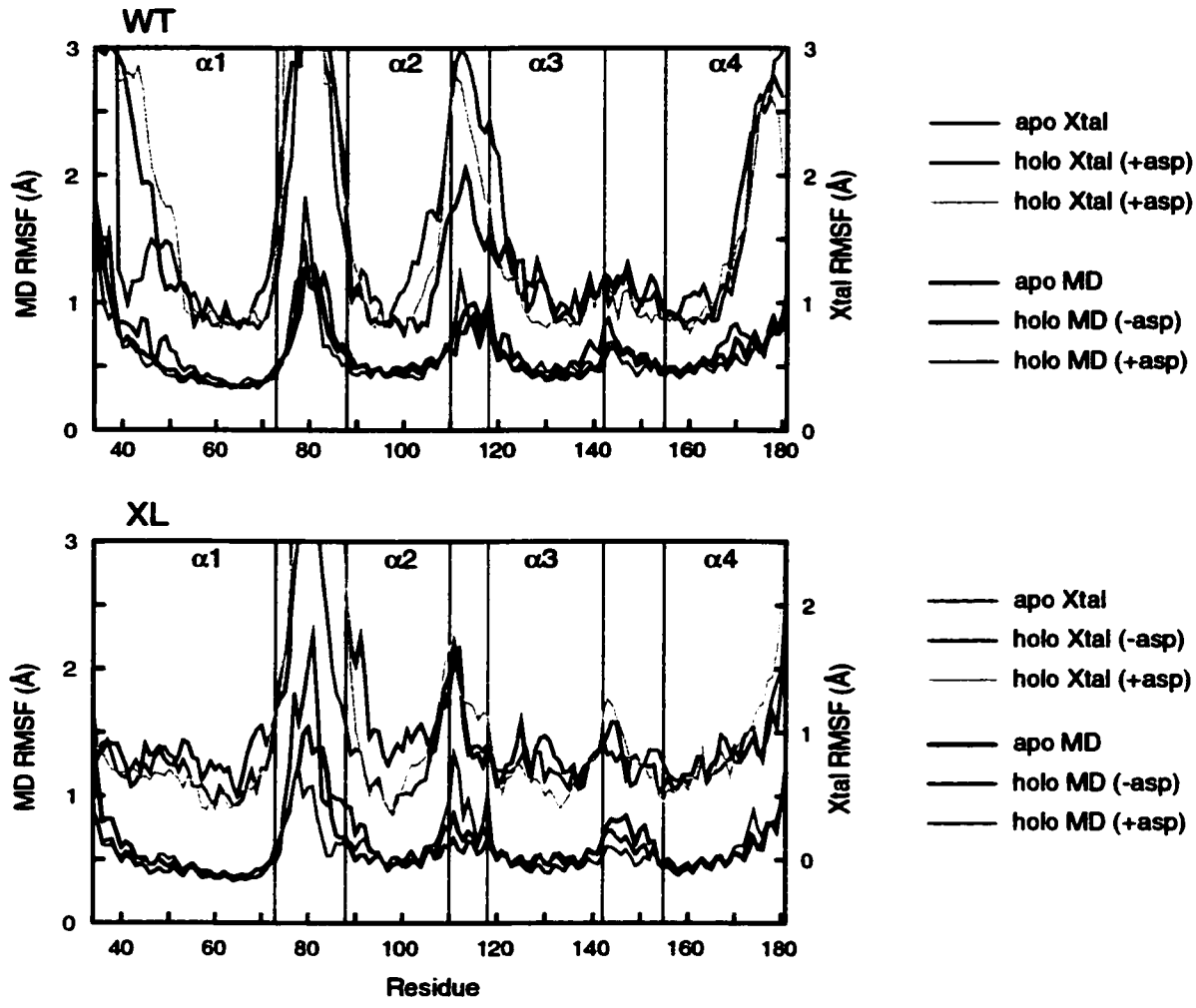

Figure 4.3: Root-mean-square fluctuations of the simulation structure backbone atoms during the 500 ps equilibrated trajectory compared to crystal structure B-factors. In each graph, the top set of lines represents the B-factors of the crystal structure, converted to RMSF values. The lower set of lines are the RMSF values from the molecular dynamics simulations. In the lower graph showing the results from the cross-linked system, the right-hand axis for the converted crystal structure RMSF values has a shifted scale for clarity. The locations of the helices are labeled and marked with vertical lines. Abbreviations: WT = wild-type structure; XL = cross-linked structure; MD = molecular dynamics; Xtal = crystal structure; asp = aspartate ligand. In the wild-type holo crystal structure, both binding sites had electron density indicating the presence of aspartate, so both subunits are marked +asp.

4.3.2 RMS fluctuations of binding site

A sketch of the residues that make up the binding site, along with a molecule of bound asparate, is shown in Figure 4.4A. The binding site consists of residues R64 and S68 on helix $\alpha 1$, residues R69′ and R73′ from helix $\alpha 1'$ in the opposite subunit, and residues Y149, F150, Q152, and T154 which form part of the loop connecting helices $\alpha 3$ and $\alpha 4$.

The values for the RMS fluctuations of the binding site atoms were calculated as above, and are shown in Figure 4.4B. The values shown are the average of the cross-linked and wild-type systems, and values for the apo structure are averages of both subunits.

The fluctuation profile for each residue has a peaked shape due to the ordering of the atoms in the residue along the x-axis (see the figure legend for details). In general, as expected, the backbone atoms of the residues are less flexible than the atoms of the sidechain.

There are significant differences in flexibility between the apo and holo subunits. Aspartate binding reduces the dynamic fluctuations of the three arginine residues R64, R69′, and R73′ which form the positively charged binding pocket, along with the backbones of residues Y149 and F150.

Interestingly, aspartate binding to one subunit also reduces to some extent the fluctuations of the other, empty subunit in the holo structure. Two of the arginine residues R69′ and R73′ show smaller fluctuations than in the apo structure, as does F150. This may be part of a mechanism for the negative cooperativity that is seen in the Tar receptor, where aspartate binding at one of the sites reduces the affinity for aspartate at the second binding site. A reduction in the dynamic motion of the second binding site could make it more difficult for aspartate to enter the site and bind.

4.4 Conformational analysis

In the absence of any overall dynamic differences between apo and holo structures, outside of the limited region of the binding site, we looked at conformational differences between the two forms in an attempt to gather more information on potential helical sliding or rota-

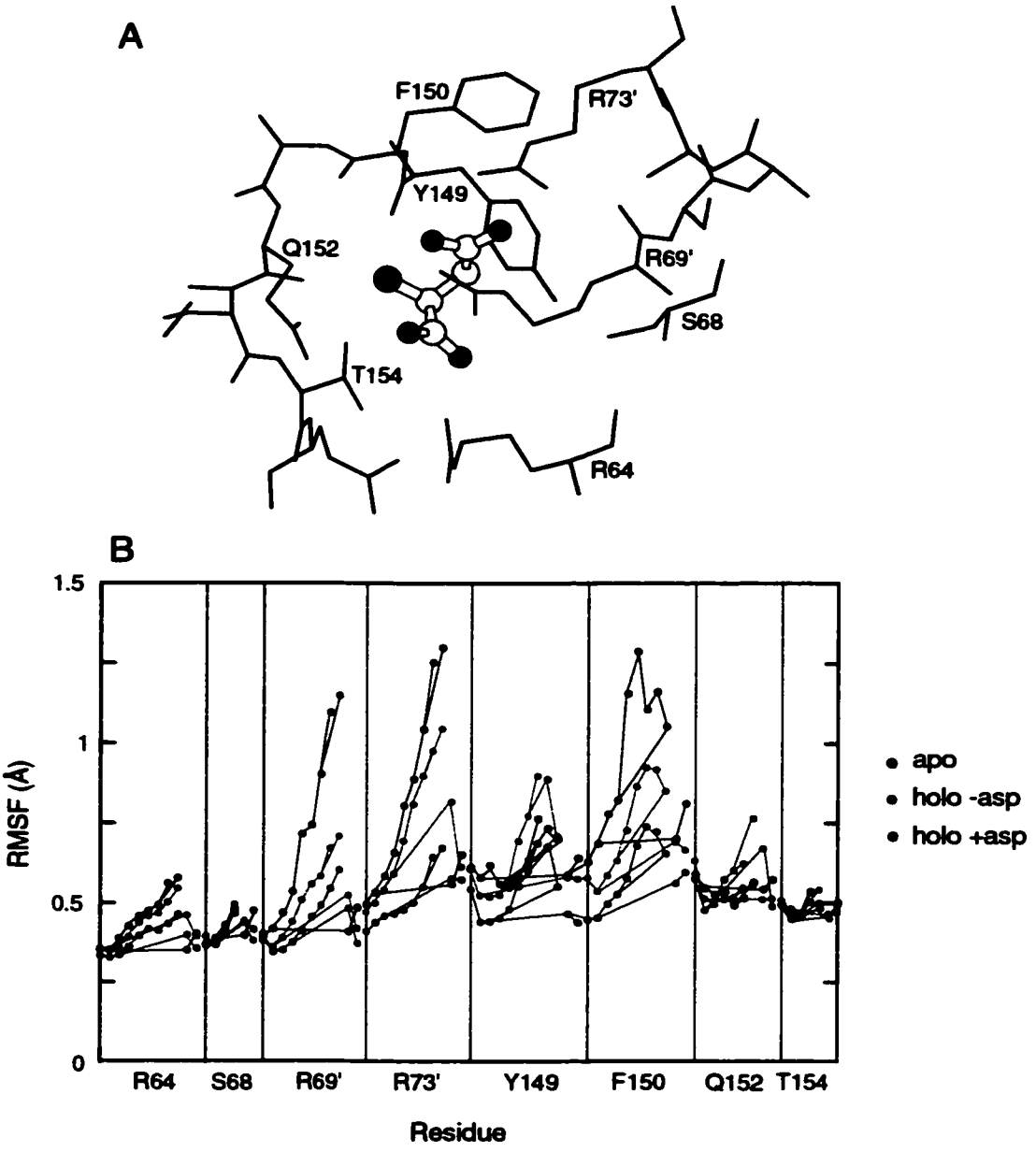

Figure 4.4: (A) The binding site residues (line representation) along with a molecule of bound aspartate (ball-and-stick representation). (B) Root-mean-square fluctuations of all atoms in the residues involved in aspartate binding. The ordering of the atoms along the x-axis within each residue begins with the backbone nitrogen, then the Cα atom, then the Cβ, γ, δ, etc. atoms to the tip of the sidechain, and lastly the backbone C and O atoms. The lines connecting the data points show the atomic connectivity.

tional motions in the solvated dynamic periplasmic domain of the receptor.

4.4.1 Distance difference matrices

Distance difference matrices are commonly used for analysing differences between two structures [111]. The advantage of this method is that it makes no *a priori* assumptions about what differences in conformation might be occurring. This is useful when the changes in the structure after a conformational shift are complex and small, as in the case of the crystal structures of the periplasmic domain of the chemotaxis receptors. When these structures are superimposed onto one another using an RMS fit, the changes seen depend on which atoms are used for the superposition. For example, if we assume that an inter-subunit conformational change occurs upon ligand binding, and align the backbone atoms of the A subunit in the apo structure with the backbone atoms of the A subunit in the holo structure, and then compare the positions of the B subunits in the two structures, the difference between them is a small rotation about a pivot axis perpendicular to the dimer interface (Figure 4.5A and 4.5B). This is also the case when the B subunits are aligned and the A subunits are compared [106, 161, 162, 44]. On the other hand, if we assume that ligand binding causes an intra-subunit conformational change and align individual ligand-bound subunits to ligand-free subunits through the central, most well-ordered residues in helix $\alpha 1$, the vertical position of helix $\alpha 4$ is on average about 1 Å lower in the ligand-bound subunits (Figure 4.5C). Thus, alternative RMS superpositions of the crystal structures can show either a small displacement of $\alpha 4$ within a monomer or a rotation betweeen monomers.

A distance difference matrix is a very simple method of comparing two structures that eliminates these difficulties. Each element in the matrix shows the difference in the distance between two Cα atoms in the apo structure and the distance between those atoms in the holo structure. This gives a clear picture of what regions of the structure are changing and which are static between the two different forms.

Such distance difference matrices have been plotted for both of the two available pairs of apo/holo crystal structures of the truncated Tar periplasmic domain, one with an inter-

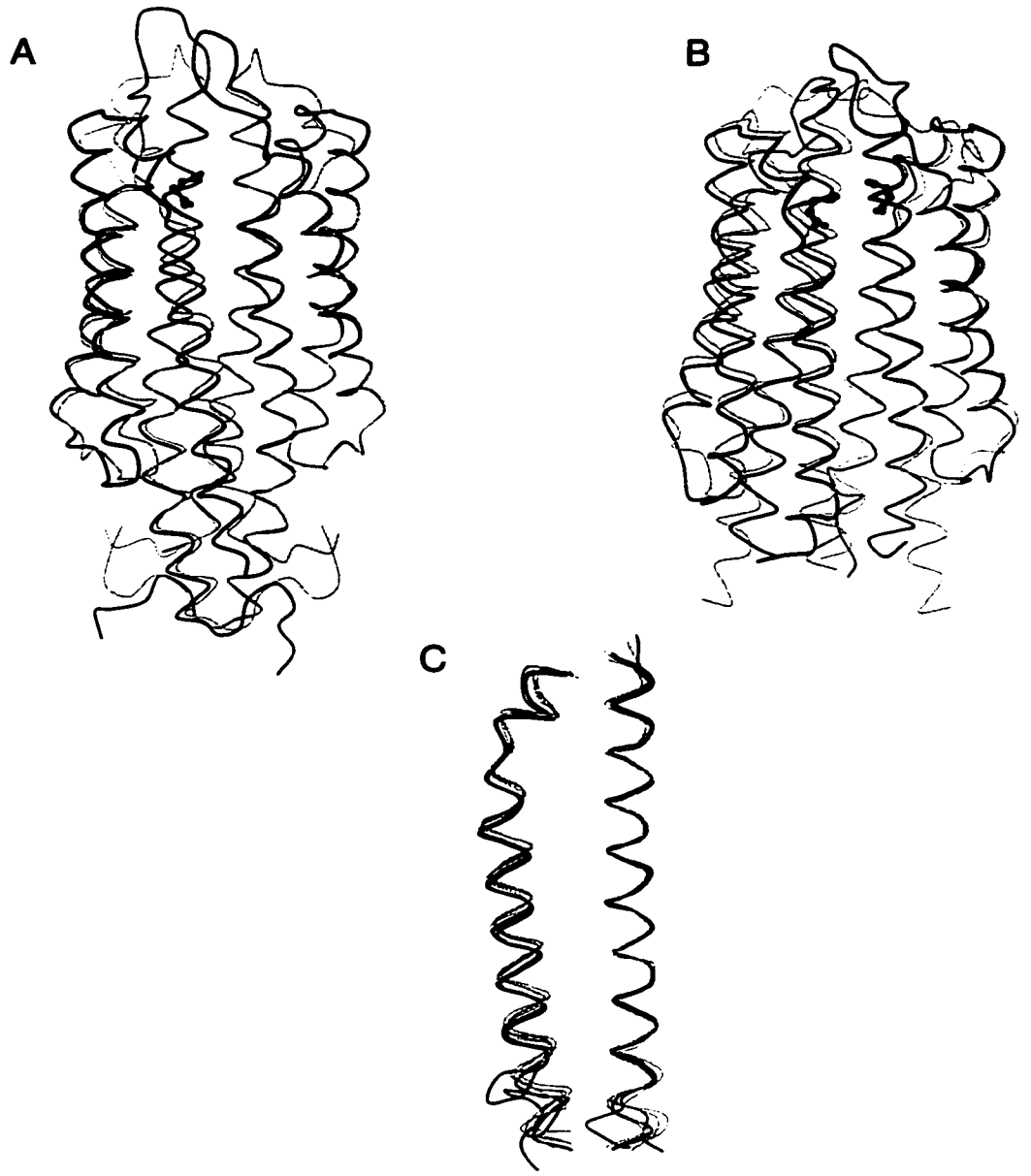

Figure 4.5: A comparison of different RMS overlays of the available crystal structures of the Tar periplasmic domain. (A) One subunit of the apo cross-linked structure (gray line) aligned with the corresponding subunit in the holo cross-linked structure (black line) (B) One subunit of the apo wild-type structure (gray line) aligned with the corresponding subunit in the holo wild-type structure (black line). The aspartate ligand is shown in ball-and-stick representation. (C) Ligand-bound subunits (black line) aligned with ligand-free subunits (gray line) through the central residues in helix $\alpha 1$. Helices $\alpha 2$ and $\alpha 3$ are omitted for clarity. This figure was made using Molscript [89].

subunit cross-link between residues 36-36′ and one without. However, they have not shed any light on the controversy of the conformational change in the receptor upon ligand binding because they show somewhat different ligand-induced conformational changes in the two pairs [42, 162, 28]. Both structures show inter-subunit changes, although these are larger in the wild-type structure. In the cross-linked structure, there is also a fairly large movement of helix α4 in the ligand-bound subunit relative to the rest of the receptor.

Our molecular dynamics simulations allow us to calculate an ensemble averaged distance difference matrix for the 2500 structures generated during the 500 ps of equilibrated simulation. The advantage of this method over traditional distance difference analysis is that our structures are in solution and free of any crystal packing forces, and having 2500 frames for each conformation allows us to measure the statistical significance of each distance difference by calculating the standard deviation at each position.

Each element in the ensemble averaged distance difference matrix is described by [1]:

$$\overline{\Delta d_{ij}} = (MN)^{-1} \sum_{p=1}^{M} \sum_{q=1}^{N} \left(d_{ij,p}^{(A)} - d_{ij,q}^{(B)} \right) \tag{4.2}$$

and the standard deviations for each element in the matrix are [1]:

$$\sigma(\Delta d_{ij}) = \sqrt{(MN)^{-1} \sum_{p=1}^{M} \sum_{q=1}^{N} \left(d_{ij,p}^{(A)} - d_{ij,q}^{(B)} - \overline{\Delta d_{ij}} \right)^2} \tag{4.3}$$

where $\overline{\Delta d_{ij}}$ is the average distance difference between atoms i and j in the two ensembles A and B (i.e. the apo and the holo systems), the sizes of the two ensembles A and B are M and N, respectively, and $d_{ij,p}^{(A)}$ is the distance between atoms i and j in the pth structure (i.e. frame) of ensemble A.

The results for intra- and inter-subunit distance difference comparisons of the apo and holo structures in both the cross-linked and wild-type systems are shown in Figures 4.6 and 4.7. In these figures, the locations of the helices are indicated along the edges of the matrices. The sequences of the apo structures run along the x-dimension, and the holo structures run along the y-dimension. Regions with non-statistically significant differences, or differences less than 0.5 Å in magnitude are colored white. Regions with a positive distance

difference, meaning that they are farther apart in the holo structure than in the apo structure, are colored light blue for differences between 0.5 and 1.5 Å and dark blue for differences greater than 1.5 Å. Regions with a negative distance difference are colored orange for differences between -0.5 and -1.5 Å and red for differences greater in magnitude than -1.5 Å.

Aside from the loop regions in all the structures and the N-terminal and C-terminal ends of the helices in the wild-type structures, which are highly mobile as shown by their RMS fluctuations (Figure 4.3), all four of the intra-subunit distance difference matrices show virtually no differences between the apo and holo forms of the four subunits. There is a small motion at the top of helix α2, indicating that it moves slightly closer to helix α3. This may be a slight change in the conformation of the binding site, leading or contributing to negative cooperativity in the binding site in the opposite subunit. In contrast, the inter-subunit distance difference matrices show much larger conformational changes, especially in the wild-type system. There are rotational movements of α1, α2, and α3 in the cross-linked structure. Similar but larger movements are also seen in the wild-type structure, along with movements of α4.

These results suggest that the shift in the position of α4 relative to the rest of the structure that is seen in the cross-linked crystal structures [42] is actually not significant, and may be an artifact of the crystallization conditions. The major difference between the apo and holo structures of the periplasmic domain seems to be a rotation of the subunits relative to one another.

4.4.2 Signaling motions

The authors of the original papers on the crystal structures had suggested that the differences between the two apo/holo pairs of crystal structures of the periplasmic domain may have underestimated the magnitude of inter-subunit rotation, since even in the un-liganded forms an ion occupies the binding site [106, 162]. This was confirmed by a structure of Tar_E with both binding sites empty, in which the inter-subunit rotation was approximately

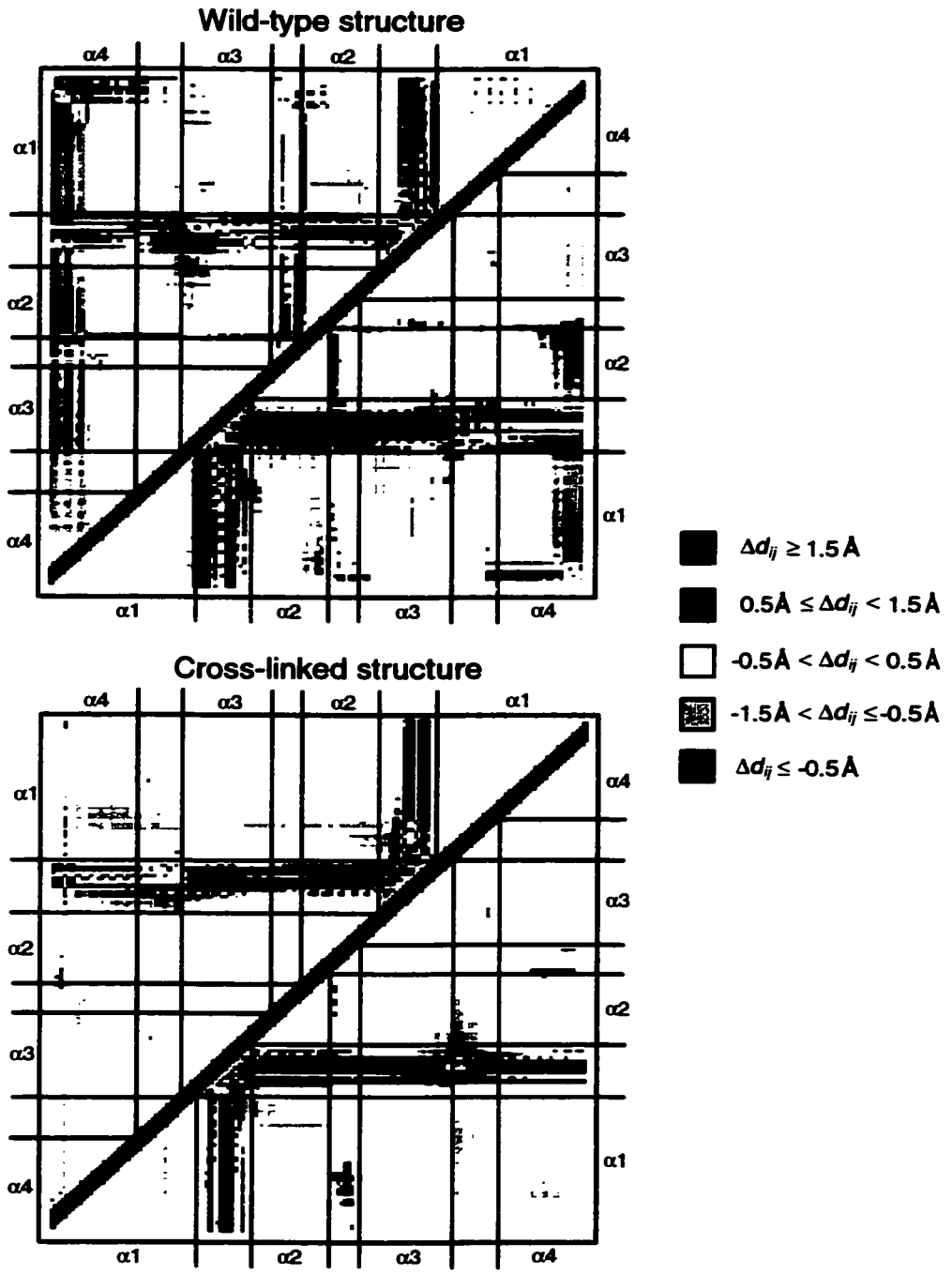

Figure 4.6: Ensemble averaged distance difference matrices showing ligand-induced differences in structure within receptor subunits. Each element in the matrix, Δd_{ij}, is the difference in the distance between two atoms i and j in the apo and holo structures. The locations of the helices are indicated along the edges of the matrix, and the boundaries between loops and helices are marked with black lines.

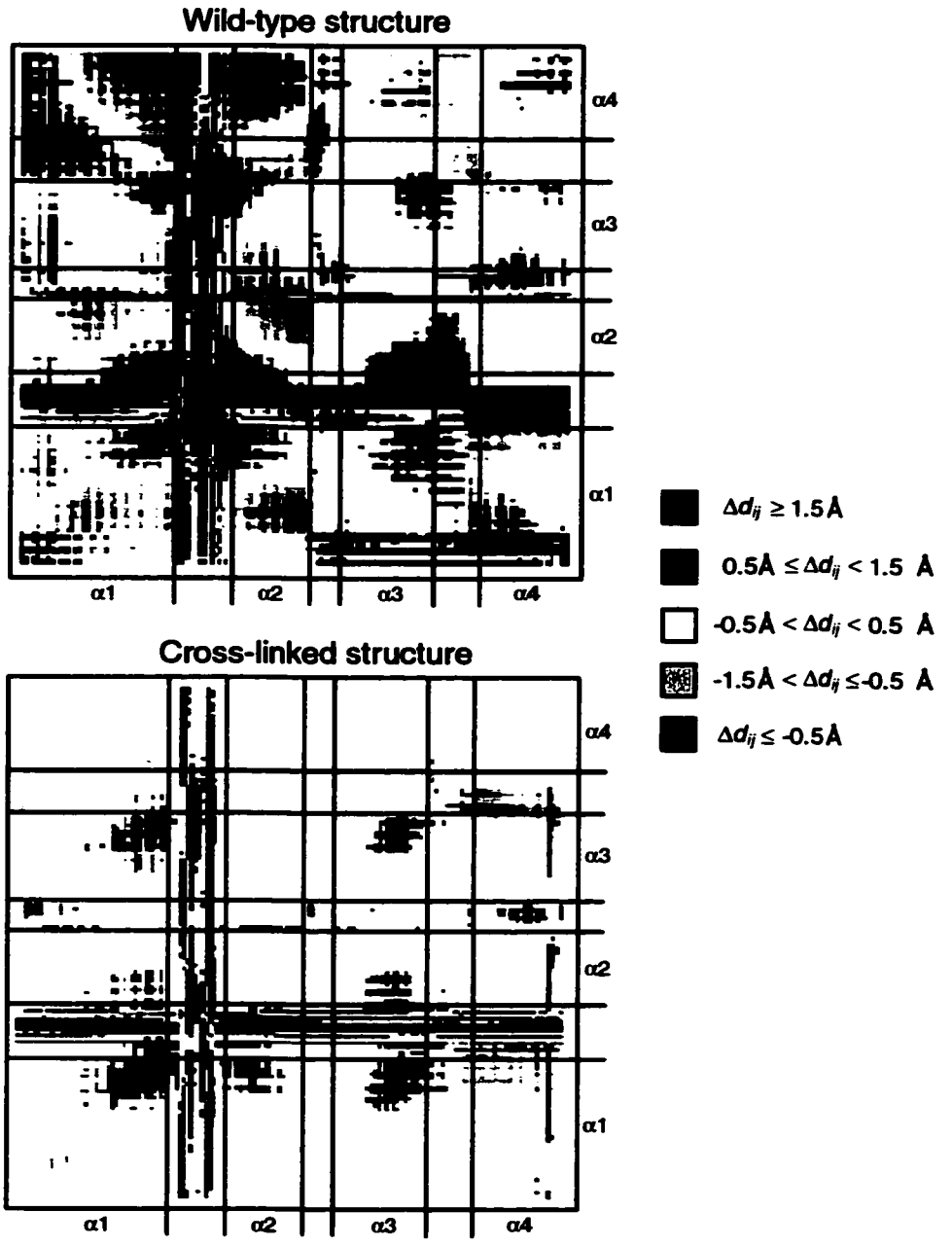

Figure 4.7: Ensemble averaged distance difference matrices showing ligand-induced differences in structure between receptor subunits. Each element in the matrix, Δd_{ij}, is the difference in the distance between two atoms i and j in the apo and holo structures. The locations of the helices are indicated along the edges of the matrix, and the boundaries between loops and helices are marked with black lines.

twice as large [44].

As our studies with models of cross-linked mutants of Trg and Tar showed (Chapter 3), the difference in the subunit interaction angle is much larger between the three available apo structures of the receptor periplasmic domain than between either of the apo/holo pairs of structures. This suggests that the crystallization conditions or crystal packing environments have a greater effect on the inter-subunit rotation angle than ligand binding, although the direction and magnitude of the change in rotation angle upon ligand binding are similar for both apo/holo structure pairs.

In light of our distance difference results, we examined the two proposed signaling motions for the chemotaxis receptors, an axial sliding motion of helix α4 and an inter-subunit rotation, over the course of our calculated molecular dynamics trajectories.

Axial sliding of α4

Fluctuations in the position of α4 relative to the other helices in the subunit were calculated for each frame in the trajectory by performing a mass-weighted RMS fit of residues 48-73 and 88-110, the central well-ordered residues in helices α1 and α2, to a reference structure, which was the first frame of the simulation. (This reference structure is the crystal structure, after undergoing minimization and thermalization). After the RMS fit, we calculated the position of the center of mass of the backbone atoms in residues 48-73 in α1, and the position of the center of mass of the backbone atoms in residues 155-169 in α4, using the program CARNAL [124]. We then repeated this procedure for the other subunit.

The top part of Figure 4.8 shows the backbone of the periplasmic domain with the centers of mass of helices α1, α4, α1′, and α4′ indicated by black dots, and an arrow drawn between α1 and α4 in each subunit. This reference is in the same orientation and scale as the traces in the bottom part of the figure. Here, for both the wild-type and cross-linked structures, the centers of mass of α1 and α1′ are also indicated with black dots, and are aligned for each frame in the simulation. The variation in the position of the center of mass of α4 is shown with a traced line for the apo structure (in black) and the holo structure (in

grey). The line connecting the center of mass of α1 and α4 indicates the position of the center of mass of α4 in the starting structure. There is a 2 Å grid behind these traces.

In the cross-linked system, the α4 helix in one of the apo subunits explores an area of conformational space that is slightly higher along the helix axis than the other subunits. Aside from this, there is virtually no difference in the vertical positioning of α4 in any of the four systems. The position of the helix varies in all directions over an area of about 2 $Å^3$, which is typical for the size of a thermal motion in a soluble protein structure [34]. This suggests that differences of approximately 1 Å in size seen in the crystal structures may not be significant, supporting our conclusions from the distance difference analysis.

Inter-subunit rotation

Fluctuations in the inter-subunit angle were measured through the angle of α1 relative to its starting position in the reference structure. For each frame in the trajectory we aligned the ligand-free subunits to the reference structure through residues 48-73, 88-110, and 118-169, the most well-ordered residues in the structure. In the other, non-aligned subunit, we then calculated the center of mass of the backbone atoms in residues 68-73 at the top of α1, and the center of mass of the backbone atoms in residues 48-53 at the bottom of α1, using the program CARNAL [124].

The top part of Figure 4.9 shows the backbone of one subunit of the periplasmic domain, with the plane of the subunit interface oriented approximately parallel to the plane of the page. The locations of the center of mass of the top region and bottom region of helix α1 are marked with black dots, and an arrow is drawn to indicate the helix axis. This reference is in the same orientation and scale as the traces in the bottom part of the figure. Here, for both the wild-type and cross-linked structures, the variation in the positions of the top and bottom of helix α1 are shown with a traced line for the apo simulation (in black) and the holo simulation (in grey). The lines connecting the centers of mass of the top and bottom of α1 indicate the positions of the helix axes in the starting structure. There is a 2 Å grid behind these traces.

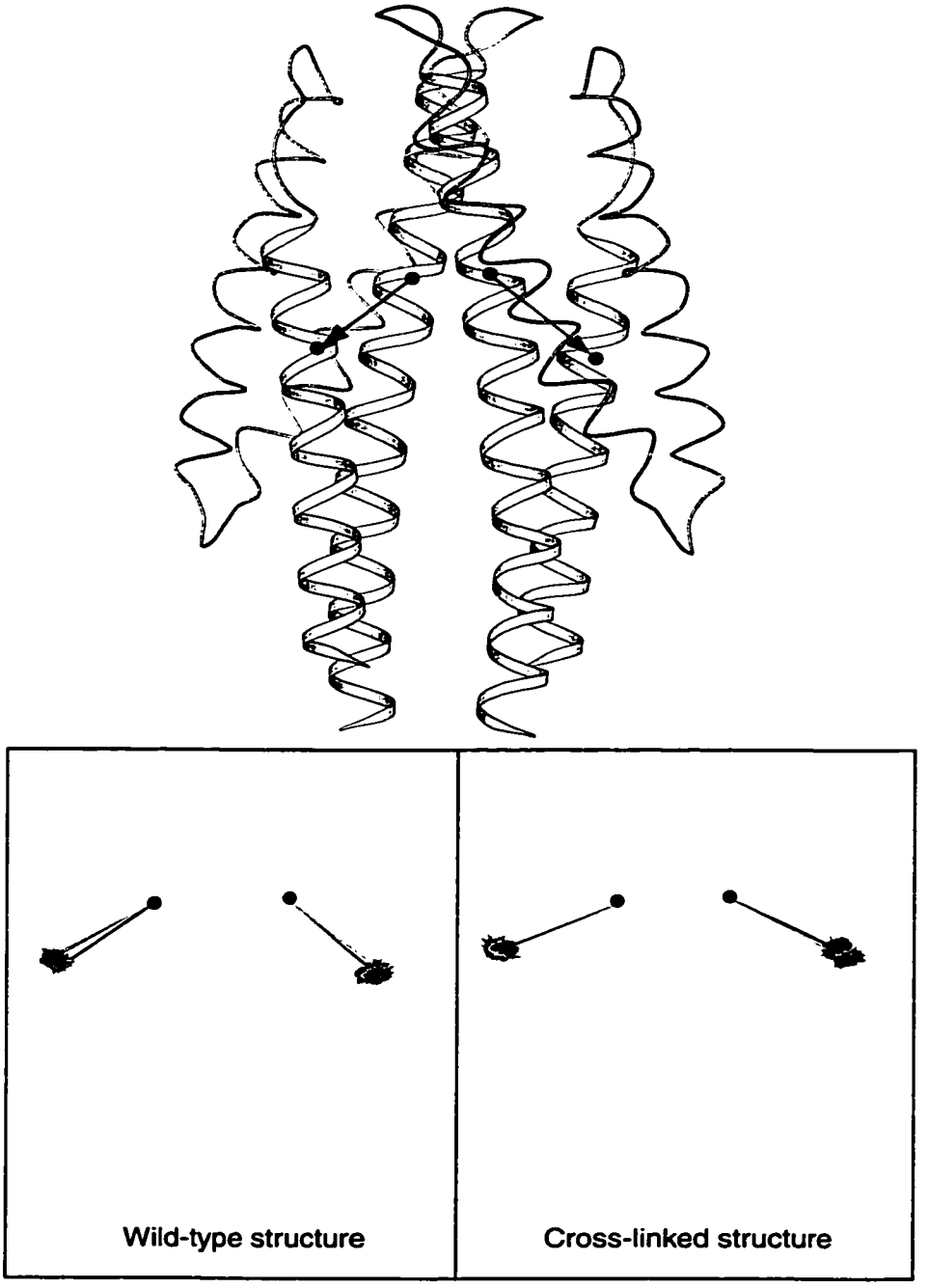

Figure 4.8: Variation in the position of the center of mass of helix α4 relative to the rest of the subunit structure, for the apo trajectory (black line) and the holo trajectory (grey line). The reference structure at the top was made using MolScript [89]. The positions of the center of mass of the helices are indicated with black dots. The grid has a 2 Å mesh.

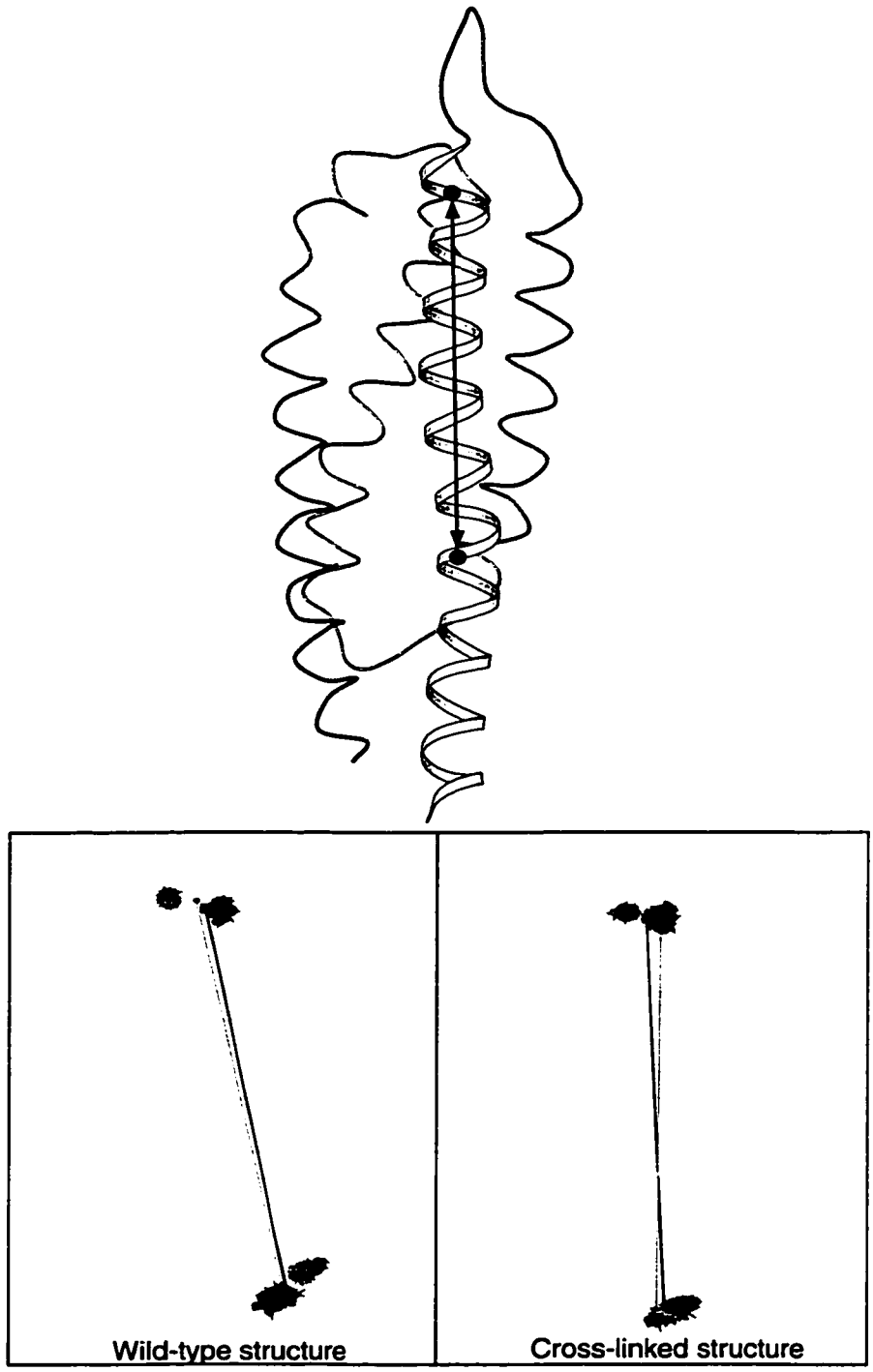

Figure 4.9: Variation in the inter-subunit angle as measured by the position of the axis of helix α1 relative to the opposite subunit for the apo trajectory (black line) and the holo trajectory (grey line). The reference structure at the top was made using MolScript [89]. The positions of the center of mass of the top and bottom of helix α1 are indicated with black dots. The grid has a 2 Å mesh.

Figure 4.9 shows that the variation in the inter-subunit angle over the course of the molecular dynamics simulations is much larger than that seen in the crystal structures. For both the cross-linked and wild-type structures, the crystallized periplasmic domain shows a much smaller difference in inter-subunit angle between the apo and holo forms than is seen in the solvated simulation structures. The direction and magnitude of rotation is qualitatively similar for the cross-linked and wild-type structures, although in the cross-linked structure rotation occurs mainly in the plane of the page, whereas in the wild-type structures the rotation has a component directed out of the page. The disulfide linkage at the bottom of $\alpha 1$ in the cross-linked structure impedes the rotation slightly in that area.

4.5 Conclusions

We did not see any overall difference in the size of the dynamic fluctuations between the apo and holo periplasmic domains of Tar. However, differences in the dynamics of some of the residues in the binding site could be the source of the negative cooperativity of this receptor.

We also resolved some of the confusion due to differences in the two available pairs of apo/holo crystal structures of the truncated periplasmic domain. Crystallization conditions or the removal of the transmembrane and cytoplasmic domains appear to have slightly but insignificantly affected the positioning of the helix $\alpha 4$ in the holo cross-linked structure; they also appear to have damped the size of the inter-subunit rotation that occurs upon aspartate binding. We saw no evidence for an intra-subunit helical sliding motion in the periplasmic domain.

The results from our distance difference analysis and our molecular dynamics simulations of the truncated periplasmic domain of Tar_S provide support for the idea that the conformational change in the chemotaxis receptors upon ligand binding is a rotation of the subunits relative to one another, as was originally suggested by the crystallographers who solved the structure of the periplasmic domain [106, 161, 162, 44]. This model, however, is

at odds with experimental cross-linking studies and our modeling studies (Chapter 3) of the conformational change that takes place in the transmembrane domain of the intact receptor.

Chapter 5

MOLECULAR DYNAMICS OF THE SPIN-LABELED TRG TRANSMEMBRANE DOMAIN

Along with disulfide cross-linking experiments, another alternative method for reliably determining the three-dimensional structure of membrane proteins is the technique of spin-labeling—using nitroxide radicals (or any paramagnetic chemical species) with EPR spectroscopy to obtain information on the local chemical environment and structure around the spin label [35]. This biochemical technique has been used since the 1950s, but it is only in the last decade that spin labels have been incorporated into proteins and used to elucidate their structure. Most of the work in this regard has been pioneered by Dr. Wayne L. Hubbell's laboratory, at UCLA. He has shown that nitroxide spin labels can be used to give both static and dynamic information about membrane proteins: the solvent accessibility, secondary structure, mobility, electrostatic potential, and depth in the membrane of spin-labeled sidechains, as well as changes in these parameters that occur during signaling and function [77].

5.1 Background

5.1.1 EPR spectroscopy

Electron paramagnetic resonance spectroscopy (EPR), which is also sometimes called ESR, or electron spin resonance spectroscopy, is based on the interaction of a magnetic field with the spin or magnetic dipole moment of an unpaired election [35]. A variety of chemical species with unpaired electrons can be used, but the one most often used with membrane proteins is S-(1-oxy-2,2,5,5-tetramethylpyrroline-3-methyl) methanethiosulfonate, shown

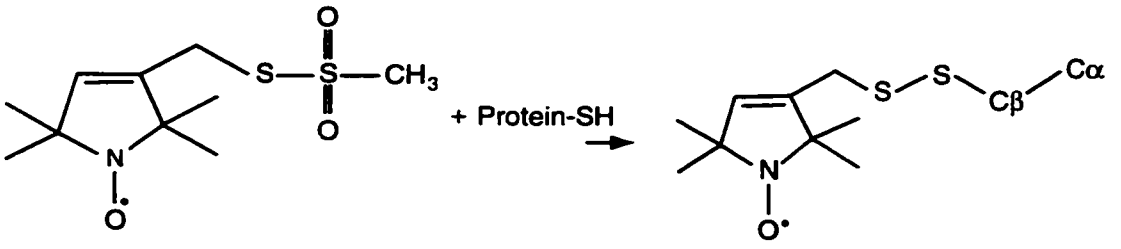

Figure 5.1: The chemical structure of a nitroxide spin label, shown as a free molecule reacting with a cysteine residue, and bound to a protein backbone [78].

in Figure 5.1. This molecule reacts with cysteine residues on a protein to form what is commonly called a nitroxide spin label [78]. The general approach for studying protein structure is to use site-directed mutagenesis to replace amino acids in the protein one at a time with cysteine, and then react the mutants with nitroxide to produce spin-labeled sidechains. Unlike other free radicals, the nitroxide group in this spin label is extremely stable and non-reactive because it is stabilized by the four methyl groups [112]. The unpaired electron is delocalized over the oxygen and the nitrogen, and it interacts with the nuclear spin of the nitrogen atom. The EPR spectra of nitroxides are very sensitive to the local environment of the spin label which makes them ideally suited for examining the details of protein structure [98].

Nitroxide spin labels have a characteristic spectrum with three peaks, corresponding to the interaction of the electron with each of the three spins of the nitrogen nucleus [98]. When spin labels are freely tumbling in solution, this three-peaked spectrum can be described as a superposition of Lorentzian lines. However, when the motion of the spin label is restricted, anisotropies in the signal don't cancel out and the spectrum becomes much more complicated [63]. Generally, interactions between the free electron and neighboring sidechains or solvent molecules, or restrictions in the rotation of the spin label about any of its bonds, show as a loss of resolution in the spectrum or a widening of the lines [98]. In these cases, the EPR spectra cannot be described in simple mathematical terms [5].

Because of the difficulty in analyzing the EPR spectra of spin labels in proteins in a quantitative way, simpler methods have been developed for comparing the spectra of two spin labels at different sites in a protein, under the same experimental conditions. From the differences in EPR spectra, it is possible to deduce information about sidechain packing and solvent accessibility of the spin-labeled sidechain. If a series of mutants is made, with amino acids mutated to cysteine and spin-labeled in sequential order along the polypeptide chain, periodic patterns in the spectra of these mutants can be used to deduce the secondary structure of that region of the protein [3].

The first method for comparing spectra uses the relationship between the amplitude of the signal output and the power of the microwave input. From a graph of power vs. signal amplitude, one can extract a number called $P_{1/2}$ which is a numerical measure of how easily the system can be saturated. The value of $P_{1/2}$ is affected by the environment of the spin label, and can be altered by adding paramagnetic species such as molecular oxygen to the system. When a paramagnetic reagent is present, it can collide directly with a spin label, exchanging spin with the electron, and allowing the system to relax more rapidly to thermal equilibrium [3]. The effect of paramagnetic reagents on the power saturation curve for a protein with a spin label at a given position depends on a wide variety of factors: the concentration of the reagent, its local diffusion coefficient [35], and local steric constraints on the spin label affecting its accessibility to collisions with the reagent [150].

In addition, since the EPR signal given off by a nitroxide spin label in a protein is not a simple Lorentzian curve, the relationship between collision frequency with a paramagnetic reagent and the relaxation time of the system is not a direct one [71]. However, it can be argued that the *change* in $P_{1/2}$ ($\Delta P_{1/2}$) between the same spin-labeled protein with and without a paramagnetic reagent reflects only a difference in relaxation times due to a difference in collision frequency with the reagent, and all other factors will cancel out [3]. Thus the value of $\Delta P_{1/2}$ for spin labels at different positions in a protein is a measure of the relative solvent accessibilities of the spin-labeled residues. A further refinement of this argument uses a normalization of $\Delta P_{1/2}$ to the lipids used to reconstitute the membrane

protein and to the performance of the spectrometer, to give a dimensionless "accessibility parameter" Π:

$$\Pi = \frac{\Delta P_{1/2}(\text{spinlabel})}{P_{1/2}(\text{lipid})} \times \frac{\Delta H(\text{lipid})}{\Delta H(\text{spinlabel})} \tag{5.1}$$

where ΔH is the peak-to-peak line width of the central resonance for each species. Π can be considered a "pure" measure of the frequency of collisions between the reagent and the spin label [60].

The second method for comparing the spectra of two spin labels at different sites in a protein is to use the width and general shape of the EPR signal. Two parameters can be extracted from an EPR signal plot: the total width of the signal along the magnetic field axis, and the line width of the central peak (H_o) [105]. The exact mathematical relationship between these spectral parameters and the motion of the spin label is difficult to calculate, but in general line width depends on the speed of the electron's motion, and the degree of isotropy in its motion. The more rapid and isotropic the motion, the narrower the spectrum [98].

The motion of the nitroxide spin label depends on the flexibility and rotational freedom of the bonds in the spin label itself, the local structure of the protein backbone around the spin labeled residue, interactions of the spin label with neighboring sidechains, and the nature of the surrounding solvent [98]. In general, however, the line width of the EPR spectrum can be considered a qualitative or semi-quantitative measure of the rotational mobility of the spin label [3], where "mobility" is a generalized term meaning both the amplitude and the frequency of the spin label's motion [105]. As with power saturation measurements, the *difference* between two spectral linewidths (ΔH_o) for proteins spin-labeled at different positions gives an indication of differences in mobility between the two positions, because of differences in secondary structure or sidechain packing.

5.1.2 Membrane protein flexibility and dynamics

Dr. Gerald Hazelbauer's group at Washington State University/University of Missouri–Columbia has collaborated with Dr. Hubbell to do spin-labeling experiments with the chemotaxis receptor Trg. Interestingly, the spin-labeling data for Trg do not correlate well with data gathered for other membrane proteins, including bacteriorhodopsin [5, 4], bovine rhodopsin [6], lactose permease from *E. coli* [150, 151], a potassium channel from *Streptomyces lividans* [118, 69], diptheria toxin T domain [113], annexin XII [91], colicin E1 [126], as well as the soluble protein T4 lysozyme [105]. The experimental procedures were very similar for all the proteins, however the average values of the collision frequency Π with (O_2) and the mobility $(1/\Delta H_o)$ were higher for Trg than for any of the other proteins.

One explanation for the discrepancies between Trg and the other membrane proteins is that Trg might simply be a much more structurally dynamic protein, with larger thermal fluctuations of its backbone and/or sidechains. This could be related to the fact that the membrane-spanning region of Trg is a four-helix bundle, whereas the other proteins form larger seven, eight, or twelve-helix bundles. It could also be related to the extensive periplasmic and cytoplasmic domains found in Trg but not in the other proteins.

The folding and packing of integral membrane proteins is driven by the energy of matching hydrophobic regions of the protein sequence with the lipid bilayer, and hydrophilic regions of sequence with water [97]. Within the membrane-spanning portions of the protein, packing of helices depends on the association of hydrophilic residues from different helices, forming hydrogen bonds and electrostatic interactions. This locks the helices into position: they are prevented from moving up and down because of the hydrophobic effect (and often the presence of charged residues at the membrane/water interface) and they are prevented from moving side-to-side because of hydrophilic interactions with the other helices in the protein [149]. Thus, proteins with more transmembrane helices may be more stable, due to more tertiary interactions within the helical bundle.

The mechanism for small-molecule diffusion in a membrane is different from the diffu-

sion of lipids and proteins. If the lipid tails are well-packed around a protein there will be few vacant pockets into which molecular oxygen can diffuse and interact with spin-labels [11]. Thus, for Trg, if the lipid tails are not well-packed around the transmembrane helices, perhaps because it is undergoing large conformational fluctuations, then spin-labeled residues on its surface may be more accessible to O_2 than comparable residues in bacteriorhodopsin or other large and fairly static membrane proteins.

In recent years molecular dynamics (MD) simulations of lipid bilayers have also become a powerful tool for gaining a better understanding of the structure and dynamics of membrane proteins and peptides (see [62] for a recent review). MD simulations can not only provide an atomic-resolution picture of the protein-membrane structure, but can also assist in the interpretation of experimental results. Results from other molecular dynamics studies have shown that it is feasible and useful to perform simulations on membrane proteins to extract information about their dynamic properties and overall flexibility, and that information from such simulations can be correlated with experimental results.

5.1.3 Molecular dynamics of spin labels

It is in theory possible to calculate an EPR spectrum from a molecular dynamics trajectory containing the positions of all atoms in the system over time, by computing the magnetization as a function of time, then taking a Fourier transform [122]. However, since the rotational correlation times of a spin label on a protein range between 10^{-11} and 10^{-6} seconds, a simulation on the order of hundreds of nanoseconds in length is necessary to sample enough conformations of the spin label [134]. Simulations of this length can be done using Brownian dynamics (in which aqueous solvent around the system is approximated by a diffusion tensor added to the interaction energy of the atoms), or stochastic dynamics (in which only a small "reaction zone" directly around the spin label is simulated explicitly, and the rest of the system is only included in the calculations in the form of mean forces) [34], but molecular dynamics simulation times longer than a few nanoseconds remain out of the limit of current computing power, especially for a large system consisting of protein,

lipids, and explicit solvent.

Nevertheless, useful information can be extracted from simulations on the picosecond time scale. In this regime, the nitroxide mainly fluctuates around one potential energy well, with occasional jumps to a different well [135]. Such simulations would allow the contributions of the internal rotation of the spin-labeled sidechain, its interactions with neighboring sidechains, and the movement of the protein backbone as a whole in the spin-labeled region to be to be assessed (at least qualitatively) by observing the behavior of a spin label in a given location. These parameters cannot be independently extracted from an EPR spectrum since the internal dynamics of a nitroxide spin label can be quite complex [105], and EPR spectra for nitroxides attached to a protein are usually heterogeneous, with contributions from several different populations, due to individual spin labels in different proteins sampling different environments [150].

Since spin-labeling of proteins using site-directed mutagenesis to introduce a series of spin labels at different positions is a relatively new technique, little is known about the atomic details of the interactions of spin labels with protein sidechains and lipid molecules. No molecular dynamics simulations (to our knowledge) have been performed on a spin-labeled membrane protein in a bilayer, and only a few MD simulations have been done on spin-labeled proteins of any kind [135, 84]. In fact, the majority of structural and computational studies on membrane proteins have been performed on either larger proteins, such as the G-protein coupled receptors, or on small peptides [26]. The differences in the accessibility and mobility of spin-labeled residues between Trg and other membrane proteins illustrates the need for further studies on a wider range of membrane protein classes. Thus, we performed a set of three molecular dynamics simulations of the transmembrane domain of Trg, spin-labeled at a different position in each simulation, and embedded in a patch of solvated lipid bilayer.

5.2 Methods

We began with our model of the transmembrane domain of Trg, consisting of residues 14-48 in TM1 and residues 196-228 in TM2. These sequences include the hydrophobic lipid-embedded regions, as well as several charged residues on each end that presumably interact with the lipid headgroups. The helix ends were capped with neutral acetyl (Ace) and methyl amide (Nme) terminal residues.

We constructed three systems, with spin labels placed at three different positions on TM1 of Trg: at residue 18 near the N-terminal, a residue which demonstrates unusually high O_2 accessibility and mobility; at residue 31 near the center of the bilayer, which has values for O_2 accessibility and mobility that are close to those of other membrane proteins; and at residue 44 near the C-terminal, which also has unusually high O_2 accessibility and mobility [14]. Residue 18 faces TM1′ in the other subunit, residue 31 faces out toward the lipids and TM2, and residue 44 faces the lipids and TM2′. In all cases the spin label was constructed in an all-trans configuration, with minor adjustments to eliminate steric clashes.

5.2.1 Nitroxide spin label parameters

A nitroxide spin label contains an unpaired electron, which cannot be modeled using standard atom types or residues. Nor is it possible to account for the extra electron by modifying any of the parameters that describe atoms in a forcefield. Therefore, we simply added an extra hydrogen to the structure (Figure 5.2). Although the EPR spectrum of the spin label exists because of its paramagnetic character, the shape of the spectrum is mainly influenced by rotation around the χ angles of the sidechain. Therefore its behavior in the simulation can still be reasonably compared to experimental results, even though the chemical structure of the modeled spin label is slightly different.

The partial charges for an all-atom model of a nitroxide spin label were calculated semi-empirically, using the program MOPAC [137] and the MNDO Hamiltonian [52]. MOPAC uses the electrostatic potential calculation method of Merz and Besler [23], where the elec-

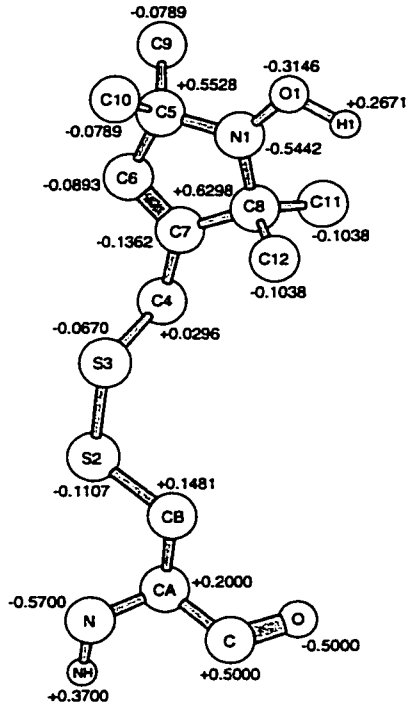

Figure 5.2: Sketch of the modeled structure of a nitroxide spin label residue. The nomenclature used for each atom is indicated, as well as the calculated partial charges on each atom.

trostatic potential of a molecule is calculated on a grid of points, then the resulting surface is fitted to atom centered charges. We refined the results from MOPAC by collapsing the charges on hydrogens bound to non-aromatic carbon atoms to give united atom parameters, setting the backbone and Cβ charges to be close to those of a cysteine residue [155], and forcing the overall charge on the spin label to be zero. Figure 5.2 shows a sketch of this nitroxide spin label structure with the calculated partial charges.

5.2.2 DPPC lipid parameters

The full physiological activity of cellular membranes is certainly due to the interactions between all their constituents, such as lipids, proteins and sugars, but modeling of these

complex molecular assemblies is currently unfeasible. However, simpler model membranes can provide valuable insights into the interactions between peptides and lipid molecules. One convenient model system is a hydrated bilayer consisting of dipalmitoylphosphatidylcholine (DPPC) lipids, since this bilayer has been well characterized through experiments and molecular dynamics studies.

The initial structure of the DPPC lipids was derived from the X-ray crystal structure of the dihydrate of the closely related lipid dimyristoylphosphatidylcholine (DMPC) [117]. The unit cell contains two distinct conformations of the DMPC molecule, labeled A and B. The head groups of these two conformers exhibit approximate mirror image symmetry [73]. We constructed the DPPC molecule using the coordinates of both DMPC conformers as templates, by adding two carbon atoms to the ends of the hydrocarbon chains. The dihedral angles were arranged in an all-trans conformation.

Partial charges for the phosphocholine head group as well as the glycerol backbone were derived from electrostatic potential calculations using the program GAUSSIAN 90 with a 6-31G* basis set [64]. The final atomic charges were obtained by fitting the calculated charges to a united atom model of zero total charge using CHELPG [33]. The same charge parameters were used for both head group conformers. Standard AMBER parameters were used for bond, angle, and torsion interactions [155], with OPLS parameters for the van der Waals interactions [83]. Figure 5.3 shows a sketch of this DPPC lipid structure with the calculated partial charges.

5.2.3 Bilayer construction

The best way to build a starting structure for a membrane protein in a bilayer is still under some debate. Difficulties include inserting the protein into the bilayer while eliminating steric clashes between lipid and protein atoms, as well as establishing the correct surface area for the lipids and protein, which is vital for keeping the system in the right phase [74, 141] and reproducing experimental data [61]. In general, two different methods have been used. The protocol developed by Woolf and Roux [158] involves randomly selecting lipids

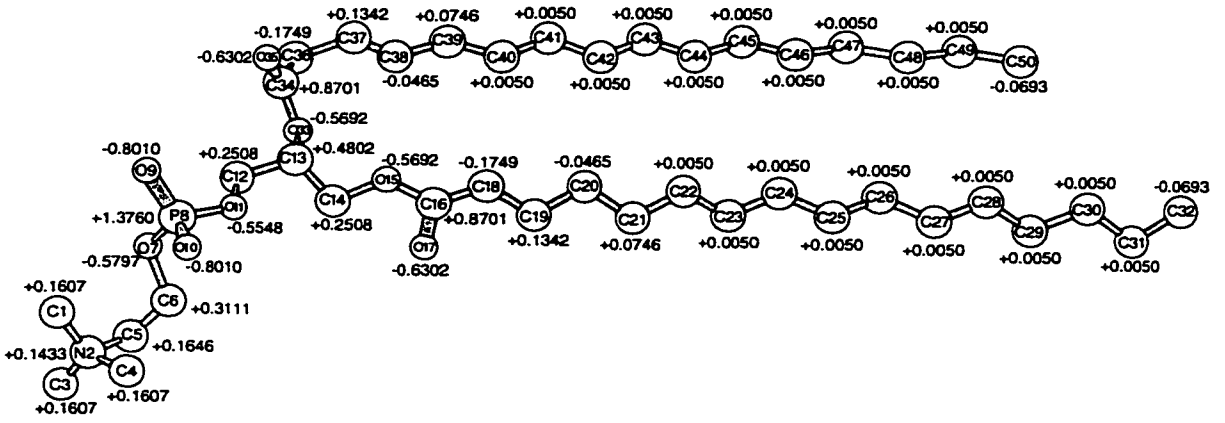

Figure 5.3: Sketch of the structure of a dipalmitoylphosphatidylcholine molecule. The nomenclature used for each atom is indicated, as well as the calculated partial charges on each atom.

from a library of pre-equilibrated conformers, which are then placed around the protein with the appropriate area per headgroup, and rotated to reduce or eliminate overlap of lipid and protein atoms. The second general method, first proposed by Shen et al. [129] involves starting with a pre-equilibrated bilayer, then deleting lipids and (optionally) using a weak repulsive force to clear out a hole into which the protein is inserted. This latter method works best for small, symmetric proteins. A disadvantage of the first method is that it is difficult to construct large amounts of bilayer around the protein, which is necessary for simulations in which protein-lipid interactions are to be analyzed [142].

The thermalization and equilibration procedure that we apply in our simulations, as outlined below, makes the choice of the initial configuration less critical. Our initial configuration is constructed so as to be structurally very different from the equilibrated bilayer structure, and the subsequent equilibration of our molecular dynamics simulations is accelerated by incorporating a specifically devised "simulated annealing" protocol.

We first constructed a lipid monolayer by placing the phosphorus atoms of the DPPC lipids on a rectangular lattice in the x-y plane. The lattice sites of the phosphorus atoms

were equally spaced along the Cartesian coordinate axes, leading to an area per lipid molecule of 49 Å. The two lipid conformers were placed in alternating order along the x-axis, which allows the charged headgroups to stack against each other without unfavorable electrostatic interactations. The hydrocarbon chains of each lipid molecule were aligned parallel to the z-axis, while the dipole moments of the two conformers were pointed along the two x-y plane diagonals, respectively. The opposing leaflet of the bilayer was then obtained by rotational symmetry about the y-axis. The bilayer thickness, defined by the distance between the phosphorus atoms of the opposing leaflets, was initially set to 48.5 Å.

Some lipids were removed from the center of this bilayer to make a hole big enough for the receptor transmembrane domain, and the three spin-labeled Trg structures were each inserted into a separate bilayer. The resulting structure consisted of 142 lipid molecules. We positioned the receptor in the bilayer based on the positions of tryptophan and arginine residues on either side of the transmembrane domain. These residues are known to interact with the lipid headgroups, and are preferentially found on edges of TM domains [121, 158]. We added twelve chloride counter-ions to neutralize the system, placing them on a 1 Å grid using a Coulombic potential. Figure 5.4 shows the positioning of the receptor in the bilayer, and the locations of the chloride counter-ions, which are clustered around the positively charged arginine residues at the ends of the helices. The bilayer was centered in a periodic box with dimensions measuring 78 Å $\times$ 76 Å $\times$ 75 Å. Voids in the box above and below the bilayer were filled with TIP3P water molecules [82], excluding the region occupied by the lipid hydrocarbon chains.

The advantages of this method for constructing a protein-bilayer system are that there is no need of a pre-equilibrated bilayer or a library of lipid conformers, and it is easy to incorporate membrane proteins of any size and shape by simply deleting lipids from the lattice-like starting bilayer configuration. There is also no need to carefully choose the surface area values for the system components; these are difficult to determine experimentally for membrane proteins anyway. As shown below, our system "collapses" from an initial area per lipid and bilayer thickness that are somewhat larger than those measured experi-

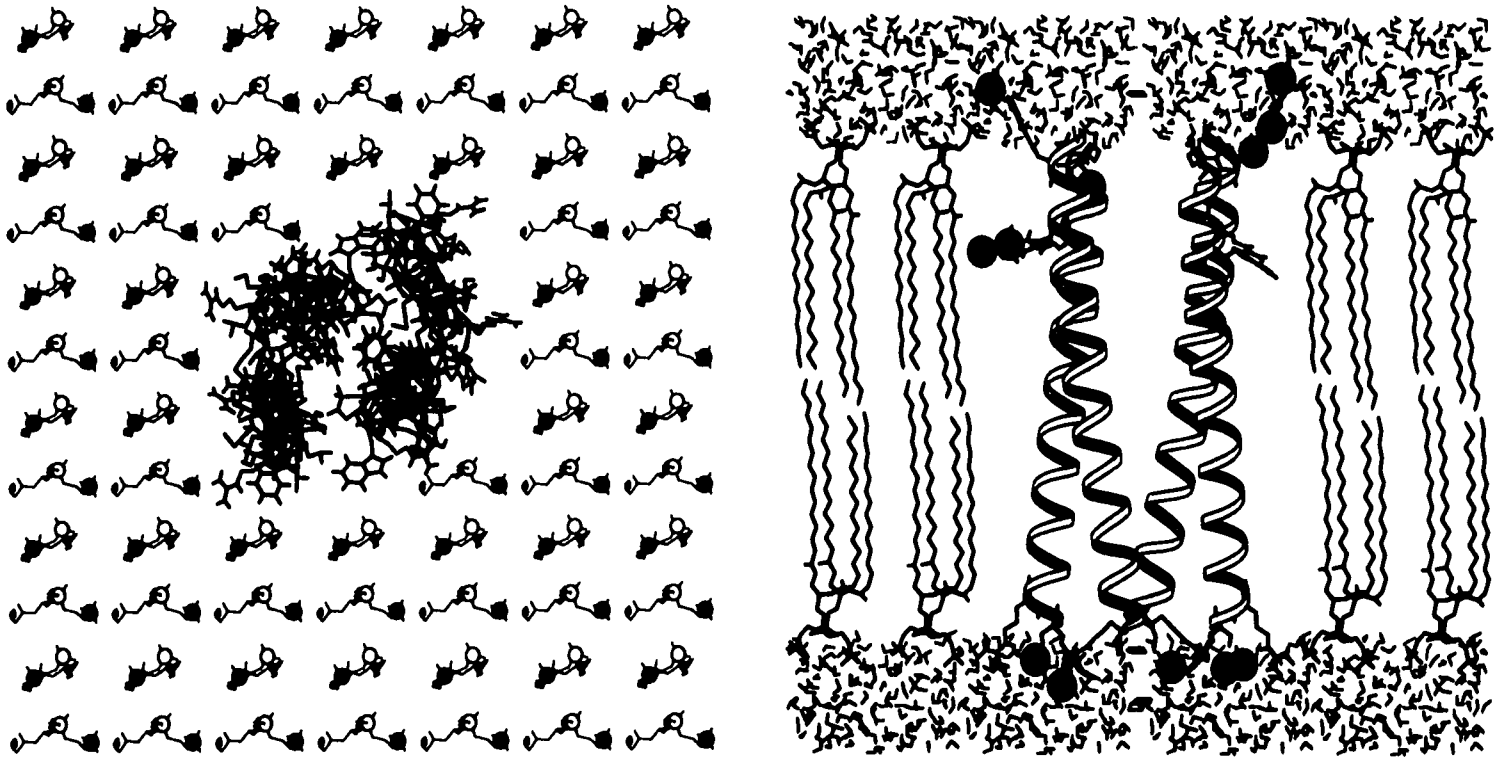

Figure 5.4: Top and side views of the starting configuration of Trg in the bilayer. In the top view, the phosphorus and nitrogen atoms of the lipids are represented by yellow and blue spheres, respectively. Only the upper layer of lipids is shown in the top view for clarity. In the side view water molecules are included in line drawing representation to illustrate the initial hydration level of the lipid head groups. Note the symmetry of the initial structure about the y-axis as well as the interdigitation of the hydrocarbon chain ends. Arginine residues, which mark the boundaries of the transmembrane domains, are shown in red. The chloride counter-ions are shown as green spheres. This figure was made using MolScript [89].

mentally to equilibrium values that are in reasonable agreement with experimental data and other simulations.

5.2.4 Computational details

All molecular dynamics was run using AMBER 5.0 [38]. A residue-based cutoff of 10 Å for the non-bonded interactions was employed. Long-range electrostatic interactions were modeled by the particle-mesh Ewald summation technique [51]. Periodic boundary conditions were used in all simulations resulting in an infinite multilayer system. The integration time step was set to 1 fs, and a dielectric constant of 1 was used. All hydrogen bond lengths were restrained to their equilibrium values using SHAKE [125]. The system temperature of 320 K was maintained using the Berendsen algorithm [22] with time constants for heat bath coupling of 0.5 ps for the solvent and 1.0 ps for the solute. The system pressure was coupled anisotropically to a Berendsen pressure piston [22] at 1 atm with a relaxation time of 1.0 ps. The coordinates of the system were written to disk every 200 steps, or 0.2 ps.

5.3 Equilibration protocol

We developed a procedure for the equilibration of lipid bilayers to rapidly induce disorder and bring the bilayer to thermal equilibrium [88]. A variation on this thermalization and equilibration protocol was applied to insure proper equilibration, and to achieve values for the area per lipid and the bilayer thickness that are close to experimentally observed values. This protocol imparts a large amount of disorder to the lipid hydrocarbon tails in a fairly short amount of time. The system moves from the initial crystalline lattice-like state to the physiologically relevent L_α state in two stages—first the hydrocarbon tails in the interior of the bilayer are melted, and then the headgroups follow. In comparison, systems that were started without the simulated annealing protocol did not yield a equilibrated system in which the geometric parameters of the lipid phase converged towards their experimental values (data not shown). With our method we are ensuring that the lipids have had fully

enough time to react to the presence of the protein. Since our starting structure is very different from the final equilibrated structure, we eliminate any effects of the initial configuration on our simulation results, and the system does not retain any "memory" of its starting configuration.

5.3.1 Thermalization

The three systems were first minimized for 100 steps with only water molecules and ions allowed to move, then for 200 steps with all atoms moving. Since the water boxes were constructed by abutting several small equilibrated boxes of water, any periodic structure remaining in the water was removed by running 5000 steps of molecular dynamics at constant volume and low temperature, allowing only water molecules and ions to move. This eliminates the possibility of spurious forces acting on the protein structure during subsequent dynamics runs [9, 70].

The systems were brought to thermal equilibrium by running constant volume molecular dynamics in 10 runs of 200 steps each, reassigning the atomic velocites to a different Maxwell-Boltzmann distribution at 320 K after each run.

5.3.2 Hydrocarbon chain relaxation

To rapidly induce disorder in the lipid hydrocarbon chains, the lipid headgroups and water atoms were held fixed over the course of the next 50 ps, and the hydrocarbon chains were gradually relaxed. For the first 10 ps, only the terminal methyl group plus two ethyl groups were allowed to move, then for the next 10 ps those atoms plus three more ethyl groups were allowed to move, and so on, increasing the number of moving carbon atoms in groups of three until the entire lipid tail was free to move.

5.3.3 Simulated annealing

During the third part of the equilibration procedure, the water and the lipid head groups were constrained, and simulated annealing was performed in the following way: (1) the temperature was raised to 500 K in increments of 50 K over a time period of 10 ps; (2) the temperature was held constant at 500 K for an additional 10 ps; (3) the temperature was gradually lowered to 292 K in steps of 10 K, over the course of 40 ps. Steps (1) through (3) were repeated three times to assure satisfactory randomization of the lipid sidechain conformations.

As a lipid bilayer moves from the initial highly ordered crystalline state to the physiologically relevant liquid L_α phase, the thickness of the bilayer is reduced. With an increase in thermal disorder, the overall length of the lipid tails shortens due to an increase in the number of *gauche* dihedral configurations in the hydrocarbon chain. To accelerate the phase change in the simulated bilayer, we manually reduced the bilayer thickness during the simulated annealing phase of equilibration. Before cooling down for the third time, we wrote out the coordinates of the atoms in the system and altered the structure of the bilayer by translating the leaflets towards one another by 6 Å. We then added new TIP3P water to fill the gap in the periodic box, and repeated the thermalization and simulated annealing procedures. Once again, before cooling down for the third time during the simulated annealing, we wrote out the coordinates of the atoms to a file and translated the leaflets of the bilayer towards one another by 3 Å. We then added new TIP3P water, and repeated the thermalization and simulated annealing procedures for the third time.

5.3.4 Equilibration

Following the simulated annealing of the hydrocarbon chains, we continued the thermalization of the system by switching to an isotropic constant pressure ensemble (NPT) and allowing the dimensions of the periodic box to relax. The backbone atoms of the receptor were tethered in place with a 25 kcal/mol restraint for the next 400 ps of molecular dynam-

ics. The simulations were then run for a total of 2 ns at constant pressure and temperature. The final 1000 ps of the trajectories was used for subsequent analyses.

As with the Tar simulations (Chapter 4), we assessed the progression of the simulations toward equilibrium by monitoring the RMS deviation of the receptor backbone from its starting configuration. This gives an indication of the stability of the receptor in the bilayer.

Any global translation or rotation due to diffusion of the protein was removed by superimposing the backbone atoms in each frame onto the starting conformation of the protein, using a mass-weighted root-mean-square fitting algorithm. The value of the RMS deviation of the coordinates of each frame was calculated using the analysis program PTraj, which is part of AMBER [38]. The time evolution of the RMS deviation from the starting structure for the three systems is shown in Figure 5.5. For all the systems, the RMSD gradually reaches a stable value of about 3.5 Å, after approximately 1000 ps of equilibration.

5.4 Bilayer geometry

In order to validate our molecular dynamics simulations and ensure that they had reached equilibrium, we examined the structural features of the bilayer. The geometric measurements we made included the area per lipid, the bilayer thickness, and the periodic box dimensions. We calculated the area per lipid by simply dividing the periodic box area in the x-y plane by the number of lipid molecules in one membrane layer. The thickness of the bilayer was determined by the average distance between phosphorus atoms in opposing leaflets.

The convergence of these three structural parameters, along with the total energy of the system (the sum of the kinetic and potential energies) is displayed in Figure 5.6. Our simulations reach equilibrium after a simulation time of approximately 1000 picoseconds. This is a rather long equilibration time compared to methods for constructing protein-bilayer systems which rely on a pre-equilibrated bilayer, where the system is typically re-equilibrated after the insertion of the protein for 100–300 ps [129, 142, 45, 12]. However, it is not

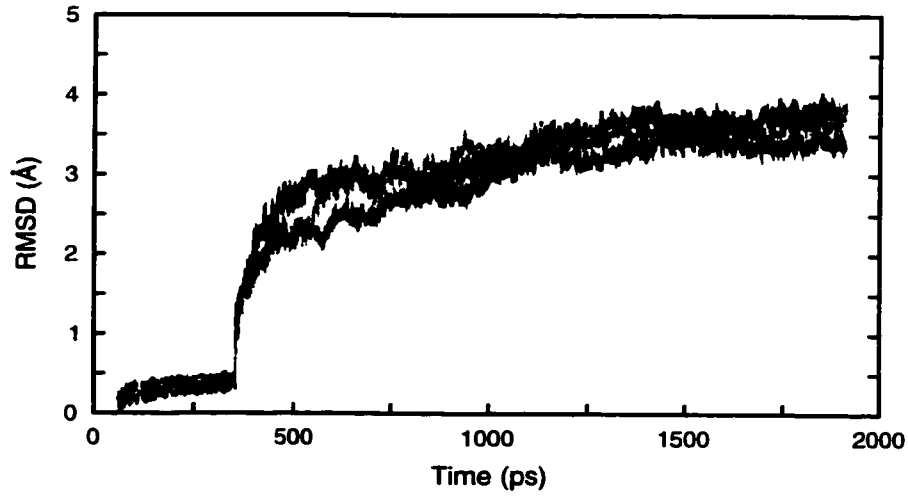

Figure 5.5: Root mean square deviations of the Trg receptor backbone in the three spin-labeled systems from its starting coordinates, monitored as a function of simulation time. The black line represents the system spin-labeled on residue 18, the dark gray line represents the system spin-labeled on residue 31, and the light gray line indicates the system spin-labeled on residue 44. All simulations reach an equilibrium after approximately 1000 ps of simulation time. During the first 400 ps of the simulation, the backbone atoms of the receptor were fixed in place.

clear whether a bilayer that has been severely perturbed by the insertion of a membrane protein has really returned to equilibrium after only a few hundred picoseconds. While the energy of a bilayer system has typically stabilized after a relatively short time [61, 45], longer-term molecular dynamics and stochastic dynamics simulations have found, as we did (Figure 5.6), that the structural properties of the bilayer such as the area per lipid and the thickness can take 500 ps or longer to reach equilibrium [146, 131].

The equilibrium values for our geometric measurements of area per lipid and bilayer thickness are slightly below the values of these parameters from experimental measurements [145]. This is due to the fact that using OPLS parameters for the lipids yields a smaller lipid volume than that observed experimentally [133].

5.5 Behavior of spin-labeled sidechains

To assess the overall mobility and behavior of the spin-labeled sidechains in our simulations, we examined their internal rotation and the movement of the protein backbone as a whole in the spin-labeled region. The contributions from these different factors cannot be distinguished experimentally, but our molecular dynamics simulations allow us to examine the motion of the nitroxide spin label at an atomic level of detail.

5.5.1 Internal rotation

In the experiments with Trg, EPR spectra for some of the spin-labeled residues showed contributions from two mobility states of the spin label [14]. Two or more mobility states can arise if the spin-labeled protein is present in more than one folded form, or if the spin label itself exists in two or more different rotamers that are not averaged out on the time scale of the EPR measurements [105]. This latter possibility may be particularly likely with the homodimeric Trg, since if it is spin-labeled at one position in the polypeptide chain, there will be two spin-labeled residues present in the folded receptor. For reference during the discussion in the following section, the structure of a nitroxide spin-labeled sidechain

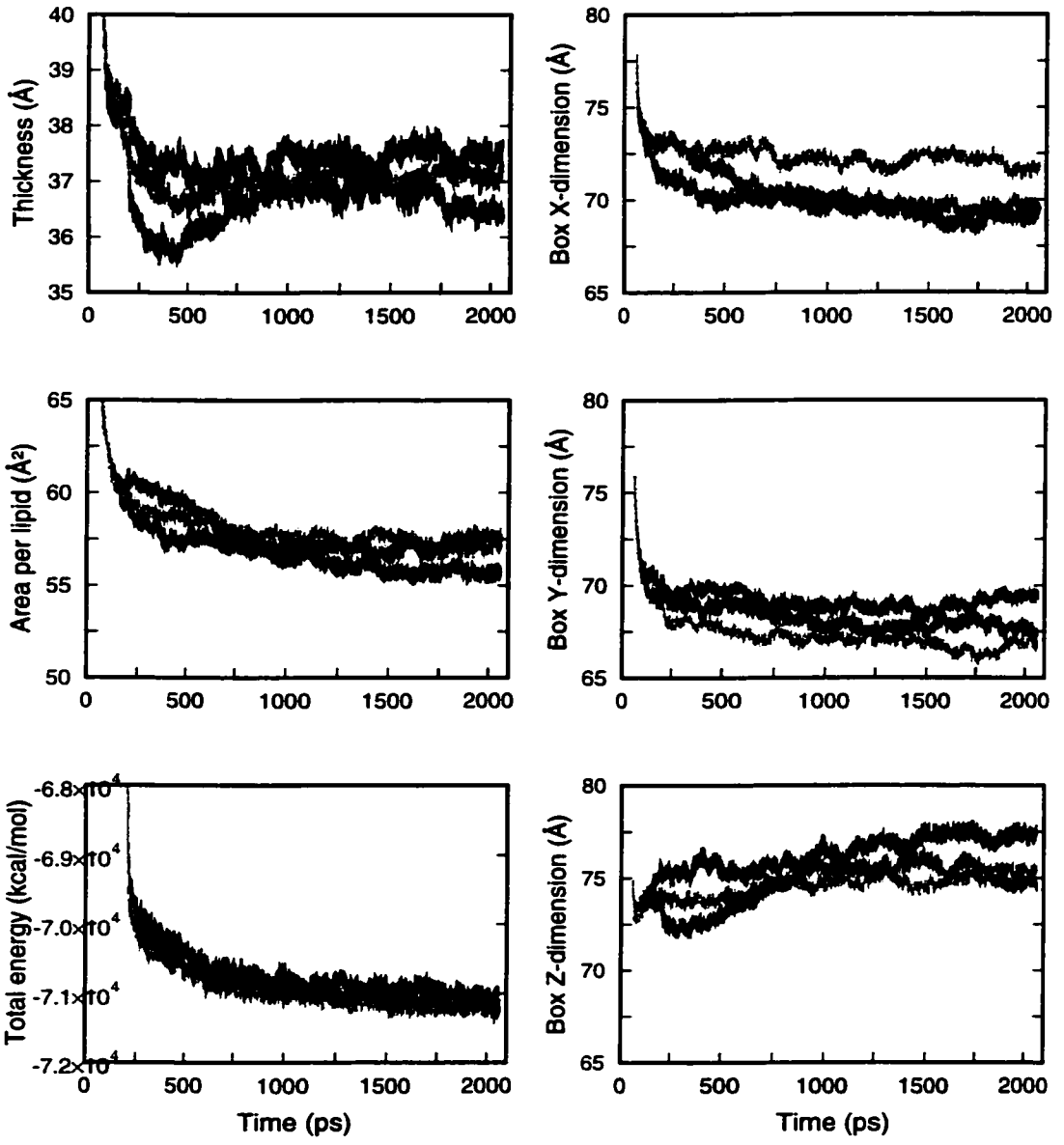

Figure 5.6: Lipid bilayer thickness, area per lipid, and periodic box dimensions for the three spin-labeled Trg systems monitored over the course of the simulations. Black lines represent the system spin-labeled on residue 18, dark gray lines represent the system spin-labeled on residue 31, and light gray lines indicate the system spin-labeled on residue 44. All simulations reach an equilibrium after approximately 1000 ps of simulation time.

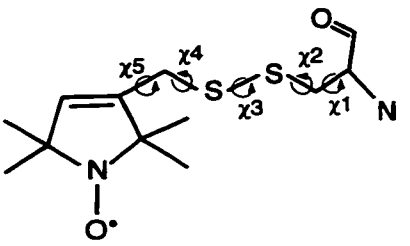

Figure 5.7: The dihedral angles χ_1, χ_2, χ_3, χ_4, and χ_5 of a nitroxide spin-labeled sidechain.

with the dihedral angles labeled is shown in Figure 5.7. The EPR spectrum of the spin label depends on the rate of rotation of all of these bonds, as well as on the movement of the protein backbone in the region of the spin-labeled residue [105].

To assess the contribution of internal rotation of the spin label about its dihedral χ angles to its overall mobility, we examined the rotameric states of the spin labels during the molecular dynamics simulation. For each frame in the equilibrated simulation, the χ angles of each nitroxide spin label were calculated using the analysis program CARNAL [124]. The distributions of these dihedral angles are shown in Figure 5.8.

We see that all three spin-labeled sidechains in our simulation adopt conformations about their χ_1 and χ_2 angles that are similar to those seen in crystal structures of spin-labeled T4 lysozyme [92], with narrow distributions at either $-60°$ or $180°$. The exception to this is the spin label at position 31, which shows χ_1 angles of $\sim -90°$ and $\sim -50°$, for reasons that are unclear.

The spin labels at positions 18 and 31 show similar distributions of the χ_3 angle around $90°$, which is the minimum energy configuration of a disulfide bond. Rotation about a disulfide bond has a barrier of $\sim$7 kcal/mol, so on the time scale of EPR and molecular dynamics this dihedral angle is essentially static [105]. However, χ_3 in the spin label at position 44 shows a population in one subunit at an angle of $-90°$. This would give rise to two distinct components in the EPR spectrum.

For a solvent-exposed disulfide on the surface of a helix, rotation about χ_1 is restricted

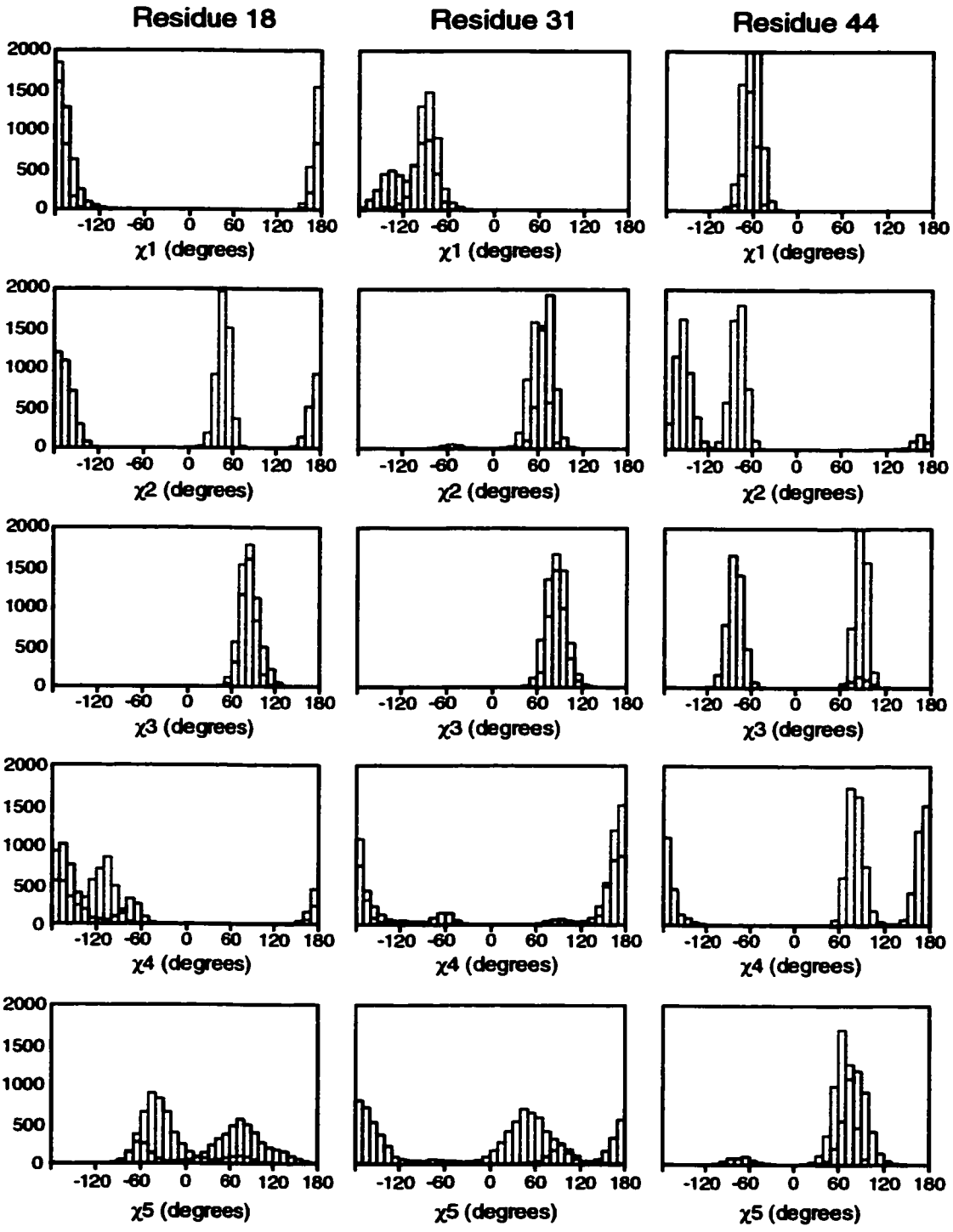

Figure 5.8: Histograms of the dihedral angle distributions of spin-labeled sidechains over the course of the simulation, binned in 10-degree increments. The three columns show χ values for the systems spin-labeled on residues 18, 31, and 44, respectively. Sidechains from the two different subunits are indicated with red and blue lines.

by steric interactions of the Cβ atom with the backbone of the helix. The crystal structures of spin-labeled T4 lysozyme showed that the disulfide linkage also interacts with the protein backbone, perhaps through a non-conventional hydrogen bond between the S3 atom (see Figure 5.2) and the Cα hydrogen atom [92] or through van der Waals interactions [105]. This implies that for spin labels in regions of helical secondary structure, χ_1, χ_2, and χ_3 are essentially static. The degree of mobility of the nitroxide is thus thought to be determined by the motion of the protein backbone and by rotations of the nitroxide ring itself about χ_5 [92]. In our simulations, the spin labels at positions 18 and 31 both show a wide distribution of angles for the χ_4 and χ_5 dihedrals, suggesting that spin labels at these positions would exhibit high mobility. The spin label at position 44 is more restricted.

These results suggest that the force field parameters we used are reasonable, and the trajectory provides a good picture of the behavior of a nitroxide spin label in a nanosecond time regime. However, perhaps because these trajectories are not long enough, we do not see any indication of higher-than-normal mobility in the spin labeled residues being caused by increased rotation about the sidechain dihedral angles.

5.5.2 Motion of protein backbone

To examine the contribution of the size of the thermal fluctuations of the protein backbone to the overall mobility of the spin labels, we calculated the root-mean-square fluctuations of the backbone atoms of the receptor over the course of our molecular dynamics simulations. As with the RMSD calculations, we removed any global translation or rotation by superimposing the backbone atoms in each frame in the equilibrated portion of the trajectory (5000 frames for each simulation) onto the starting conformation of the protein, using a mass-weighted root-mean-square fitting algorithm. The values of the RMS fluctuations for the backbone atoms in each residue were calculated using PTraj [38], averaged, and are shown in Figure 5.9.

There is no indication that the spin-labeled residues have larger backbone fluctuations than the rest of the residues. In fact, the spin labels seem to stabilize the helices, especially

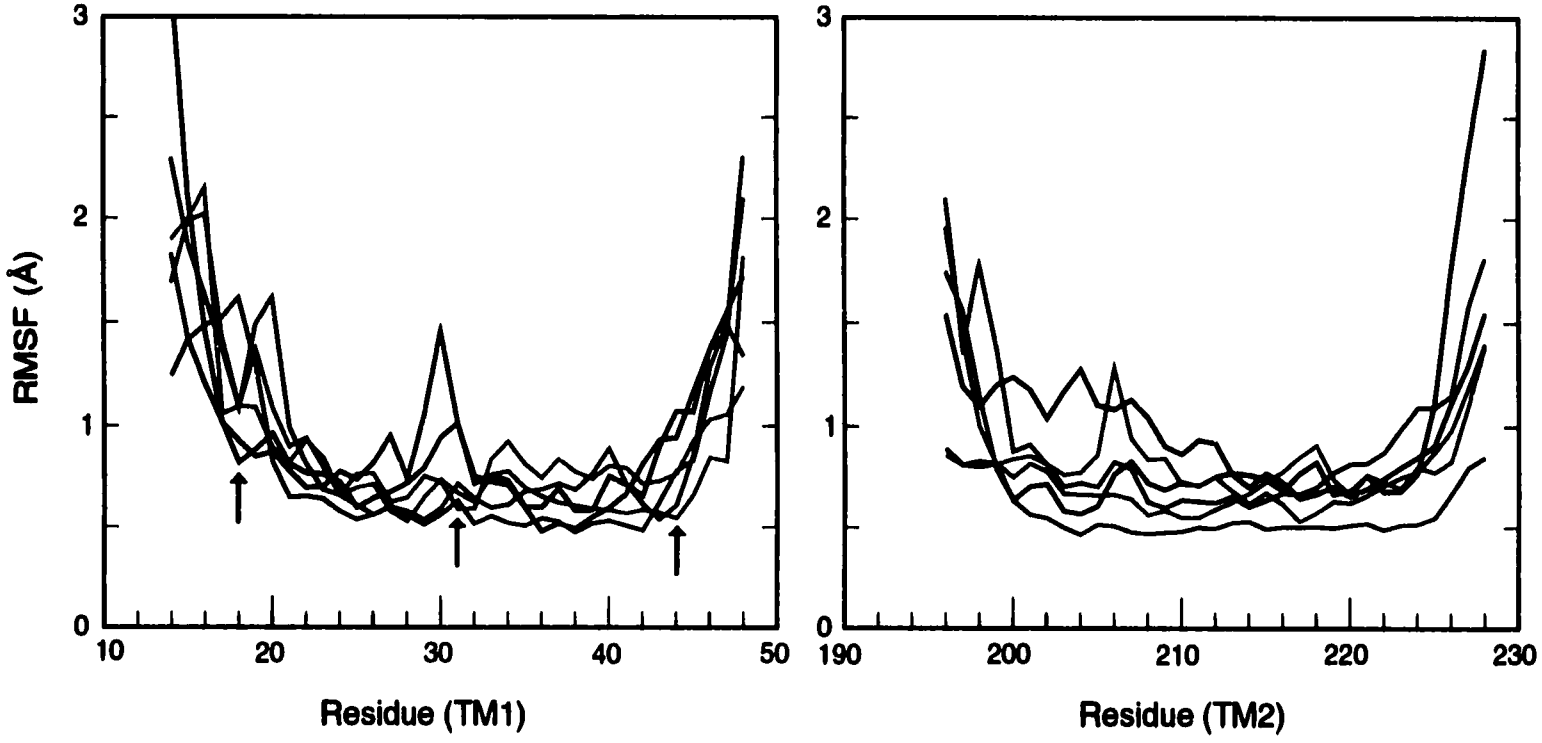

Figure 5.9: Root-mean-square fluctuations of the spin-labeled Trg receptor backbone over the course of the 1000 ps equilibrated trajectories. The left panel shows the fluctuations of TM1, and the right panel shows TM2. The blue lines represent the system spin-labeled on residue 18, the red lines represent the system spin-labeled on residue 31, and the green lines indicate the system spin-labeled on residue 44. The locations of the spin-labeled residues are indicated by arrows.

in the case of residues 18 and 44, where receptors spin-labeled at those positions show lower RMS fluctuation values than the other receptors. In comparison with the RMS fluctuations of the periplasmic domain of Tar (Figure 4.3), however, the transmembrane domain of Trg shows much greater mobility, as well as greater variation in the flexibility of individual helices within the membrane-spanning helical bundle. The core hydrophobic regions of the transmembrane helices in Trg also show somewhat greater RMS fluctuations than those reported in other molecular dynamics studies of membrane proteins: bacteriophodopsin in a patch of purple membrane [55], the β-sheet regions of the OmpF porin [142], alamethicin [143], and a potassium channel [132].

One concern in a simulation with the isolated transmembrane domain of the receptor is that, in the absence of the periplasmic and cytoplasmic domains, the helical ends might display abnormally dynamic behavior and so influence the flexibility of the protein backbone in the region of the spin label. As shown in Figure 5.9, however, all three spin labels seem to be in stable helical regions of the receptor. The helix ends do display increased amplitude of motion, but for the most part the portion of the helices, including the spin-labeled residues, that is in the hydrophobic part of the bilayer remains fairly stable.

5.6 Conclusions

It appears that the high mobility and O_2 accessibility of spin-labeled residues in Trg relative to other membrane proteins may be due to higher flexibility of the protein backbone. The traditional view of the flexibility of membrane proteins is that while their internal flexibility is comparable to soluble proteins [49], the sidechains in contact with lipids are far more restricted than external sidechains in contact with water, because water as a solvent promotes flexibility and conformational changes through hydrogen bond exchange, whereas lipids cannot form hydrogen bonds and so they tend to stabilize protein conformations [10].

However, in a ^{13}C-NMR experiment comparing crystals of cytochrome-c oxidase in detergent to crystals of lysozyme, Tuzi et al. found that the backbone carbonyl and α-carbons

were more flexible in cytochrome-c oxidase than in lysozyme, whereas the mobilities of sidechain carbons were similar for the two proteins [148]. Additionally, elastic incoherent neutron scattering experiments on bacteriorhodopsin have shown that within this protein there are regions that differ in their flexibility. There appears to be a "rigid anchor" region, composed of the retinal binding pocket and the extracellular half of the protein. (The photo-isomerization of the retinal from *cis* to *trans* and back to *cis* during the photocycle needs a fairly rigid structural environment for optimal function.) In contrast to this rigid region, the cytoplasmic half of the structure is more flexible, and it is here that the larger conformational changes that change the solvent accessibility of the Schiff base take place [120].

This experimental work is supported by computer simulations of bacteriorhodopsin. In a simulated annealing study of the M412 intermediate, Xu et al. found significant conformational changes (bending) in the cytoplasmic portions of helices F and G, and a small translational change in helix E, but no large movements in any of the other helices [159]. In a molecular dynamics study of a trimer of bacteriorhodopsin, complete with purple membrane lipids and water, Edholm et al. found that the RMS fluctuations of the loops and helices in the cytoplasmic half of the membrane were greater than those in the periplasmic half [55]. Another molecular dynamics study by Woolf on the individual helices of bacteriorhodopsin, surrounded by a DMPC lipid bilayer in a hexagonal periodic lattice, found that the helices differed strikingly in the types of motions they exhibited, in their hydrogen bonding patterns, and in their backbone $\phi - \psi$ angles. Two overall patterns of helix motions were observed: one in which the helix fluctuates evenly along its axis, and the other in which greater fluctuations were observed near the membrane boundary, with smaller fluctuations at the interior of the membrane. He concluded that the amino acid sequence of a transmembrane helix can have a strong effect on its stability and interactions with the surrounding membrane [157].

These results suggest that different parts of the same membrane protein can have widely varying conformational flexibilities and types of motion. It seems possible therefore that

different proteins could also exhibit variations in their ranges of dynamic behavior, based on differences in sequence and in function. A variety of experimental evidence suggests that the transmembrane domain of the chemotaxis receptors is flexible and loosely packed. This may be essential for their function: as we showed in Chapter 3, signaling by these receptors appears to require large movements of the transmembrane helices relative to one another, which could occur with low energy in a flexible transmembrane domain.

Chapter 6

SUMMARY AND CONCLUSIONS

Ligand binding to the periplasmic domain of a bacterial chemotaxis receptor leads to a conformational change in the receptor that sends a signal through the membrane and initiates the signaling pathway of bacterial chemotaxis. Although chemotaxis is perhaps the most well-understood and thoroughly studied cell signaling pathway, some aspects are still unknown, notably the nature of the conformational change that occurs in the chemotaxis receptors upon ligand binding. Since this conformational change has a broad relevance to many other signal transduction pathways, a greater understanding of this process would be useful.

There is a large amount of experimental data available on the structure of the chemotaxis receptors, yet much of it seems contradictory. We therefore performed a series of computer modeling studies to consolidate and resolve the contradictions in the available experimental data, and to formulate a description of how the receptor structure changes with signaling.

6.1 Models refined by experimental data

The first step in our modeling was to create detailed models of the periplasmic and transmembrane domains of the chemotaxis receptor for aspartate, Tar, and the receptor for ribose and galactose, Trg. These two receptors have been the focus of most of the experimental work to date on the structure of chemotaxis receptors.

High-resolution structural information is not available for the transmembrane domains of these receptors, so we needed to build molecular models of this four-helix domain. In the first stage of modeling, we used the coordinates of an unrelated four-helix coiled coil

as a template for the transmembrane domain, positioning this template by fusing it with the X-ray structure of the periplasmic domain of Tar_S. There is significant experimental data about transmembrane structure for the closely related receptor Tar_E, as well as for the more distantly related Trg. Thus we created models of the periplasmic plus transmembrane domains of both Tar and Trg. Preliminary studies indicate that the periplasmic domain of Tar_S provides a valid template for the periplasmic domain of Trg even though sequence relationship is marginal.

We used data from oxidative cross-linking experiments to test and refine these first-stage models of the transmembrane domain, and found that for the most part the models corresponded well with the experimental data. One exception to this was the register of helix TM2 relative to TM1. We found that adjusting the position of TM2 by sliding it along its long axis toward the periplasm by several Ångströms provided a good alignment of residues in the TM1–TM2 interface with high propensities for cross-linking.

The fact that this correction was necessary in order to make models of the transmembrane domain derived from extending the helices of the periplasmic domain agree with experimental data on cross-linking propensities implies that the position of α4/TM2 that is seen in the crystal structures of the truncated periplasmic domain is shifted toward the cytoplasm relative to the average conformation of intact, membrane-embedded receptor, the state probed in cross-linking studies.

6.2 Ligand-induced conformational changes

Three general theories about the nature of the conformational change upon ligand binding in the chemotaxis receptors have been proposed: a sliding motion of helix α4/TM2 along its axis, a rotation of the two subunits in the receptor dimer relative to one another, or a change in the dynamic motion of the receptor as a whole. The next step in our modeling was to use our detailed models for the transmembrane and periplasmic domains of Trg and Tar to examine how the structural relationships among the helices are altered by these

proposed conformational changes. We tested the three theories using a method related to targeted energy minimization [56] on our refined structures of the periplasmic plus transmembrane domains of Trg and Tar, coupled with molecular dynamics simulations of the isolated periplasmic domain of Tar and the transmembrane domain of Trg in fully solvated environments.

Many studies of ligand-induced conformational changes in the chemotaxis receptors have used oxidative cross-links between cysteines introduced into adjacent helical segments (reviewed in [58]). Several studies determined whether signaling was blocked by specific cross-links [128, 43, 41, 96]. An assumption in these original investigations of the effects of disulfide cross-links on receptor signaling was that cross-links that blocked signaling would identify helical interfaces that were shifted by the conformational change whereas cross-links that allowed signaling would identify interfaces that were essentially static. Thus, different effects on specific interfaces could distinguish between alternative notions of what moved in conformational signaling. However, there could be complications if disulfide cross-links across a static interface deformed receptor structure sufficiently to block signaling or if the conformational change of signaling were sufficiently modest to occur within the limits imposed by specific disulfide bonds.

We used our refined models to explore these issues, creating cross-linked models with cysteine pairs that had been studied experimentally, and calculating an energy parameter for the disulfide bonds to investigate the degree to which the engineered disulfides actually do constrain two proposed ligand-induced conformational changes: axial sliding of helix α4/TM2, and inter-subunit rotation.

We found that α1/TM1–α4/TM2 cross-links that blocked receptor signaling would cause little deformation of our modeled structures, suggesting that our refined models showed the "off" or non-signaling conformation of the receptor. Our results confirmed the original conclusion of the cross-linking studies that ligand-induced signaling includes an axial sliding of α4/TM2 of about 5 Å toward the cytoplasm. Previous analysis of one of the pairs of apo/holo crystal structures of the truncated periplasmic domain had showed

a much smaller difference (~1 Å) in the vertical positioning of helix α4 upon ligand binding [42]. The ensemble-averaged distance difference matrices we constructed from our molecular dynamics simulations of the Tar periplasmic domain suggested that this small difference may be an artifact.

The discrepancy between the position of helix α4/TM2 seen in the crystal structures and its position in our refined model based on disulfide cross-linking data was in approximately the same size and direction as the helical sliding motion of transmembrane signaling. This suggests that the position of helix α4 that is captured in the crystals, which is translated down toward the cytoplasm relative to the resting structure of the intact receptor, is in fact the signaling conformation. This may imply that the truncated, isolated periplasmic domain does not undergo a sliding motion of helix α4 upon ligand binding, even though that motion is an important component of the conformational change upon signaling in the full-length, intact receptor.

In contrast to our studies of α1/TM1–α4/TM2 cross-links we found that α1/TM1–α1′/TM1′ cross-links that disrupted receptor function would also strain and deform the receptor whereas α1/TM1–α1′/TM1′ cross-links that allowed signaling not only caused little strain in the structure of the unoccupied receptor but also would not constrain the ligand-induced rotation between the subunits that is observed in the crystals of the periplasmic domain of Tar_S. Thus signaling by receptors with α1/TM1–α1′/TM1′ cross-links does not in itself address the functional significance of the observed subunit rotation. We found that an inter-subunit rotational motion could not necessarily be ruled out as a component of receptor signaling based on the disulfide cross-linking experiments.

In our molecular dynamics simulations of the periplasmic domain of Tar in solution, we found that the difference in inter-subunit angle between the holo and apo periplasmic domains was much greater than the apo/holo rotational differences seen in the crystal structures. In our modeling of the inter-subunit rotation, we also saw that each of the five different crystal structures of the periplasmic domain has a different inter-subunit packing angle. This suggests that the truncated periplasmic domain is sensitive to crystal packing forces

and so the crystal structures underestimate the magnitude of subunit rotation upon ligand binding.

Our results also suggested that the receptor structure, especially the transmembrane domain, has a great deal of dynamic flexibility. In our analysis of the potential energies of α1/TM1–α4/TM2 cross-links with high propensities for formation, we saw that they would stabilize the interface between those helices in a wide variety of conformations, suggesting that the α4/TM2 helix undergoes large sliding and rotational motions in its membrane-embedded functional state. We also saw, in our molecular dynamics simulations of the isolated transmembrane domain in a patch of solvated lipid bilayer, that the RMS fluctuations of the helices were quite large, offering an explanation for why EPR experiments have shown larger values for solvent acessibility and mobility for spin-labeled residues in Trg than in many other membrane proteins.

There is also a variety of experimental evidence supporting the idea of flexibility and loose packing in the transmembrane domain of the chemotaxis receptors. For example, this domain is quite insensitive to mutation [43, 41, 94, 19, 80], and when TM2 is replaced entirely by a series of randomly selected hydrophobic residues, in some cases the mutant receptors are still able to perform chemotaxis to aspartate [81, 104]. Furthermore, Tar can be reconstructed without any transmembrane domain at all, by fusing the periplasmic domain to the linker region. This soluble protein retains some signaling ability, implying that to some extent the transmembrane domain is not required at all for transmitting the ligand-binding signal from the periplasmic to the cytoplasmic domain of the receptor [114].

Our analysis of the RMS fluctuations in the periplasmic domain during our molecular dynamics simulations showed that, although the flexibility of the transmembrane domain may be necessary for receptor function, a change in the dynamics of receptor motion is most likely not part of the signaling mechanism. In the periplasmic domain, the two equivalent, non-overlapping ligand-binding sites span the subunit interface and occupancy at one of the sites drastically reduces affinity for ligand at the second site [25]. This negative cooperativity for asparate binding in Tar may be regulated by a localized change in backbone

and sidechain dynamics in the vicinity of the ligand binding sites.

6.3 New model for receptor signaling

Taken together, our results lead to a suggestion for a new model of receptor signaling, in which both inter-subunit rotation and intra-subunit helical sliding play a part.

Rotation cannot be sufficient for transmembrane signaling, since α1/TM1–α4/TM2 cross-links that block signaling do not block subunit rotation. However, ligand binding to the chemotaxis receptors has multiple effects. In the cytoplasmic domain, the associated histidine kinase is deactivated. Chemotaxis receptors can also adjust to increasing levels of ligand by modifying their signaling through the methylation of several glutamate residues in the cytoplasmic domain. Thus it seems plausible that in the intact receptor both proposed ligand-induced conformational changes would occur and have functional roles. The two proposed signal transduction mechanisms may be involved in different aspects of signaling or adaptation. However, the situation is probably not simple and clear-cut. For example, several constitutively signaling mutants of Trg have been isolated [160]. These mutations are nearly all located at the interface of α1 and α1′ in the periplasmic domain, suggesting that they influence the inter-subunit rotation of the receptor, but they have also been shown to affect the vertical positioning of TM2 [21]. This suggests that if both the inter-subunit rotational and intra-subunit helical sliding motions are involved in receptor signaling, they are not independent of one another, but instead may be functionally coupled.

Since in the isolated periplasmic domain ligand binding induces an inter-subunit rotation, in the intact receptor this motion would still occur as a first step in the signaling mechanism. This rotational motion would then be converted to a helical sliding motion in the transmembrane and cytoplasmic domains, perhaps through the action of the linker region. This region connects the transmembrane domain to the cytoplasmic domain and is known to have a partially non-helical but well-defined secondary structure [40, 36]. It may act as a transducer to couple the rotational motion to the sliding motion, pulling helix

α4/TM2 downward when the subunits rotate.

Interestingly, sequence analysis studies have shown that similar linker-type regions are found in a wide variety of bacterial signaling proteins, so the coupling of rotational and sliding motions may be a common theme in signaling. This suggests a theoretical mechanism for signaling in the eukaryotic tyrosine kinase receptors, which signal through dimerization. The chemotaxis receptors are always dimeric, but the rotational re-orientation of the subunits upon ligand binding may be equivalent to a dimerization event with the tyrosine kinase receptors. In both cases, this rotation could be transduced into a sliding motion that is also involved in signaling.

REFERENCES

[1] Akke, M., S. Forsén, and W. J. Chazin. 1995. Solution structure of $(Cd^{2+})_1$ – calbindinD_{9K} reveals details of the stepwise structural changes along the apo $\rightarrow$ $(Ca^{2+})_1^{II}$ $\rightarrow$ $(Ca^{2+})_2^{I,II}$ binding pathway. *Journal of Molecular Biology* 252:102–121.

[2] Alex, L. A. and M. I. Simon. 1994. Protein histidine kinases and signal transduction in prokaryotes and eukaryotes. *Trends in Genetics* 10:133–138.

[3] Altenbach, C., S. L. Flitsch, H. G. Khorana, and W. L. Hubbell. 1989. Structural studies on transmembrane proteins. 2. Spin labeling of bacteriorhodopsin mutants at unique cysteines. *Biochemistry* 28:7806–7812.

[4] Altenbach, C., D. A. Greenhalgh, H. G. Khorana, and W. L. Hubbell. 1994. A collision gradient method to determine the immersion depth of nitroxides in lipid bilayers: Application to spin-labeled mutants of bacteriorhodopsin. *Proceedings of the National Academy of Sciences USA* 91:1667–1671.

[5] Altenbach, C., T. Marti, H. G. Khorana, and W. L. Hubbell. 1990. Transmembrane protein structure: Spin labeling of bacteriorhodopsin mutants. *Science* 248:1088–1092.

[6] Altenbach, C., K. Yang, D. L. Farrens, Z. T. Farahbakhsh, H. G. Khorana, and W. L. Hubbell. 1996. Structural features and light-dependent changes in the cytoplasmic interhelical E-F loop of rhodopsin: A site-directed spin-labeling study. *Biochemistry* 35:12470–12478.

[7] Altschul, S. F., T. L. Madden, A. A. Schäffer, J. Zhang, Z. Zhang, W. Miller, and D. J. Lipman. 1997. Gapped BLAST and PSI-BLAST: A new generation of protein database search programs. *Nucleic Acids Research* 25:3389–3402.

[8] Aravind, L. and C. P. Ponting. 1999. The cytoplasmic helical linker domain of receptor histidine kinase and methyl-accepting proteins is common to many prokaryotic signalling proteins. *FEMS Microbiology Letters* 176:111–116.

[9] Arnold, G. E. and R. L. Ornstein. 1994. An evaluation of implicit and explicit solvent model systems for the molecular dynamics simulation of bacteriophage T4 lysozyme. *Proteins: Structure, Function, and Genetics* 18:19–33.

[10] Arumugam, S., S. Pascal, C. L. North, W. Hu, K. C. Lee, M. Cotten, R. R. Ketchem, F. Xu, M. Brenneman, F. Kovacs, F. Tian, A. Wang, S. Huo, and T. A. Cross. 1996. Conformational trapping in a membrane environment: A regulatory mechanism for protein activity? *Proceedings of the National Academy of Sciences USA* 93:5872–5876.

[11] Ashikawa, I., J. J. Yin, W. K. Subczynski, T. Kouyama, J. S. Hyde, and A. Kusumi. 1994. Molecular organization and dynamics in bacteriorhodopsin-rich reconstituted membranes: Discrimination of lipid environments by the oxygen transport parameter using a pulse ESR spin-labeling technique. *Biochemistry* 33:4947–4952.

[12] Bachar, M. and O. M. Becker. 2000. Protein-induced membrane disorder: A molecular dynamics study of melittin in a dipalmitoylphosphatidylcholine bilayer. *Biophysical Journal* 78:1359–1375.

[13] Bajorath, J., R. Stenkamp, and A. Aruffo. 1993. Knowledge-based model building of proteins: Concepts and examples. *Protein Science* 2:1798–1810.

[14] Barnakov, A., C. Altenbach, W. L. Hubbell, and G. L. Hazelbauer. 2001. Site-directed spin labeling of a bacterial chemoreceptor identifies specific but loose packing in the transmembrane domain. *In preparation* .

[15] Barrett, J. F., R. M. Goldschmidt, L. E. Lawrence, B. Foleno, R. Chen, J. P. Demers, S. Johnson, R. Kanojia, J. Fernandez, J. Bernstein, L. Licata, A. Donetz, S. Huang, D. J. Hlasta, M. J. Macielag, K. Ohemeng, R. Frechette, M. B. Frosco, D. H. Klaubert, J. M. Whiteley, L. Wang, and J. A. Hoch. 1998. Antibacterial agents that inhibit two-component signal transduction systems. *Proceedings of the National Academy of Sciences USA* 95:5317–5322.

[16] Barton, G. J. 1993. ALSCRIPT: a tool to format multiple sequence alignments. *Protein Engineering* 6:37–40.

[17] Barton, G. J. and M. J. E. Sternberg. 1987. Evaluation and improvements in the automatic alignment of protein sequences. *Protein Engineering* 1:89–94.

[18] Barton, G. J. and M. J. E. Sternberg. 1987. A strategy for the rapid multiple alignment of protein sequences. *Journal of Molecular Biology* 198:327–337.

[19] Baumgartner, J. W. and G. L. Hazelbauer. 1996. Mutational analysis of a transmembrane segment in a bacterial chemoreceptor. *Journal of Bacteriology* 178:4651–4660.

[20] Baumgartner, J. W., C. Kim, R. E. Brissette, M. Inouye, C. Park, and G. L. Hazelbauer. 1994. Transmembrane signaling by a hybrid protein: Communication from the domain of chemoreceptor Trg that recognizes sugar-binding proteins to the kinase/phosphatase domain of osmosensor EnvZ. *Journal of Bacteriology* 176:1157–1163.

[21] Beel, B. D. and G. L. Hazelbauer. 2001. Signaling substitutions in the periplasmic domain of chemoreceptor Trg induce or reduce helical sliding in the transmembrane domain. *Molecular Microbiology* 40:824–834.

[22] Berendsen, H. J. C., J. P. M. Postma, W. F. van Gunsteren, A. DiNola, and J. R. Haak. 1984. Molecular dynamics with coupling to an external bath. *Journal of Chemical Physics* 81:3684–3690.

[23] Besler, B. H., Jr, K. M. Merz, and P. A. Kollman. 1990. Atomic charges derived from semiempirical methods. *Journal of Computational Chemistry* 11:431–439.

[24] Biemann, H. P., S. L. Harmer, and D. E. Koshland, Jr. 1996. An aspartate/insulin receptor chimera mitogenically activates fibroblasts. *Journal of Biological Chemistry* 271:27927–27930.

[25] Biemann, H. P. and D. E. Koshland, Jr. 1994. Aspartate receptors of *Escherichia coli* and *Salmonella typhimurium* bind ligand with negative and half-of-the-sites cooperativity. *Biochemistry* 33:629–634.

[26] Biggin, P. C. and M. S. P. Sansom. 1999. Interactions of α-helices with lipid bilayers: a review of simulation studies. *Biophysical Chemistry* 76:161–183.

[27] Biosym/Molecular Simulations, Inc., San Diego. 1997. *Insight II.*

[28] Björkman, A. M., P. Dunten, M. O. J. Sandgren, V. N. Dwarakanath, and S. L. Mowbray. 2001. Mutations that affect ligand binding to the Escherichia coli aspartate receptor. *Journal of Biological Chemistry* 276:2808–2815.

[29] Bollinger, J., C. Park, S. Harayama, and G. L. Hazelbauer. 1984. Structure of the Trg protein: Homologies with and differences from other sensory transducers of *Escherichia coli*. *Proceedings of the National Academy of Sciences USA* 81:3287–3291.

[30] Bower, M. J., F. E. Cohen, and R. L. Dunbrack, Jr. 1997. Prediction of protein side-chain rotamers from a backbone-dependent rotamer library: A new homology modeling tool. *Journal of Molecular Biology* 267:1268–1282.

[31] Bowie, J. U., A. A. Pakula, and M. I. Simon. 1995. The three-dimensional structure of the aspartate receptor from *Escherichia coli*. *Acta Crystallographica section D* 51:145–154.

[32] Bray, D., M. D. Levin, and C. J. Morton-Firth. 1998. Receptor clustering as a cellular mechanism to control sensitivity. *Nature* 393:85–88.

[33] Breneman, C. and K. B. Wiberg. 1990. Determining atom-centered monopoles from molecular electrostatic potentials. The need for high sampling density in formamide conformational analysis. *Journal of Computational Chemistry* 11:361–373.

[34] Brooks, C. L., M. Karplus, and B. M. Pettitt. 1988. *Proteins: A Theoretical Perspective of Dynamics, Structure, and Thermodynamics*, volume LXXI of *Advances in Chemical Physics*. New York: John Wiley & Sons.

[35] Brudvig, G. W. 1995. Electron paramagnetic resonance spectroscopy. *Methods in Enzymology* 246:536–554.

[36] Butler, S. L. and J. J. Falke. 1998. Cysteine and disulfide scanning reveals two amphiphilic helices in the linker region of the aspartate chemoreceptor. *Biochemistry* 37:10746–10756.

[37] Careaga, C. L. and J. J. Falke. 1992. Thermal motions of surface α-helices in the D-galactose chemosensory receptor. *Journal of Molecular Biology* 226:1219–1235.

[38] Case, D. A., D. A. Pearlman, J. W. Caldwell, T. E. Cheatham, III, W. S. Ross, C. L. Simmerling, T. A. Darden, K. M. Merz, R. V. Stanton, A. L. Cheng, J. J. Vincent, M. Crowley, D. M. Ferguson, R. J. Radmer, G. L. Seibel, U. C. Singh, P. K. Weiner, and P. A. Kollman. 1997. *AMBER*. University of California, San Francisco.

[39] Chen, X. and D. E. Koshland, Jr. 1995. The N-terminal cytoplasmic tail of the aspartate receptor is not essential in signal transduction of bacterial chemotaxis. *Journal of Biological Chemistry* 270:24038–24042.

[40] Chen, X. and D. E. Koshland, Jr. 1997. Probing the structure of the cytoplasmic domain of the aspartate receptor by targeted disulfide cross-linking. *Biochemistry* 36:11858–11864.

[41] Chervitz, S. A. and J. J. Falke. 1995. Lock on/off disulfides identify the transmembrane signaling helix of the aspartate receptor. *Journal of Biological Chemistry* 270:24043–24053.

[42] Chervitz, S. A. and J. J. Falke. 1996. Molecular mechanism of transmembrane signaling by the aspartate receptor: A model. *Proceedings of the National Academy of Sciences USA* 93:2545–2550.

[43] Chervitz, S. A., C. M. Lin, and J. J. Falke. 1995. Transmembrane signaling by the aspartate receptor: Engineered disulfides reveal static regions of the subunit interface. *Biochemistry* 34:9722–9733.

[44] Chi, Y. I., H. Yokota, and S. H. Kim. 1997. Apo structure of the ligand-binding domain of aspartate receptor from *Escherichia coli* and its comparison with ligand-bound or pseudoligand-bound structures. *FEBS Letters* 414:327–332.

[45] Chiu, S. W., S. Subramaniam, and E. Jakobsson. 1999. Simulation study of a gramicidin/lipid bilayer system in excess water and lipid. I. Structure of the molecular complex. *Biophysical Journal* 76:1929–1938.

[46] Cochran, A. G. and P. S. Kim. 1996. Imitation of *Escherichia coli* aspartate receptor signaling in engineered dimers of the cytoplasmic domain. *Science* 271:1113–1116.

[47] Cornell, W. D., P. Ciepiak, C. I. Bayly, I. R. Gould, K. M. Merz, Jr, D. M. Ferguson, D. C. Spellmeyer, T. Fox, J. W. Caldwell, and P. A. Kollman. 1995. A second generation force field for the simulation of proteins, nucleic acids, and organic molecules. *Journal of the American Chemical Society* 117:5179–5197.

[48] Creighton, T. E. 1984. Disulfide bond formation in proteins. *Methods in Enzymology* 107:305–329.

[49] Creighton, T. E. 1993. *Proteins: Structures and Molecular Properties*. New York: W. H. Freeman and Company, 2nd edition.

[50] Danielson, M. A., R. B. Bass, and J. J. Falke. 1997. Cysteine and disulfide scanning reveals a regulatory α-helix in the cytoplasmic domain of the aspartate receptor. *Journal of Biological Chemistry* 272:32878–32888.

[51] Darden, T., D. York, and L. Pedersen. 1993. Particle mesh Ewald. An N·log(N) method for Ewald sums in large systems. *Journal of Chemical Physics* 98:10089–10092.

[52] Dewar, M. J. S. and W. Thiel. 1977. The MNDO method. Approximations and parameters. *Journal of the American Chemical Society* 99:4899–4907.

[53] Djordjevic, S. and A. M. Stock. 1998. Structural analysis of bacterial chemotaxis proteins: Components of a dynamic signaling system. *Journal of Structural Biology* 124:189–200.

[54] Dunbrack, R. L., Jr and K. Martin. 1993. Backbone-dependent rotamer library for proteins. *Journal of Molecular Biology* 230:543–574.

[55] Edholm, O., O. Berger, and F. Jähnig. 1995. Structure and fluctuations of bacteriorhodopsin in the purple membrane: A molecular dynamics study. *Journal of Molecular Biology* 250:94–111.

[56] Engels, M., E. Jacoby, P. Krüger, J. Schlitter, and A. Wollmer. 1992. The T↔R structural transition of insulin; pathways suggested by targeted energy minimization. *Protein Engineering* 5:669–677.

[57] Falke, J. J., R. B. Bass, S. L. Butler, S. A. Chervitz, and M. A. Danielson. 1997. The two-component signaling pathway of bacterial chemotaxis: A molecular view of signal transduction by receptors, kinases, and adaptation enzymes. *Annual Review of Cell and Developmental Biology* 13:457–512.

[58] Falke, J. J. and G. L. Hazelbauer. 2001. Transmembrane signaling in bacterial chemoreceptors. *Trends in Biochemical Sciences* 26:257–265.

[59] Falke, J. J. and D. E. Koshland, Jr. 1987. Global flexibility in a sensory receptor: A site-directed cross-linking approach. *Science* 237:1596–1600.

[60] Farahbakhsh, Z. T., C. Altenbach, and W. L. Hubbell. 1992. Spin labeled cysteines as sensors for protein-lipid interaction and conformation in rhodopsin. *Photochemistry and Photobiology* 6:1019–1033.

[61] Feller, S. E., R. M. Venable, and R. W. Pastor. 1997. Computer simulation of a DPPC phospholipid bilayer: Structural changes as a function of molecular surface area. *Langmuir* 13:6555–6561.

[62] Forrest, L. R. and M. S. P. Sansom. 2000. Membrane simulations: bigger and better? *Current Opinion in Structural Biology* 10:174–181.

[63] Freed, J. H. 1976. Theory of slow tumbling ESR spectra for nitroxides. In *Spin Labeling Theory and Applications* (L. J. Berliner, ed.), pp. 53–132. New York: Academic Press.

[64] Frisch, M. J., M. Head-Gordon, G. W. Trucks, J. B. Foresman, H. B. Schlegel, K. Raghavachari, M. A. Robb, J. S. Binkley, C. Gonzalez, D. J. Defrees, D. J. Fox, R. Whiteside, R. Seeger, C. Melius, J. Baker, R. L. Martin, L. Kahn, J. P. Stewart, J. Topiol, and J. A. Pople. 1990. *Gaussian 90.* Gaussian, Inc.

[65] Gardina, P., C. Conway, M. Kossman, and M. Manson. 1992. Aspartate and maltose-binding protein interact with adjacent sites in the Tar chemotactic signal transducer of *Escherichia coli. Journal of Bacteriology* 174:1528–1536.

[66] Gerstein, M., A. M. Lesk, and C. Chothia. 1994. Structural mechanisms for domain movements in proteins. *Biochemistry* 33:6739–6749.

[67] Gracy, J., L. Chiche, and J. Sallantin. 1993. Improved alignment of weakly homologous protein sequences using structural information. *Protein Engineering* 6:821–829.

[68] Gregoret, L. M. and F. E. Cohen. 1990. Novel method for the rapid evaluation of packing in protein structures. *Journal of Molecular Biology* 211:959–974.

[69] Gross, A., L. Columbus, K. Hideg, C. Altenbach, and W. L. Hubbell. 1999. Structure of the KcsA potassium channel from *Streptomyces lividans*: a site-directed spin labeling study of the second transmembrane segment. *Biochemistry* 38:10324–10335.

[70] Guenot, J. and P. A. Kollman. 1992. Molecular dynamics studies of a DNA-binding protein: 2. An evaluation of implicit and explicit solvent models for the molecular dynamics simulation of the *Escherichia coli trp* repressor. *Protein Science* 1:1185–1205.

[71] Haas, D. A., C. Mailer, and B. H. Robinson. 1993. Using nitroxide spin labels. *Biophysical Journal* 64:594–604.

[72] Harbury, P. B., T. Zhang, P. S. Kim, and T. Alber. 1993. A switch between two, three, and four-stranded coiled coils in GCN4 leucine zipper mutants. *Science* 262:1401–1406.

[73] Hauser, H., I. Pascher, R. H. Pearson, and S. Sundell. 1981. Preferred conformation and molecular packing of phosphatidylethanolamine and phosphatidylcholine. *Biochimica et Biophysica Acta* 650:21–51.

[74] Heller, H., M. Schaefer, and K. Schulten. 1993. Molecular dynamics simulation of a bilayer of 200 lipids in the gel and in the liquid-crystal phases. *Journal of Physical Chemistry* 97:8343–8360.

[75] Henikoff, S. and J. G. Henikoff. 1992. Amino acid substitution matrices from protein blocks. *Proceedings of the National Academy of Sciences USA* 8910915-9:10915–10919.

[76] Howard, A. E. and P. A. Kollman. 1992. Molecular dynamics studies of a DNA-binding protein: 1. A comparison of the *trp* repressor and *trp* aporepressor aqueous simulations. *Protein Science* 1:1173–1184.

[77] Hubbell, W. L. and C. Altenbach. 1994. Investigation of structure and dynamics in membrane proteins using site-directed spin labeling. *Current Opinion in Structural Biology* 4:566–573.

[78] Hubbell, W. L., A. Gross, R. Langen, and M. A. Lietzow. 1998. Recent advances in site-directed spin labeling of proteins. *Current Opinion in Structural Biology* 8:649–656.

[79] Hughson, A. G. and G. L. Hazelbauer. 1996. Detecting the conformational change of transmembrane signaling in a bacterial chemoreceptor by measuring effects of disulfide cross-linking in vivo. *Proceedings of the National Academy of Sciences USA* 93:11546–11551.

[80] Hughson, A. G., G. F. Lee, and G. L. Hazelbauer. 1997. Analysis of protein structure in intact cells: Crosslinking *in vivo* between introduced cysteines in the transmembrane domain of a bacterial chemoreceptor. *Protein Science* 6:315–322.

[81] Jeffery, C. J. and D. E. Koshland, Jr. 1999. The *Escherichia coli* aspartate receptor: sequence specificity of a transmembrane helix studied by hydrophobic-biased random mutagenesis. *Protein Engineering* 12:863–871.

[82] Jorgensen, W. L., J. Chandrasekhar, J. D. Madura, R. W. Impey, and M. L. Klein. 1983. Comparison of simple potential functions for simulating liquid water. *Journal of Chemical Physics* 79:926–935.

[83] Jorgensen, W. L. and J. Tirado-Rives. 1988. The OPLS potential functions for proteins. Energy minimizations for crystals of cyclic peptides and crambin. *Journal of the Americal Chemical Society* 110:1657–1666.

[84] Keyes, R. S., Y. Y. Cao, E. V. Bobst, J. M. Rosenberg, and A. M. Bobst. 1996. Spin-labeled nucleotide mobility in the boundary of the EcoRI endonuclease binding site. *Journal of Biomolecular Structure and Dynamics* 14:163–172.

[85] Kim, K. K., H. Yokota, and S.-H. Kim. 1999. Four-helical-bundle structure of the cytoplasmic domain of a serine chemotaxis receptor. *Nature* 400:787–792.

[86] Kim, S.-H. 1994. "Frozen" dynamic dimer model for transmembrane signaling in bacterial chemotaxis receptors. *Protein Science* 3:159–165.

[87] Kim, S.-H., G. G. Privé, J. Yeh, W. G. Scott, and M. V. Milburn. 1992. A model for transmembrane signaling in a bacterial chemotaxis receptor. *Cold Spring Harbor Symposia on Quantitative Biology* 57:17–24.

[88] Krammer, A., M. L. Peach, R. Henne, V. Vogel, and T. P. Lybrand. 2001. Molecular dynamics simulation of a bombesin-like peptide embedded in a dipalmitoylphosphatidylcholine bilayer. *In preparation* .

[89] Kraulis, P. J. 1991. MOLSCRIPT: a program to produce both detailed and schematic plots of protein structures. *Journal of Applied Crystallography* 24:946–950.

[90] Lai, W.-C., M. L. Peach, T. P. Lybrand, and G. L. Hazelbauer. 2002. *in preparation* .

[91] Langen, R., J. M. Isas, W. L. Hubbell, and H. T. Haigler. 1998. A transmembrane form of annexin XII detected by site-directed spin labeling. *Proceedings of the National Academy of Sciences USA* 95:14060–14065.

[92] Langen, R., K. J. Oh, D. Cascio, and W. L. Hubbell. 2000. Crystal structures of spin labeled T4 lysozyme mutants: Implications for the interpretation of EPR spectra in terms of structure. *Biochemistry* 39:8396–8405.

[93] Lee, G. F., G. G. Burrows, M. R. Lebert, D. P. Dutton, and G. L. Hazelbauer. 1994. Deducing the organization of a transmembrane domain by disulfide cross-linking. *Journal of Biological Chemistry* 269:29920–29927.

[94] Lee, G. F., D. P. Dutton, and G. L. Hazelbauer. 1995. Identification of functionally important helical faces in transmembrane segments by scanning mutagenesis. *Proceedings of the National Academy of Sciences USA* 92:5416–5420.

[95] Lee, G. F. and G. L. Hazelbauer. 1995. Quantitative approaches to utilizing mutational analysis and disulfide crosslinking for modeling a transmembrane domain. *Protein Science* 4:1100–1107.

[96] Lee, G. F., M. R. Lebert, A. A. Lilly, and G. L. Hazelbauer. 1995. Transmembrane signaling characterized in bacterial chemoreceptors by using sulfhydryl cross-linking *in vivo*. *Proceedings of the National Academy of Sciences USA* 92:3391–3395.

[97] Lenaz, G. 1987. Lipid fluidity and membrane protein dynamics. *Bioscience Reports* 7:823–837.

[98] Likhtenshtein, G. I. 1976. *Spin Labeling Methods in Molecular Biology*. New York: John Wiley & Sons, translated by Philip S. Shelnitz edition.

[99] Liu, Y., M. Levit, R. Lurz, M. G. Surette, and J. B. Stock. 1997. Receptor-mediated protein kinase activation and the mechanism of transmembrane signaling in bacterial chemotaxis. *EMBO Journal* 16:7231–7240.

[100] Livingstone, C. D. and G. J. Barton. 1993. Protein sequence alignments: a strategy for the hierarchical analysis of residue conservation. *Computer Applications in the Biosciences* 9:745–756.

[101] Longati, P., P. M. Comoglio, and A. Bardelli. 2001. Receptor tyrosine kinases as therapeutic targets: the model of the MET oncogene. *Current Drug Targets* 2:41–55.

[102] Lynch, B. A. and D. E. Koshland, Jr. 1992. Structural similarities between the aspartate receptor of bacterial chemotaxis and the *trp* repressor of *E. coli*. *FEBS Letters* 307:3–9.

[103] Macnab, R. M. 1987. Motility and chemotaxis. In *Escherichia coli and Salmonella typhimurium: Cellular and Molecular Biology* (F. C. Neidhardt, ed.), volume 1, pp. 732–759. Washington, D.C.: American Society for Microbiology, 1st edition.

[104] Maruyama, I. N., Y. G. Mikawa, and H. I. Maruyama. 1995. A model for transmembrane signalling by the aspartate receptor based on random-cassette mutagenesis and site-directed disulfide cross-linking. *Journal of Molecular Biology* 253:530–546.

[105] Mchaourab, H. S., M. A. Lietzow, K. Hideg, and W. L. Hubbell. 1996. Motion of spin-labeled side chains in T4 lysozyme. Correlation with protein structure and dynamics. *Biochemistry* 35:7692–7704.

[106] Milburn, M. V., G. G. Privé, D. L. Milligan, W. G. Scott, J. Yeh, J. Jancarik, D. E. Koshland, Jr, and S.-H. Kim. 1991. Three-dimensional structures of the ligand-binding domain of the bacterial aspartate receptor with and without a ligand. *Science* 254:1342–1347.

[107] Milligan, D. L. and D. E. Koshland, Jr. 1991. Intrasubunit signal transduction by the aspartate chemoreceptor. *Science* 254:1651–1654.

[108] Mosimann, S., R. Meleshko, and M. N. G. James. 1995. A critical assessment of comparative molecular modeling of tertiary structures of proteins. *Proteins: Structure, Function, and Genetics* 23:301–317.

[109] Murphy, O. J., III, F. A. Kovacs, E. L. Sicard, and L. K. Thompson. 2001. Site-directed solid-state NMR measurement of a ligand-induced conformational change in the serine bacterial chemoreceptor. *Biochemistry* 40:1358–1366.

[110] Needleman, S. B. and C. D. Wunsch. 1970. A general method applicable to the search for similarities in the amino acid sequence of two proteins. *Journal of Molecular Biology* 48:443–453.

[111] Nishikawa, K., T. Ooi, Y. Isogai, and N. Saito. 1972. Tertiary structure of proteins. I. Representation and computation of the conformations. *Journal of the Physical Society of Japan* 32:1331–1337.

[112] Nordio, P. L. 1976. General magnetic resonance theory. In *Spin Labeling Theory and Applications* (L. J. Berliner, ed.), pp. 5–52. New York: Academic Press.

[113] Oh, K. J., H. Zhan, C. Cui, K. Kideg, R. J. Collier, and W. L. Hubbell. 1996. Organization of diphtheria toxin T domain in bilayers: A site-directed spin labeling study. *Science* 273:810–812.

[114] Ottemann, K. M. and D. E. Koshland, Jr. 1997. Converting a transmembrane receptor to a soluble receptor: Recognition domain to effector domain signaling after excision of the transmembrane domain. *Proceedings of the National Academy of Sciences USA* 94:11201–11204.

[115] Ottemann, K. M., T. E. Thorgeirsson, A. F. Kolodziej, Y.-K. Shin, and D. E. Koshland, Jr. 1998. Direct measurement of small ligand-induced conformational changes in the aspartate chemoreceptor using EPR. *Biochemistry* 37:7062–7069.

[116] Pakula, A. A. and M. I. Simon. 1992. Determination of transmembrane protein structure by disulfide cross-linking: The *Escherichia coli* Tar receptor. *Proceedings of the National Academy of Sciences USA* 89:4144–4148.

[117] Pearson, R. H. and I. Pascher. 1979. The molecular structure of lecithin dihydrate. *Nature* 281:499–501.

[118] Perozo, E., D. M. Cortes, and L. G. Cuello. 1998. Three-dimensional architecture and gating mechanism of a K+ channel studied by EPR spectroscopy. *Nature Structural Biology* 5:459–469.

[119] Post, C. B., B. R. Brooks, M. Karplus, C. M. Dobson, P. J. Artymiuk, J. C. Cheetham, and D. C. Phillips. 1986. Molecular dynamics simulations of native and substrate-bound lysozyme. *Journal of Molecular Biology* 190:455–479.

[120] Réat, V., H. Patzelt, M. Ferrand, C. Pfister, D. Oesterhelt, and G. Zaccai. 1998. Dynamics of different functional parts of bacteriorhodopsin: H-2H labeling and neutron scattering. *Proceedings of the National Academy of Sciences USA* 95:4970–4975.

[121] Reithmeier, R. A. F. 1995. Characterization and modeling of membrane proteins using sequence analysis. *Current Opinion in Structural Biology* 5:491–500.

[122] Robinson, B. H., L. J. Slutsky, and F. P. Auteri. 1992. Direct simulation of continuous wave electron paramagnetic resonance spectra from Brownian dynamics trajectories. *Journal of Chemical Physics* 96:2609–2616.

[123] Robinson, S. C., J. A. Tynan, and D. J. Donoghue. 2000. RTK mutations and human syndromes: When good receptors turn bad. *Trends in Genetics* 16:265–271.

[124] Ross, W. S. 1995. *CARNAL*. University of California, San Francisco.

[125] Ryckaert, J.-P., G. Ciccotti, and H. J. C. Berendsen. 1977. Numerical integration of the Cartesian equations of motion of a system with constraints: Molecular dynamics of n-alkanes. *Journal of Computational Physics* 23:327–341.

[126] Salwinski, L. and W. L. Hubbell. 1999. Structure in the channel forming domain of colicin E1 bound to membranes: the 402-424 sequence. *Protein Science* 8:562–572.

[127] Scott, W. G., D. L. Milligan, M. V. Milburn, G. G. Privé, J. Yeh, D. E. Koshland, Jr, and S.-H. Kim. 1993. Refined structures of the ligand-binding domain of the aspartate receptor from *Salmonella typhimurium*. *Journal of Molecular Biology* 232:555–573.

[128] Scott, W. G. and B. L. Stoddard. 1994. Transmembrane signalling and the aspartate receptor. *Structure* 2:877–887.

[129] Shen, L., D. Bassolino, and T. Stouch. 1997. Transmembrane helix structure, dynamics, and interactions: Multi-nanosecond molecular dynamics simulations. *Biophysical Journal* 73:3–20.

[130] Shimizu, T. S., N. Le Novère, M. D. Levin, A. J. Beavil, B. J. Sutton, and D. Bray. 2000. Molecular model of a lattice of signalling proteins involved in bacterial chemotaxis. *Nature Cell Biology* 2:792–796.

[131] Shinoda, W., N. Namiki, and S. Okazaki. 1997. Molecular dynamics study of a lipid bilayer: Convergence, structure, and long-time dynamics. *Journal of Chemical Physics* 106:5731–5743.

[132] Shrivastava, I. H. and M. S. P. Sansom. 2000. Simulations of ion permeation through a potassium channel: Molecular dynamics of KcsA in a phospholipid bilayer. *Biophysical Journal* 78:557–570.

[133] Smondyrev, A. M. and M. L. Berkowitz. 1999. United atom force field for phospholipid membranes: Constant pressure molecular dynamics simulation of dipalmitoylphosphatidicholine/water system. *Journal of Computational Chemistry* 20:531–545.

[134] Steinhoff, H. J. and W. L. Hubbell. 1996. Calculation of electron paramagnetic resonance spectra from Brownian dynamics trajectories: Application fo nitroxide side chains in proteins. *Biophysical Journal* 71:2201–2212.

[135] Steinhoff, H. J. and C. Karim. 1993. Protein dynamics and EPR-spectroscopy: Comparison of molecular dynamics simulations with experiments. *Berichte der Bunsen-Gesellschaft für Physikalische Chemie* 97:163–171.

[136] Stephenson, K., Y. Yamaguchi, and J. A. Hoch. 2000. The mechanism of action of inhibitors of bacterial two-component signal transduction systems. *Journal of Biological Chemistry* 275:38900–38904.

[137] Stewart, J. J. P. 1990. MOPAC: A semiempirical molecular orbital program. *Journal of Computer-Aided Molecular Design* 4:1–105.

[138] Stock, J. 1996. Receptor signaling: Dimerization and beyond. *Current Biology* 6:825–827.

[139] Stoddard, B. L., H. P. Biemann, and D. E. Koshland, Jr. 1992. Receptors and transmembrane signaling. *Cold Spring Harbor Symposia on Quantitative Biology* 57:1–15.

[140] Tatsuno, I., L. Lee, I. Kawagishi, M. Homma, and Y. Imae. 1994. Transmembrane signalling by the chimeric chemosensory receptors of *Escherichia coli* Tsr and Tar with heterologous membrane-spanning regions. *Molecular Microbiology* 14:755–762.

[141] Tieleman, D. P. and H. J. C. Berendsen. 1996. Molecular dynamics simulations of a fully hydrated dipalmitoylphosphatidylcholine bilayer with different macroscopic boundary conditions and parameters. *Journal of Chemical Physics* 105:4871–4880.

[142] Tieleman, D. P. and H. J. C. Berendsen. 1998. A molecular dynamics study of the pores formed by *Escherichia coli* OmpF porin in a fully hydrated palmitoyloleoylphosphatidylcholine bilayer. *Biophysical Journal* 74:2786–2801.

[143] Tieleman, D. P., M. S. P. Sansom, and H. J. C. Berendsen. 1999. Alamethicin helices in a bilayer and in solution: Molecular dynamics simulations. *Biophysical Journal* 76:40–49.

[144] Trammell, M. A. and J. J. Falke. 1999. Identification of a site critical for kinase regulation on the central processing unit (CPU) helix of the aspartate receptor. *Biochemistry* 38:329–336.

[145] Tristam-Nagle, S., R. Zhang, R. Suter, C. R. Worthington, W.-J. Sun, and J. F. Nagle. 1993. Measurement of chain tilt angle in fully hydrated bilayers of gel phase lecithins. *Biophysical Journal* 64:1097–1109.

[146] Tu, K., D. J. Tobias, J. K. Blasie, and M. L. Klein. 1996. Molecular dynamics investigation of the structure of a fully hydrated gel-phase dipalmitoylphosphatidylcholine bilayer. *Biophysical Journal* 70:595–608.

[147] Tung, C. S., S. C. Harvey, and J. A. McCammon. 1984. Large-amplitude bending motions in phenylalanine transfer RNA. *Biopolymers* 23:2173–2193.

[148] Tuzi, S., K. Shinzawa-Itoh, T. Erata, A. Naito, S. Yoshikawa, and H. Saitô. 1992. A high-resolution solid-state 13C-NMR study on crystalline bovine heart cytochrome-c oxidase and lysozyme. *European Journal of Biochemistry* 208:713–720.

[149] Veld, G. I., A. J. M. Driessen, and W. N. Konings. 1993. Bacterial solute transport proteins in their lipid environment. *FEMS Microbiology Reviews* 12:293–314.

[150] Voss, J., M. M. He, W. L. Hubbell, and H. R. Kaback. 1996. Site-directed spin labeling demonstrates that transmembrane domain XII in the lactose permease of *Escherichia coli* is an α-helix. *Biochemistry* 35:12915–12918.

[151] Voss, J., W. L. Hubbell, J. Hernandez-Borrell, and H. R. Kaback. 1997. Site-directed spin-labeling of transmembrane domain VII and the 4B1 antibody epitope in the lactose permease of *Escherichia coli*. *Biochemistry* 36:15055–15061.

[152] Vriend, G. 1990. WHAT IF: a molecular modeling and drug design program. *Journal of Molecular Graphics* 8:52–56.

[153] Wallin, E., T. Tsukihara, S. Yoshikawa, G. von Heijne, and A. Elofsson. 1997. Architecture of helix bundle membrane proteins: An analysis of cytochrome c oxidase from bovine mitochondria. *Protein Science* 6:808–815.

[154] Weerasuriya, S., B. M. Schneider, and M. D. Manson. 1998. Chimeric chemoreceptors in *Escherichia coli*: Signaling properties of Tar-Tap and Tap-Tar hybrids. *Journal of Bacteriology* 180:914–920.

[155] Weiner, S. J., P. A. Kollman, D. A. Case, U. C. Singh, C. Ghio, G. Alagona, S. Profeta, Jr, and P. Weiner. 1984. A new force field for molecular mechanical simulation of nucleic acids and proteins. *Journal of the American Chemical Society* 106:765–784.

[156] Weiner, S. J., P. A. Kollman, D. T. Nguyen, and D. A. Case. 1986. An all atom force field for simulations of proteins and nucleic acids. *Journal of Computational Chemistry* 7:230–252.

[157] Woolf, T. B. 1997. Molecular dynamics of individual α-helices of bacteriorhodopsin in dimyristoyl phosphatidylcholine. I. Structure and dynamics. *Biophysical Journal* 73:2376–2392.

[158] Woolf, T. B. and B. Roux. 1996. Structure, energetics, and dynamics of lipid-protein interactions: A molecular dynamics study of the gramicidin A channel in a DMPC bilayer. *Proteins: Structure, Function, and Genetics* 24:92–114.

[159] Xu, D., M. Sheves, and K. Schulten. 1995. Molecular dynamics study of the M412 intermediate of bacteriorhodopsin. *Biophysical Journal* 69:2745–2760.

[160] Yaghmai, R. and G. L. Hazelbauer. 1992. Ligand occupancy mimicked by single residue substitutions in a receptor: Transmembrane signaling induced by mutation. *Proceedings of the National Academy of Sciences USA* 89:7890–7894.

[161] Yeh, J. I., H. P. Biemann, J. Pandit, D. E. Koshland, Jr, and S.-H. Kim. 1993. The three-dimensional structure of the ligand-binding domain of a wild-type bacterial chemotaxis receptor. Structural comparison to the cross-linked mutant forms and conformational changes upon ligand binding. *Journal of Biological Chemistry* 268:9787–9792.

[162] Yeh, J. I., H.-P. Biemann, G. G. Privé, J. Pandit, D. E. Koshland, Jr, and S.-H. Kim. 1996. High-resolution structures of the ligand binding domain of the wild-type bacterial aspartate receptor. *Journal of Molecular Biology* 262:186–201.

Appendix A

INPUT PARAMETER FILES

A.1 Conformational change simulation protocol

A.1.1 Helical sliding

```
#BIOSYM btcl 3

begin topology = 42-203.mdf coordinate = 42-203.car
set tblfile [open down42-203.tbl w]
set tcl_precision 17

forcefield scale coulomb = 0.0 hbond = 0.0 vdw_1_4 = 0.5 \
                coulomb_1_4 = 0.0
set disulfides "TRG:(13..41,43..202,204..729):Atom;*"

subset define Subset "*:*:backbone" "CA,N,C"
subset get fixBone "*:(13..729):backbone"
subset get TM2bone "TRG:(165..229):backbone"

puts $tblfile "Frame\tTotal\tBond\tAngle\tTorsion\tInternal"

atomMovability set fixed ex1 $fixBone
atomMovability set excluded ex2 $disulfides
minimize method = steepest iteration_limit = 20000 \
    sd convergence = 10.0 final_convergence = 10.0
minimize method = conjugate iteration_limit = 20000 \
    final_convergence = 0.1
atomMovability unset ex1

set total [energy]
database handle edb Energy.
$edb select Bond Values.Name row
$edb get BE .Value $row
$edb select Angle Values.Name row
$edb get AE .Value $row
$edb select Torsion Values.Name row
$edb get TE .Value $row
$edb select Internal Values.Name row
$edb get IE .Value $row
puts $tblfile [format "%3.3f\t%8.4f\t%8.4f\t%8.4f\t%8.4f\t%8.4f" \
                  0.000 $total [object BE] [object AE] [object TE] \
                  [object IE] ]
```

```
flush $tblfile
atomMovability unset ex2

writeFile archive frame = 1
$nframe = 2
$dist = 0.125

for {$count = 0.125} {$count <= 10.000} {$count = $count + $dist} {
    molGeom get lsqLine axis $TM2bone
    geometry direction vector $axis
    molGeom translate $direction $dist $TM2bone

    atomMovability set fixed ex1 $fixBone
    atomMovability set excluded ex2 $disulfides
    minimize method = steepest iteration_limit = 20000 \
        sd convergence = 10.0 final_convergence = 10.0
    minimize method = conjugate iteration_limit = 20000 \
        final_convergence = 0.1
    atomMovability unset ex1

    set total [energy]
    database handle edb Energy.
    $edb select Bond Values.Name row
    $edb get BE .Value $row
    $edb select Angle Values.Name row
    $edb get AE .Value $row
    $edb select Torsion Values.Name row
    $edb get TE .Value $row
    $edb select Internal Values.Name row
    $edb get IE .Value $row
    puts $tblfile [format "%3.3f\t%8.4f\t%8.4f\t%8.4f\t%8.4f\t%8.4f" \
                            $count $total [object BE] [object AE] \
                    [object TE] [object IE] ]
    flush $tblfile
    atomMovability unset ex2

    writeFile archive frame = $nframe
    $nframe = $nframe + 1
}
close $tblfile
```

A.1.2 Subunit rotation

```
#BIOSYM btcl 3

begin topology = start36.mdf coordinate = start36.car
set tblfile [open rotate36.tbl w]
set tcl_precision 17
```

```
proc MoveAtoms { x y } {
    global dbh
    global template
    global distlist
    global step
    global numsteps
    global index

    $dbh get moving Coord $x
    $template get fixed Coord $y
    geometry dir vector $moving $fixed
    set dist $distlist($index)
    vector v subtract $numsteps $step
    vector target multiply $dist $v
    geometry currdist distance $moving $fixed
    vector trans subtract $currdist $target
    geometry moving transform translate $trans $dir
    $dbh set $moving Coord $x
    $index = $index + 1
}

proc GetDist { x y } {
    global dbh
    global template
    global distlist
    global numsteps
    global index

    $dbh get starting Coord $x
    $template get ending Coord $y
    geometry totdist distance $starting $ending
    vector size divide $totdist $numsteps
    set distlist($index) [object size]
    $index = $index + 1
}

forcefield scale coulomb = 0.0 hbond = 0.0 vdw_1_4 = 0.5 \
                coulomb_1_4 = 0.0
set disulfides "START:(3..35,37..535,537..715):Atom;*"

subset define Subset "*:*:backbone" "CA,N,C"
subset get fixBone "START:(3..715):backbone"

#########################################################################

database handle dbh
readFile molecular_system filename = end-2lig system_name = temp
database handle template temp

$step = 0
```

```
$numsteps = 10

puts $tblfile "1lih-2lig"

atomMovability set fixed ex1 $fixBone
atomMovability set excluded ex2 $disulfides
minimize method = steepest iteration_limit = 20000 \
    sd convergence = 10.0 final_convergence = 10.0
minimize method = conjugate iteration_limit = 20000 \
    final_convergence = 0.1
atomMovability unset ex1

$dbh select {N CA C} Atom.Name a "START:(3..74,89..215):Atom;*"
$dbh get allmove Coord $a
$template select {N CA C} Atom.Name b "END:(3..74,89..215):Atom;*"
$template get allfix Coord $b
geometry Dist distance $allmove $allfix
vector Square power $Dist 2
vector Av average $Square
vector RMS sqrt $Av

database handle edb Energy.
$edb select Internal Values.Name row
$edb get IE .Value $row
puts $tblfile [format "%8.4f\t%8.4f" [object RMS] [object IE] ]
flush $tblfile
atomMovability unset ex2

$index = 0
for {$i = 3} {$i <= 215} {$i = $i + 1} {
    if {$i <= 88 && $i >= 75} {
        continue
    }
    select mon START:$i
    $dbh get AAtype Monomer.Type $mon

    switch [object AAtype] {
        ACE {
            $dbh select {CH3} Atom.Name a "START:$i:Atom;*"
            $template select {CH3} Atom.Name b "END:$i:Atom;*"
            GetDist $a $b

            $dbh select {C} Atom.Name c "START:$i:Atom;*"
            $template select {C} Atom.Name d "END:$i:Atom;*"
            GetDist $c $d
        }
        NME {
            $dbh select {N} Atom.Name a "START:$i:Atom;*"
            $template select {N} Atom.Name b "END:$i:Atom;*"
            GetDist $a $b
```

```
            $dbh select {CH3} Atom.Name c "START:$i:Atom;*"
            $template select {CH3} Atom.Name d "END:$i:Atom;*"
            GetDist $c $d
        }
        default {
            $dbh select {N} Atom.Name a "START:$i:Atom;*"
            $template select {N} Atom.Name b "END:$i:Atom;*"
            GetDist $a $b

            $dbh select {CA} Atom.Name c "START:$i:Atom;*"
            $template select {CA} Atom.Name d "END:$i:Atom;*"
            GetDist $c $d

            $dbh select {C} Atom.Name e "START:$i:Atom;*"
            $template select {C} Atom.Name f "END:$i:Atom;*"
            GetDist $e $f
        }
    }
}

for {$step = 1} {$step <= $numsteps} {$step = $step + 1} {
    $index = 0

    for {$i = 3} {$i <= 215} {$i = $i + 1} {
        if {$i <= 88 && $i >= 75} {
            continue
        }
        select mon START:$i
        $dbh get AAtype Monomer.Type $mon

        switch [object AAtype] {
            ACE {
                $dbh select {CH3} Atom.Name a "START:$i:Atom;*"
                $template select {CH3} Atom.Name b "END:$i:Atom;*"
                MoveAtoms $a $b

                $dbh select {C} Atom.Name c "START:$i:Atom;*"
                $template select {C} Atom.Name d "END:$i:Atom;*"
                MoveAtoms $c $d
            }
            NME {
                $dbh select {N} Atom.Name a "START:$i:Atom;*"
                $template select {N} Atom.Name b "END:$i:Atom;*"
                MoveAtoms $a $b

                $dbh select {CH3} Atom.Name c "START:$i:Atom;*"
                $template select {CH3} Atom.Name d "END:$i:Atom;*"
                MoveAtoms $c $d
            }
```

```
            default {
                $dbh select {N} Atom.Name a "START:$i:Atom;*"
                $template select {N} Atom.Name b "END:$i:Atom;*"
                MoveAtoms $a $b

                $dbh select {CA} Atom.Name c "START:$i:Atom;*"
                $template select {CA} Atom.Name d "END:$i:Atom;*"
                MoveAtoms $c $d

                $dbh select {C} Atom.Name e "START:$i:Atom;*"
                $template select {C} Atom.Name f "END:$i:Atom;*"
                MoveAtoms $e $f
            }
        }
    }

    atomMovability set fixed ex1 $fixBone
    atomMovability set excluded ex2 $disulfides
    minimize method = steepest iteration_limit = 20000 \
        sd convergence = 10.0 final_convergence = 10.0
    minimize method = conjugate iteration_limit = 20000 \
        final_convergence = 0.1
    atomMovability unset ex1

    $dbh select {N CA C} Atom.Name a "START:(3..74,89..215):Atom;*"
    $dbh get allmove Coord $a
    $template select {N CA C} Atom.Name b "END:(3..74,89..215):Atom;*"
    $template get allfix Coord $b
    geometry Dist distance $allmove $allfix
    vector Square power $Dist 2
    vector Av average $Square
    vector RMS sqrt $Av

    database handle edb Energy.
    $edb select Internal Values.Name row
    $edb get IE .Value $row
    puts $tblfile [format "%8.4f\t%8.4f" [object RMS] [object IE] ]
    flush $tblfile
    atomMovability unset ex2

}

#############################################################################

database handle dbh2
readFile molecular_system filename = end-2asr system_name = temp2
database handle template temp2

$step = 0
$numsteps = 10
```

```
puts $tblfile "2lig-2asr"

atomMovability set fixed ex1 $fixBone
atomMovability set excluded ex2 $disulfides
minimize method = steepest iteration_limit = 20000 \
    sd convergence = 10.0 final_convergence = 10.0
minimize method = conjugate iteration_limit = 20000 \
    final_convergence = 0.1
atomMovability unset ex1

$dbh select {N CA C} Atom.Name a "START:(3..74,89..215):Atom;*"
$dbh get allmove Coord $a
$template select {N CA C} Atom.Name b "END:(3..74,89..215):Atom;*"
$template get allfix Coord $b
geometry Dist distance $allmove $allfix
vector Square power $Dist 2
vector Av average $Square
vector RMS sqrt $Av

database handle edb Energy.
$edb select Internal Values.Name row
$edb get IE .Value $row
puts $tblfile [format "%8.4f\t%8.4f" [object RMS] [object IE] ]
flush $tblfile
atomMovability unset ex2

$index = 0
for {$i = 3} {$i <= 215} {$i = $i + 1} {
    if {$i <= 88 && $i >= 75} {
        continue
    }
    select mon START:$i
    $dbh get AAtype Monomer.Type $mon

    switch [object AAtype] {
        ACE {
            $dbh select {CH3} Atom.Name a "START:$i:Atom;*"
            $template select {CH3} Atom.Name b "END:$i:Atom;*"
            GetDist $a $b

            $dbh select {C} Atom.Name c "START:$i:Atom;*"
            $template select {C} Atom.Name d "END:$i:Atom;*"
            GetDist $c $d
        }
        NME {
            $dbh select {N} Atom.Name a "START:$i:Atom;*"
            $template select {N} Atom.Name b "END:$i:Atom;*"
            GetDist $a $b
```

```
            $dbh select {CH3} Atom.Name c "START:$i:Atom;*"
            $template select {CH3} Atom.Name d "END:$i:Atom;*"
            GetDist $c $d
        }
        default {
            $dbh select {N} Atom.Name a "START:$i:Atom;*"
            $template select {N} Atom.Name b "END:$i:Atom;*"
            GetDist $a $b

            $dbh select {CA} Atom.Name c "START:$i:Atom;*"
            $template select {CA} Atom.Name d "END:$i:Atom;*"
            GetDist $c $d

            $dbh select {C} Atom.Name e "START:$i:Atom;*"
            $template select {C} Atom.Name f "END:$i:Atom;*"
            GetDist $e $f
        }
    }
}

for {$step = 1} {$step <= $numsteps} {$step = $step + 1} {
    $index = 0

    for {$i = 3} {$i <= 215} {$i = $i + 1} {
        if {$i <= 88 && $i >= 75} {
            continue
        }
        select mon START:$i
        $dbh get AAtype Monomer.Type $mon

        switch [object AAtype] {
            ACE {
                $dbh select {CH3} Atom.Name a "START:$i:Atom;*"
                $template select {CH3} Atom.Name b "END:$i:Atom;*"
                MoveAtoms $a $b

                $dbh select {C} Atom.Name c "START:$i:Atom;*"
                $template select {C} Atom.Name d "END:$i:Atom;*"
                MoveAtoms $c $d
            }
            NME {
                $dbh select {N} Atom.Name a "START:$i:Atom;*"
                $template select {N} Atom.Name b "END:$i:Atom;*"
                MoveAtoms $a $b

                $dbh select {CH3} Atom.Name c "START:$i:Atom;*"
                $template select {CH3} Atom.Name d "END:$i:Atom;*"
                MoveAtoms $c $d
            }
            default {
```

```
                $dbh select {N} Atom.Name a "START:$i:Atom;*"
                $template select {N} Atom.Name b "END:$i:Atom;*"
                MoveAtoms $a $b

                $dbh select {CA} Atom.Name c "START:$i:Atom;*"
                $template select {CA} Atom.Name d "END:$i:Atom;*"
                MoveAtoms $c $d

                $dbh select {C} Atom.Name e "START:$i:Atom;*"
                $template select {C} Atom.Name f "END:$i:Atom;*"
                MoveAtoms $e $f
            }
        }
    }

    atomMovability set fixed ex1 $fixBone
    atomMovability set excluded ex2 $disulfides
    minimize method = steepest iteration_limit = 20000 \
        sd convergence = 10.0 final_convergence = 10.0
    minimize method = conjugate iteration_limit = 20000 \
        final_convergence = 0.1
    atomMovability unset ex1

    $dbh select {N CA C} Atom.Name a "START:(3..74,89..215):Atom;*"
    $dbh get allmove Coord $a
    $template select {N CA C} Atom.Name b "END:(3..74,89..215):Atom;*"
    $template get allfix Coord $b
    geometry Dist distance $allmove $allfix
    vector Square power $Dist 2
    vector Av average $Square
    vector RMS sqrt $Av

    database handle edb Energy.
    $edb select Internal Values.Name row
    $edb get IE .Value $row
    puts $tblfile [format "%8.4f\t%8.4f" [object RMS] [object IE] ]
    flush $tblfile
    atomMovability unset ex2

}

#########################################################################

database handle dbh3
readFile molecular_system filename = end-1vls system_name = temp3
database handle template temp3

$step = 0
$numsteps = 20
```

```
puts $tblfile "2asr-1vls"

atomMovability set fixed ex1 $fixBone
atomMovability set excluded ex2 $disulfides
minimize method = steepest iteration_limit = 20000 \
    sd convergence = 10.0 final_convergence = 10.0
minimize method = conjugate iteration_limit = 20000 \
    final_convergence = 0.1
atomMovability unset ex1

$dbh select {N CA C} Atom.Name a "START:(3..74,89..215):Atom;*"
$dbh get allmove Coord $a
$template select {N CA C} Atom.Name b "END:(3..74,89..215):Atom;*"
$template get allfix Coord $b
geometry Dist distance $allmove $allfix
vector Square power $Dist 2
vector Av average $Square
vector RMS sqrt $Av

database handle edb Energy.
$edb select Internal Values.Name row
$edb get IE .Value $row
puts $tblfile [format "%8.4f\t%8.4f" [object RMS] [object IE] ]
flush $tblfile
atomMovability unset ex2

$index = 0
for {$i = 3} {$i <= 215} {$i = $i + 1} {
    if {$i <= 88 && $i >= 75} {
        continue
    }
    select mon START:$i
    $dbh get AAtype Monomer.Type $mon

    switch [object AAtype] {
        ACE {
            $dbh select {CH3} Atom.Name a "START:$i:Atom;*"
            $template select {CH3} Atom.Name b "END:$i:Atom;*"
            GetDist $a $b

            $dbh select {C} Atom.Name c "START:$i:Atom;*"
            $template select {C} Atom.Name d "END:$i:Atom;*"
            GetDist $c $d
        }
        NME {
            $dbh select {N} Atom.Name a "START:$i:Atom;*"
            $template select {N} Atom.Name b "END:$i:Atom;*"
            GetDist $a $b

            $dbh select {CH3} Atom.Name c "START:$i:Atom;*"
```

```
            $template select {CH3} Atom.Name d "END:$i:Atom;*"
            GetDist $c $d
        }
        default {
            $dbh select {N} Atom.Name a "START:$i:Atom;*"
            $template select {N} Atom.Name b "END:$i:Atom;*"
            GetDist $a $b

            $dbh select {CA} Atom.Name c "START:$i:Atom;*"
            $template select {CA} Atom.Name d "END:$i:Atom;*"
            GetDist $c $d

            $dbh select {C} Atom.Name e "START:$i:Atom;*"
            $template select {C} Atom.Name f "END:$i:Atom;*"
            GetDist $e $f
        }
    }
}

for {$step = 1} {$step <= $numsteps} {$step = $step + 1} {
    $index = 0

    for {$i = 3} {$i <= 215} {$i = $i + 1} {
        if {$i <= 88 && $i >= 75} {
            continue
        }
        select mon START:$i
        $dbh get AAtype Monomer.Type $mon

        switch [object AAtype] {
            ACE {
                $dbh select {CH3} Atom.Name a "START:$i:Atom;*"
                $template select {CH3} Atom.Name b "END:$i:Atom;*"
                MoveAtoms $a $b

                $dbh select {C} Atom.Name c "START:$i:Atom;*"
                $template select {C} Atom.Name d "END:$i:Atom;*"
                MoveAtoms $c $d
            }
            NME {
                $dbh select {N} Atom.Name a "START:$i:Atom;*"
                $template select {N} Atom.Name b "END:$i:Atom;*"
                MoveAtoms $a $b

                $dbh select {CH3} Atom.Name c "START:$i:Atom;*"
                $template select {CH3} Atom.Name d "END:$i:Atom;*"
                MoveAtoms $c $d
            }
            default {
                $dbh select {N} Atom.Name a "START:$i:Atom;*"
```

```
                $template select {N} Atom.Name b "END:$i:Atom;*"
                MoveAtoms $a $b

                $dbh select {CA} Atom.Name c "START:$i:Atom;*"
                $template select {CA} Atom.Name d "END:$i:Atom;*"
                MoveAtoms $c $d

                $dbh select {C} Atom.Name e "START:$i:Atom;*"
                $template select {C} Atom.Name f "END:$i:Atom;*"
                MoveAtoms $e $f
            }
        }
    }

    atomMovability set fixed ex1 $fixBone
    atomMovability set excluded ex2 $disulfides
    minimize method = steepest iteration_limit = 20000 \
        sd convergence = 10.0 final_convergence = 10.0
    minimize method = conjugate iteration_limit = 20000 \
        final_convergence = 0.1
    atomMovability unset ex1

    $dbh select {N CA C} Atom.Name a "START:(3..74,89..215):Atom;*"
    $dbh get allmove Coord $a
    $template select {N CA C} Atom.Name b "END:(3..74,89..215):Atom;*"
    $template get allfix Coord $b
    geometry Dist distance $allmove $allfix
    vector Square power $Dist 2
    vector Av average $Square
    vector RMS sqrt $Av

    database handle edb Energy.
    $edb select Internal Values.Name row
    $edb get IE .Value $row
    puts $tblfile [format "%8.4f\t%8.4f" [object RMS] [object IE] ]
    flush $tblfile
    atomMovability unset ex2

}

#########################################################################

database handle dbh4
readFile molecular_system filename = end-1vlt system_name = temp4
database handle template temp4

$step = 0
$numsteps = 10

puts $tblfile "1vls-1vlt"
```

```
atomMovability set fixed ex1 $fixBone
atomMovability set excluded ex2 $disulfides
minimize method = steepest iteration_limit = 20000 \
    sd convergence = 10.0 final_convergence = 10.0
minimize method = conjugate iteration_limit = 20000 \
    final_convergence = 0.1
atomMovability unset ex1

$dbh select {N CA C} Atom.Name a "START:(3..74,89..215):Atom;*"
$dbh get allmove Coord $a
$template select {N CA C} Atom.Name b "END:(3..74,89..215):Atom;*"
$template get allfix Coord $b
geometry Dist distance $allmove $allfix
vector Square power $Dist 2
vector Av average $Square
vector RMS sqrt $Av

database handle edb Energy.
$edb select Internal Values.Name row
$edb get IE .Value $row
puts $tblfile [format "%8.4f\t%8.4f" [object RMS] [object IE] ]
flush $tblfile
atomMovability unset ex2

$index = 0
for {$i = 3} {$i <= 215} {$i = $i + 1} {
    if {$i <= 88 && $i >= 75} {
        continue
    }
    select mon START:$i
    $dbh get AAtype Monomer.Type $mon

    switch [object AAtype] {
        ACE {
            $dbh select {CH3} Atom.Name a "START:$i:Atom;*"
            $template select {CH3} Atom.Name b "END:$i:Atom;*"
            GetDist $a $b

            $dbh select {C} Atom.Name c "START:$i:Atom;*"
            $template select {C} Atom.Name d "END:$i:Atom;*"
            GetDist $c $d
        }
        NME {
            $dbh select {N} Atom.Name a "START:$i:Atom;*"
            $template select {N} Atom.Name b "END:$i:Atom;*"
            GetDist $a $b

            $dbh select {CH3} Atom.Name c "START:$i:Atom;*"
            $template select {CH3} Atom.Name d "END:$i:Atom;*"
```

```
            GetDist $c $d
        }
        default {
            $dbh select {N} Atom.Name a "START:$i:Atom;*"
            $template select {N} Atom.Name b "END:$i:Atom;*"
            GetDist $a $b

            $dbh select {CA} Atom.Name c "START:$i:Atom;*"
            $template select {CA} Atom.Name d "END:$i:Atom;*"
            GetDist $c $d

            $dbh select {C} Atom.Name e "START:$i:Atom;*"
            $template select {C} Atom.Name f "END:$i:Atom;*"
            GetDist $e $f
        }
    }
}

for {$step = 1} {$step <= $numsteps} {$step = $step + 1} {
    $index = 0

    for {$i = 3} {$i <= 215} {$i = $i + 1} {
        if {$i <= 88 && $i >= 75} {
            continue
        }
        select mon START:$i
        $dbh get AAtype Monomer.Type $mon

        switch [object AAtype] {
            ACE {
                $dbh select {CH3} Atom.Name a "START:$i:Atom;*"
                $template select {CH3} Atom.Name b "END:$i:Atom;*"
                MoveAtoms $a $b

                $dbh select {C} Atom.Name c "START:$i:Atom;*"
                $template select {C} Atom.Name d "END:$i:Atom;*"
                MoveAtoms $c $d
            }
            NME {
                $dbh select {N} Atom.Name a "START:$i:Atom;*"
                $template select {N} Atom.Name b "END:$i:Atom;*"
                MoveAtoms $a $b

                $dbh select {CH3} Atom.Name c "START:$i:Atom;*"
                $template select {CH3} Atom.Name d "END:$i:Atom;*"
                MoveAtoms $c $d
            }
            default {
                $dbh select {N} Atom.Name a "START:$i:Atom;*"
                $template select {N} Atom.Name b "END:$i:Atom;*"
```

```
                MoveAtoms $a $b

                $dbh select {CA} Atom.Name c "START:$i:Atom;*"
                $template select {CA} Atom.Name d "END:$i:Atom;*"
                MoveAtoms $c $d

                $dbh select {C} Atom.Name e "START:$i:Atom;*"
                $template select {C} Atom.Name f "END:$i:Atom;*"
                MoveAtoms $e $f
            }
        }
    }

    atomMovability set fixed ex1 $fixBone
    atomMovability set excluded ex2 $disulfides
    minimize method = steepest iteration_limit = 20000 \
        sd convergence = 10.0 final_convergence = 10.0
    minimize method = conjugate iteration_limit = 20000 \
        final_convergence = 0.1
    atomMovability unset ex1

    $dbh select {N CA C} Atom.Name a "START:(3..74,89..215):Atom;*"
    $dbh get allmove Coord $a
    $template select {N CA C} Atom.Name b "END:(3..74,89..215):Atom;*"
    $template get allfix Coord $b
    geometry Dist distance $allmove $allfix
    vector Square power $Dist 2
    vector Av average $Square
    vector RMS sqrt $Av

    database handle edb Energy.
    $edb select Internal Values.Name row
    $edb get IE .Value $row
    puts $tblfile [format "%8.4f\t%8.4f" [object RMS] [object IE] ]
    flush $tblfile
    atomMovability unset ex2

}
```

A.2 Prep input file for a nitroxide spin-labeled residue

```
   0

nitroxide spin label residue
spl.top
SPL   INT   0
 CORRECT   OMIT   DU   BEG
 0.0
    1 DU1   DU    M     0     0     0     0.0000     0.0000     0.0000
```

```
     2 DU2   DU    M     1     0     0     1.0000     0.0000     0.0000
     3 DU3   DU    M     2     1     0     1.0000    90.0000     0.0000
     4 N     N     M     3     2     1     1.7934    90.2456   180.3377   -0.5700
     5 HN    H     E     4     3     2     1.1100    76.6659   220.4116    0.3700
     6 CA    CH    M     4     3     2     1.4580    39.3361    74.3491    0.2000
     7 CB    C2    S     6     4     3     1.5392   107.8076   213.0956    0.1481
     8 S2    S     S     7     6     4     1.8012   110.6475   302.0379   -0.1107
     9 S3    S     S     8     7     6     2.0001   109.5335   180.0000   -0.0670
    10 C4    C2    S     9     8     7     1.8004   109.4091    89.6966    0.0296
    11 C7    CM    S    10     9     8     1.5154   114.2869   184.1864   -0.1362
    12 C6    CJ    S    11    10     9     1.3350   123.2051   283.6243   -0.0893
    13 C5    CT    3    12    11    10     1.5035   112.2892   178.7892    0.5528
    14 C9    C3    E    13    12    11     1.5333   110.7815   117.7088   -0.0789
    15 C10   C3    E    13    12    11     1.5343   110.6907   241.5792   -0.0789
    16 N1    N3    B    13    12    11     1.4695   103.3895   359.5907   -0.5442
    17 O1    OH    S    16    13    12     1.3226   123.8774   180.3604   -0.3146
    18 H1    HO    E    17    16    13     1.1100   108.0001   180.0000    0.2671
    19 C8    CT    B    16    13    12     1.4719   110.6953     0.2762    0.6298
    20 C12   C3    E    19    16    13     1.5381   109.2810   240.6733   -0.1038
    21 C11   C3    E    19     1    13     1.5390   109.1350   119.2159   -0.1038
    22 C     C     M     6     4     3     1.5253   111.2222   335.1832    0.5000
    23 O     O     E    22     6     4     1.2455   118.5370   181.9712   -0.5000

LOOP
C7   C8

IMPROPER
 -M   CA   N   HN
 CA   +M   C   O
 C5   C8   N1  O1


DONE
STOP
```

A.3 Prep input file for DPPC

```
   0

DPPC
dppc.top
DPC  INT  0
 CORRECT  OMIT  DU  BEG
 0.0
    1 DU1   DU    M     0     0     0     0.0000     0.0000     0.0000
    2 DU2   DU    M     1     0     0     1.0000     0.0000     0.0000
    3 DU3   DU    M     2     1     0     1.0000    90.0000     0.0000
    4 C1    C3    M     3     2     1    18.5648   136.2411   338.2016    0.1607
    5 N2    N3    M     4     3     2     1.4487    79.6593   346.5417    0.1433
```

6	C3	C3	E	5	4	3	1.2512	116.2033	195.0175	0.1607
7	C4	C3	E	5	4	3	1.4042	108.6318	61.1094	0.1607
8	C5	C2	M	5	4	3	1.5899	116.5344	311.1408	0.1646
9	C6	C2	M	8	5	4	1.3451	119.1803	53.9709	0.3111
10	O7	OS	M	9	8	5	1.5676	118.0336	295.8109	-0.5797
11	P8	P	M	10	9	8	1.5336	118.3452	139.9963	1.3760
12	O9	O2	E	11	10	9	1.4810	108.1515	187.0334	-0.8010
13	O10	O2	E	11	10	9	1.3980	112.2157	316.3156	-0.8010
14	O11	OS	M	11	10	9	1.5554	102.3218	68.9619	-0.5548
15	C12	C2	M	14	11	10	1.4350	119.4990	62.1219	0.2508
16	C13	CH	M	15	14	11	1.5364	110.9666	163.2586	0.4802
17	C14	C2	S	16	15	14	1.4532	110.2286	57.1668	0.2508
18	O15	OS	S	17	16	15	1.4346	104.7205	182.5011	-0.5692
19	C16	C	B	18	17	16	1.3398	126.2936	184.2588	0.8701
20	O17	O	E	19	18	17	1.1826	108.5026	4.5319	-0.6302
21	C18	C2	S	19	18	17	1.3731	130.5673	168.8626	-0.1749
22	C19	C2	S	21	19	18	1.4146	126.9119	186.5443	0.1342
23	C20	C2	S	22	21	19	1.5150	116.0855	176.7605	-0.0465
24	C21	C2	S	23	22	21	1.5002	114.8227	179.5232	0.0746
25	C22	C2	S	24	23	22	1.4714	116.6337	188.9391	0.0050
26	C23	C2	S	25	24	23	1.4270	122.3223	194.4409	0.0050
27	C24	C2	S	26	25	24	1.3908	126.9503	179.1677	0.0050
28	C25	C2	S	27	26	25	1.4264	128.9236	161.4459	0.0050
29	C26	C2	S	28	27	26	1.4215	128.6513	158.2528	0.0050
30	C27	C2	S	29	28	27	1.4781	129.5319	179.8935	0.0050
31	C28	C2	S	30	29	28	1.3955	132.2515	197.3865	0.0050
32	C29	C2	S	31	30	29	1.5486	124.2659	208.4494	0.0050
33	C30	C2	S	32	31	30	1.5265	121.3278	186.1216	0.0050
34	C31	C2	S	33	32	31	1.5263	120.0780	169.7658	0.0050
35	C32	C3	E	34	33	32	1.5250	109.5181	179.9138	-0.0693
36	O33	OS	S	16	15	14	1.4651	108.8233	177.4359	-0.5692
37	C34	C	B	36	16	15	1.3592	117.2235	81.1207	0.8701
38	O35	O	E	37	36	16	1.1845	129.0604	5.2418	-0.6302
39	C36	C2	S	37	36	16	1.5018	109.1353	171.0693	-0.1749
40	C37	C2	S	39	37	36	1.5221	111.3651	274.7017	0.1342
41	C38	C2	S	40	39	37	1.1515	131.9024	86.2636	-0.0465
42	C39	C2	S	41	40	39	1.4306	137.7078	150.9116	0.0746
43	C40	C2	S	42	41	40	1.3454	142.0151	164.2625	0.0050
44	C41	C2	S	43	42	41	1.3585	134.8989	176.5249	0.0050
45	C42	C2	S	44	43	42	1.4031	130.5931	177.5832	0.0050
46	C43	C2	S	45	44	43	1.3545	129.3622	175.9730	0.0050
47	C44	C2	S	46	45	44	1.3355	130.1575	177.9372	0.0050
48	C45	C2	S	47	46	45	1.4273	134.0252	176.8713	0.0050
49	C46	C2	S	48	47	46	1.3423	135.2904	174.6863	0.0050
50	C47	C2	S	49	48	47	1.4252	139.6333	169.8815	0.0050
51	C48	C2	S	50	49	48	1.5269	151.4948	183.5513	0.0050
52	C49	C2	S	51	50	49	1.5273	150.1198	172.6036	0.0050
53	C50	C3	E	52	51	50	1.5264	150.0409	179.9161	-0.0693

IMPROPER

```
C12 C13 C14 O33

DONE
STOP
```

A.4 Bilayer equilibration protocol

A.4.1 Minimization

```
Small energy minimization with only water and ions allowed to move
 &cntrl
  imin = 1, ntpr = 10, ntf = 1, ntb = 1, ntc = 1, nrun = 0,
  nsnb = 25, idiel = 1, cut = 9.0, scee = 1.2, dielc = 1.0,
  tempi = 0.0, temp0 = 10.0, ntt = 0, ibelly = 1, maxcyc = 100
 &end
Group input for moving atoms
RES 287 4169
END
END

Small energy minimization with all atoms moving
 &cntrl
  imin = 1, ntpr = 10, ntf = 1, ntb = 1, ntc = 1, nrun = 0,
  nsnb = 25, idiel = 1, cut = 9.0, scee = 1.2, dielc = 1.0,
  tempi = 0.0, temp0 = 10.0, ntt = 0, ibelly = 0, maxcyc = 100
 &end
```

A.4.2 Water box disordering

```
MD run to disorder water molecules and ions
 &cntrl
  imin = 0, nrun = 1, nstlim = 5000, ibelly = 1,
  nsnb = 25, ntpr = 100, ntwx = 0,
  ntx = 1, init = 3, ig = 1234567,
  tempi = 100.0, temp0 = 100.0,
  ntc = 2, ntf = 2,
  idiel = 1, dielc = 1.0, scee = 1.2,
  ntb = 1, ntp = 0, taup = 0.5, npscal = 1, cut = 10.0,
  ntt = 4, dtemp = 5.0
 &end
Group input for moving atoms
RES 287 4169
END
END
```

A.4.3 Thermal equilibrium

```
Thermalization run
```

```
 &cntrl
  imin = 0, nrun = 1, nstlim = 200, ntpr = 50, ntwx = 0,
  ntx = 1, init = 3, ig = 4532177,
  tempi = 320.0, temp0 = 320.0,
  ntt = 4, dtemp = 5.0,
  ntc = 2, ntf = 2,
  idiel = 1, dielc = 1.0, scee = 1.2,
  ntb = 1, ntp = 0,
  cut = 10.0, iewald = 1
 &end
 7.8000E+01  7.6000E+01  7.5000E+01  9.0000E+01  9.0000E+01  9.0000E+01
 75 75 75 4 0 0 0
 0.00001
```

A.4.4 Hydrocarbon chain relaxation

```
Constant volume MD with moving lipid tails (last 3 carbons)
 &cntrl
  imin = 0, nrun = 1, nstlim = 10000, ntpr = 100, ntwx = 0,
  ntx = 1, init = 3, ig = 4567892,
  tempi = 320.0, temp0 = 320.0,
  ntt = 5, tautp = 0.2, tauts = 0.2,
  ntc = 2, ntf = 2,
  idiel = 1,  dielc = 1.0, scee = 1.2,
  ntb = 1, ntp = 0,
  ibelly = 1, cut = 10.0, iewald = 1
 &end
 7.8000E+01  7.6000E+01  7.5000E+01  9.0000E+01  9.0000E+01  9.0000E+01
 75 75 75 4 0 0 0
 0.00001
Moving carbon tails
FIND
C48 * * DPC
C49 * * DPC
C50 * * DPC
C32 * * DPC
C31 * * DPC
C30 * * DPC
SEARCH
RES 145 286
END
END

Constant volume MD with moving lipid tails (last 6 carbons)
 &cntrl
  imin = 0, nrun = 1, nstlim = 10000, ntpr = 100, ntwx = 0,
  ntx = 7, init = 4,
  tempi = 320.0, temp0 = 320.0,
```

```
  ntt = 5, tautp = 0.2, tauts = 0.2,
  ntc = 2, ntf = 2,
  idiel = 1,  dielc = 1.0, scee = 1.2,
  ntb = 1, ntp = 0,
  ibelly = 1, cut = 10.0, iewald = 1
 &end
 7.8000E+01  7.6000E+01  7.5000E+01  9.0000E+01  9.0000E+01  9.0000E+01
 75 75 75 4 0 0 0
 0.00001
Moving carbon tails
FIND
C45 * * DPC
C46 * * DPC
C47 * * DPC
C48 * * DPC
C49 * * DPC
C50 * * DPC
C32 * * DPC
C31 * * DPC
C30 * * DPC
C29 * * DPC
C28 * * DPC
C27 * * DPC
SEARCH
RES 145 286
END
END

Constant volume MD with moving lipid tails (last 9 carbons)
 &cntrl
  imin = 0, nrun = 1, nstlim = 10000, ntpr = 100, ntwx = 0,
  ntx = 7, init = 4,
  tempi = 320.0, temp0 = 320.0,
  ntt = 5, tautp = 0.2, tauts = 0.2,
  ntc = 2, ntf = 2,
  idiel = 1,  dielc = 1.0, scee = 1.2,
  ntb = 1, ntp = 0,
  ibelly = 1, cut = 10.0, iewald = 1
 &end
 7.8000E+01  7.6000E+01  7.5000E+01  9.0000E+01  9.0000E+01  9.0000E+01
 75 75 75 4 0 0 0
 0.00001
Moving carbon tails
FIND
C26 * * *
C25 * * *
C24 * * *
C44 * * *
C43 * * *
C42 * * *
```

```
SEARCH
RES 145 286
FIND
C27 * * *
C28 * * *
C29 * * *
C30 * * *
C31 * * *
C32 * * *
SEARCH
RES 145 286
FIND
C45 * * *
C46 * * *
C47 * * *
C48 * * *
C49 * * *
C50 * * *
SEARCH
RES 145 286
END
END

Constant volume MD with moving lipid tails (last 12 carbons)
 &cntrl
  imin = 0, nrun = 1, nstlim = 10000, ntpr = 100, ntwx = 0,
  ntx = 7, init = 4,
  tempi = 320.0, temp0 = 320.0,
  ntt = 5, tautp = 0.2, tauts = 0.2,
  ntc = 2, ntf = 2,
  idiel = 1,  dielc = 1.0, scee = 1.2,
  ntb = 1, ntp = 0,
  ibelly = 1, cut = 10.0, iewald = 1
 &end
 7.8000E+01  7.6000E+01  7.5000E+01  9.0000E+01  9.0000E+01  9.0000E+01
 75 75 75 4 0 0 0
 0.00001
Moving carbon tails
FIND
C23 * * *
C22 * * *
C21 * * *
C41 * * *
C40 * * *
C39 * * *
SEARCH
RES 145 286
FIND
C26 * * *
C25 * * *
```

```
C24 * * *
C44 * * *
C43 * * *
C42 * * *
SEARCH
RES 145 286
FIND
C27 * * *
C28 * * *
C29 * * *
C30 * * *
C31 * * *
C32 * * *
SEARCH
RES 145 286
FIND
C45 * * *
C46 * * *
C47 * * *
C48 * * *
C49 * * *
C50 * * *
SEARCH
RES 145 286
END
END

Constant volume MD with moving lipid tails (15 carbons)
 &cntrl
  imin = 0, nrun = 1, nstlim = 20000, ntpr = 100, ntwx = 0,
  ntx = 7, init = 4,
  tempi = 320.0, temp0 = 320.0,
  ntt = 5, tautp = 0.2, tauts = 0.2,
  ntc = 2, ntf = 2,
  idiel = 1,  dielc = 1.0, scee = 1.2,
  ntb = 1, ntp = 0, taup = 0.5, npscal = 1,
  ibelly = 1, cut = 10.0, iewald = 1
 &end
 7.8000E+01  7.6000E+01  7.5000E+01  9.0000E+01  9.0000E+01  9.0000E+01
 75 75 75 4 0 0 0
 0.00001
Moving carbon tails
FIND
C20 * * *
C19 * * *
C18 * * *
C38 * * *
C37 * * *
C36 * * *
SEARCH
```

```
RES 145 286
FIND
C23 * * *
C22 * * *
C21 * * *
C41 * * *
C40 * * *
C39 * * *
SEARCH
RES 145 286
FIND
C26 * * *
C25 * * *
C24 * * *
C44 * * *
C43 * * *
C42 * * *
SEARCH
RES 145 286
FIND
C27 * * *
C28 * * *
C29 * * *
C30 * * *
C31 * * *
C32 * * *
SEARCH
RES 145 286
FIND
C45 * * *
C46 * * *
C47 * * *
C48 * * *
C49 * * *
C50 * * *
SEARCH
RES 145 286
END
END
```

A.4.5 Simulated annealing

```
Simulated annealing -- raising temperature
 &cntrl
  imin = 0, nrun = 1, nstlim = 10000, ntpr = 100, ntwx = 0,
  ntx = 7, init = 4, tempi = 320.0,
  ntt = 5, tautp = 0.2, tauts = 0.2,
  ntc = 2, ntf = 2,
  idiel = 1, cut = 10.0, dielc = 1.0, scee = 1.2,
```

```
  ntb = 1, ntp = 0,
  ibelly = 1, nmropt = 1, iewald = 1
 &end
 7.8000E+01  7.6000E+01  7.5000E+01  9.0000E+01  9.0000E+01  9.0000E+01
 75 75 75 4 0 0 0
 0.00001
 &wt
  type='TEMP0', istep1=0, istep2=2500, value1=320.0, value2=400.0,
 &end
 &wt
  type='TEMP0', istep1=2501, istep2=5000, value1=400.0, value2=450.0,
 &end
 &wt
  type='TEMP0', istep1=5001, istep2=7500, value1=450.0, value2=500.0,
 &end
 &wt
  type='TEMP0', istep1=7501, istep2=10000, value1=500.0, value2=500.0,
 &end
 &wt
  type = 'END',
 &end
 &rst iat = 0, &end
Moving carbon tails
FIND
C20 * * *
C19 * * *
C18 * * *
C38 * * *
C37 * * *
C36 * * *
SEARCH
RES 145 286
FIND
C23 * * *
C22 * * *
C21 * * *
C41 * * *
C40 * * *
C39 * * *
SEARCH
RES 145 286
FIND
C26 * * *
C25 * * *
C24 * * *
C44 * * *
C43 * * *
C42 * * *
SEARCH
RES 145 286
```

```
FIND
C27 * * *
C28 * * *
C29 * * *
C30 * * *
C31 * * *
C32 * * *
SEARCH
RES 145 286
FIND
C45 * * *
C46 * * *
C47 * * *
C48 * * *
C49 * * *
C50 * * *
SEARCH
RES 145 286
END
END

Simulated annealing -- constant temperature reassignment of velocities
 &cntrl
  imin = 0, nrun = 1, nstlim = 3000, ntpr = 100, ntwx = 0,
  ntx = 1, init = 3, ig = 6547213,
  tempi = 500.0, temp0 = 500.0,
  ntt = 5, tautp = 0.2, tauts = 0.2,
  ntc = 2, ntf = 2,
  idiel = 1, cut = 10.0, dielc = 1.0, scee = 1.2,
  ntb = 1, ntp = 0,
  ibelly = 1, iewald = 1
 &end
 7.8000E+01  7.6000E+01  7.5000E+01  9.0000E+01  9.0000E+01  9.0000E+01
 75 75 75 4 0 0 0
 0.00001
Moving carbon tails
FIND
C20 * * *
C19 * * *
C18 * * *
C38 * * *
C37 * * *
C36 * * *
SEARCH
RES 145 286
FIND
C23 * * *
C22 * * *
C21 * * *
C41 * * *
```

```
C40 * * *
C39 * * *
SEARCH
RES 145 286
FIND
C26 * * *
C25 * * *
C24 * * *
C44 * * *
C43 * * *
C42 * * *
SEARCH
RES 145 286
FIND
C27 * * *
C28 * * *
C29 * * *
C30 * * *
C31 * * *
C32 * * *
SEARCH
RES 145 286
FIND
C45 * * *
C46 * * *
C47 * * *
C48 * * *
C49 * * *
C50 * * *
SEARCH
RES 145 286
END
END

Simulated annealing -- cooling
 &cntrl
  imin = 0, nrun = 1, nstlim = 36000, ntpr = 100, ntwx = 0,
  ntx = 7, init = 4, tempi = 500.0,
  ntt = 5, tautp = 0.2, tauts = 0.2,
  ntc = 2, ntf = 2,
  idiel = 1, cut = 10.0, dielc = 1.0, scee = 1.2,
  ntb = 1, ntp = 0,
  ibelly = 1, nmropt = 1, iewald = 1
 &end
 7.8000E+01  7.6000E+01  7.5000E+01  9.0000E+01  9.0000E+01  9.0000E+01
 75 75 75 4 0 0 0
 0.00001
 &wt
  type='TEMP0', istep1=0, istep2=2000, value1=490.0, value2=490.0,
 &end
```

```
&wt
 type='TEMP0', istep1=2001, istep2=4000, value1=480.0, value2=480.0,
&end
&wt
 type='TEMP0', istep1=4001, istep2=6000, value1=470.0, value2=470.0,
&end
&wt
 type='TEMP0', istep1=6001, istep2=8000, value1=460.0, value2=460.0,
&end
&wt
 type='TEMP0', istep1=8001, istep2=10000, value1=450.0, value2=450.0,
&end
&wt
 type='TEMP0', istep1=10001, istep2=12000, value1=440.0, value2=440.0,
&end
&wt
 type='TEMP0', istep1=12001, istep2=14000, value1=430.0, value2=430.0,
&end
&wt
 type='TEMP0', istep1=14001, istep2=16000, value1=420.0, value2=420.0,
&end
&wt
 type='TEMP0', istep1=16001, istep2=18000, value1=410.0, value2=410.0,
&end
&wt
 type='TEMP0', istep1=18001, istep2=20000, value1=400.0, value2=400.0,
&end
&wt
 type='TEMP0', istep1=20001, istep2=22000, value1=390.0, value2=390.0,
&end
&wt
 type='TEMP0', istep1=22001, istep2=24000, value1=380.0, value2=380.0,
&end
&wt
 type='TEMP0', istep1=24001, istep2=26000, value1=370.0, value2=370.0,
&end
&wt
 type='TEMP0', istep1=26001, istep2=28000, value1=360.0, value2=360.0,
&end
&wt
 type='TEMP0', istep1=28001, istep2=30000, value1=350.0, value2=350.0,
&end
&wt
 type='TEMP0', istep1=30001, istep2=32000, value1=340.0, value2=340.0,
&end
&wt
 type='TEMP0', istep1=32001, istep2=34000, value1=330.0, value2=330.0,
&end
&wt
 type='TEMP0', istep1=34001, istep2=36000, value1=325.0, value2=320.0,
```

```
 &end
 &wt
  type='END',
 &end
 &rst iat = 0, &end
Moving carbon tails
FIND
C20 * * *
C19 * * *
C18 * * *
C38 * * *
C37 * * *
C36 * * *
SEARCH
RES 145 286
FIND
C23 * * *
C22 * * *
C21 * * *
C41 * * *
C40 * * *
C39 * * *
SEARCH
RES 145 286
FIND
C26 * * *
C25 * * *
C24 * * *
C44 * * *
C43 * * *
C42 * * *
SEARCH
RES 145 286
FIND
C27 * * *
C28 * * *
C29 * * *
C30 * * *
C31 * * *
C32 * * *
SEARCH
RES 145 286
FIND
C45 * * *
C46 * * *
C47 * * *
C48 * * *
C49 * * *
C50 * * *
SEARCH
```

```
RES 145 286
END
END
```

A.4.6 Equilibration with backbone restraints

```
Standard molecular dynamics run
 &cntrl
  imin = 0, nrun = 1, nstlim = 10000,
  ntpr = 100, ntwr = 200, ntwx = 200, ntwe = 100,
  ntx = 7, init = 4,
  tempi = 320.0, temp0 = 320.0,
  ntt = 5, tautp = 1.0, tauts = 0.5,
  ntc = 2, ntf = 2,
  idiel = 1, dielc = 1.0, scee = 1.2, cut = 10.0,
  ntb = 2, ntp = 2, taup = 1.0,
  iewald = 1, ntr = 1
 &end
 7.8000E+01  7.6000E+01  7.5000E+01  9.0000E+01  9.0000E+01  9.0000E+01
 75 75 75 4 0 0 0
 0.00001
Group input for restrained atoms
25
FIND
* * M *
SEARCH
RES 1 144
END
END
```

VITA

MEGAN L. PEACH

EDUCATION

University of Washington, Seattle, Washington
1996 to 2001
Ph.D. in Bioengineering.

Harvey Mudd College, Claremont, California
1992 to 1996
Bachelor of Science degree in an independent program of study combining biology and engineering, with a humanities concentration in psychology.

PUBLICATIONS AND PRESENTATIONS

Peach, M. L., Hazelbauer, G. L., and Lybrand, T. P. Modeling the transmembrane domain of bacterial chemoreceptors. Submitted to *Protein Science*.

Krammer, A., Peach, M. L., Henne, R., Vogel, V., and Lybrand, T. P. Molecular dynamics simulations of a bombesin-like peptide embedded in a dipalmitoylphosphatidylcholine bilayer. Submitted to *Biophysical Journal*.

Peach, M. L., Lybrand, T. P., and Hazelbauer, G. L. Computer modeling of the structure and conformational changes of chemoreceptor Trg from *Escherichia coli*. Poster presentation at the BLAST V (Bacterial Locomotion and Signal Transduction) international meeting, Cuernavaca, Mexico, January 16-21, 1999.

Peach, M. L., and Adolph, S. C. Biophysics of water uptake by lizard eggs. Presentation at the Southern California Conference on Undergraduate Research, November 18, 1995.